AD-A039 085 GENERAL DYNAMICS SAN DIEGO CALIF CONVAIR AEROSPACE DIV F/G 1/3
SELF OPTIMIZING FLEXIBLE TECHNOLOGY WING PROGRAM, SEMISPAN WIND--ETC(U)
FEB 77 E S LEVINSKY, R H SCHAPPELLE N00014-76-C-0742
UNCLASSIFIED CASD-NSC-77-001 ONR-CR212-224-3 NL

1 OF 2
ADA039085

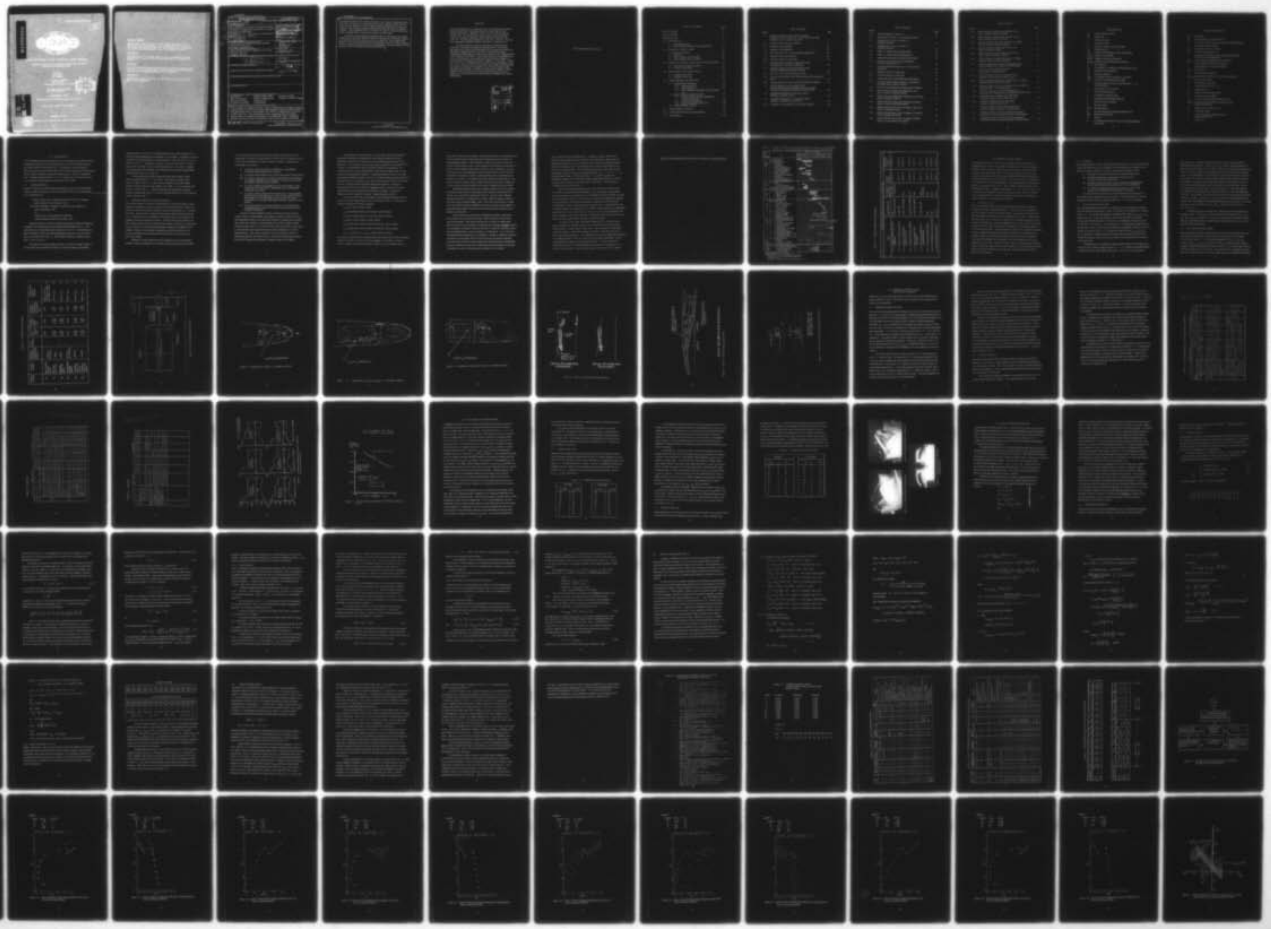

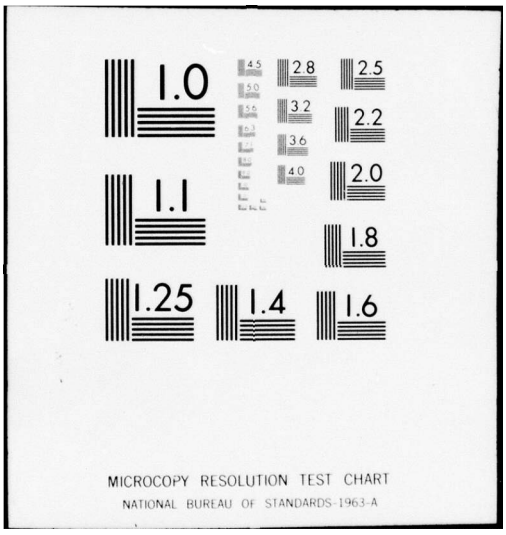
1.0
1.1
1.25
1.4
1.6
1.8
2.0
2.2
2.5
2.8
3.2
3.6
4.0
4.5
5.0
5.6
6.3
MICROCOPY RESOLUTION TEST CHART
NATIONAL BUREAU OF STANDARDS-1963-A

SELF OPTIMIZING FLEXIBLE TECHNOLOGY WING PROGR

Semispan Wind Tunnel Test of a Generalized Variable Geometry Wing Pa
Model Design and Aerodynamic Analysis

E.S. Levinsky
A.A. McClain
R.H. Schappelle

GENERAL DYNAMICS
Convair Division
P.O. Box 80847, San Diego, Calif. 92138

CONTRACT N00014-76-C-0742
ONR TASK NR 212-214

14 FEBRUARY 1977

INTERIM REPORT FOR PERIOD 15 APRIL 76 – 14 FEB 77

PREPARED FOR THE

Change of Address

Organizations receiving reports on the initial distribution list should confirm correct address. This list is located at the end of the report. Any change of address or distribution should be conveyed to the Office of Naval Research, Code 211, Arlington, VA 22217.

Disposition

When this report is no longer needed, it may be transmitted to other organizations. Do not return it to the originator or the monitoring office.

Disclaimer

The findings and conclusions contained in this report are not to be construed as an official Department of Defense or Military Department position unless so designated by other official documents.

Reproduction

Reproduction in whole or in part is permitted for any purpose of the United States Government.

Unclassified

SECURITY CLASSIFICATION OF THIS PAGE (When Data Entered)

REPORT DOCUMENTATION PAGE

READ INSTRUCTIONS BEFORE COMPLETING FORM

1. REPORT NUMBER: ONR-CR212-224-3
2. GOVT ACCESSION NO.:
3. RECIPIENT'S CATALOG NUMBER:

4. TITLE (and Subtitle): SELF OPTIMIZING FLEXIBLE TECHNOLOGY WING PROGRAM, Semispan Wind Tunnel Test of a Generalized Geometry Wing Panel, Model Design and Aerodynamic Analysis.

5. TYPE OF REPORT & PERIOD COVERED: Interim Technical Report. 15 April 1976 – 14 Feb. 1977

6. PERFORMING ORG. REPORT NUMBER: CASD-NSC-77-001

7. AUTHOR(s): S. Levinsky, R. H. Schappelle, A. A. McClain

8. CONTRACT OR GRANT NUMBER(s): N00014-76-C-0742

9. PERFORMING ORGANIZATION NAME AND ADDRESS: General Dynamics Corporation Convair Division, 5001 Kearny Villa Road, San Diego, California 92112

10. PROGRAM ELEMENT, PROJECT, TASK AREA & WORK UNIT NUMBERS: 62241N, RF 41-411-801, NR 212-224

11. CONTROLLING OFFICE NAME AND ADDRESS: Office of Naval Research - Department of the Navy, 800 North Quincy St., Arlington, VA 22217

12. REPORT DATE: February 14, 1977

13. NUMBER OF PAGES:

14. MONITORING AGENCY NAME & ADDRESS (if different from Controlling Office): F41411, RF41411801

15. SECURITY CLASS. (of this report): Unclassified

15a. DECLASSIFICATION/DOWNGRADING SCHEDULE:

16. DISTRIBUTION STATEMENT (of this Report)

Approved for Public Release; Distribution Unlimited

14 Feb 77

120 P.

17. DISTRIBUTION STATEMENT (of the abstract entered in Block 20, if different from Report)

18. SUPPLEMENTARY NOTES

19. KEY WORDS (Continue on reverse side if necessary and identify by block number)

Optimization	Mission Adaptive Wing	Interactive Testing
Wind Tunnel Models	Nonlinear Programming	Computer Controlled Testing
Wind Tunnel Testing	Transonic Flow	
Variable Camber Wing	Aerodynamics	

20. ABSTRACT (Continue on reverse side if necessary and identify by block number)

Various aspects of the design and stress, flutter, aerodynamic and computer analyses are presented for a 1/6th scale semispan Self-Optimizing Flexible Technology (SOFT) Wing Wind Tunnel Model representative of the AFTI-111 configuration, to be tested at AEDC tunnel 16T. The model features twelve independent hydraulic actuator systems which are designed to conformally vary leading edge radius, leading edge deflection about the 15% and 25% chord lines, upper surface humping, and trailing

DD FORM 1 JAN 73 1473 EDITION OF 1 NOV 65 IS OBSOLETE

Unclassified 406258

SECURITY CLASSIFICATION OF THIS PAGE (When Data Entered)

edge deflection about the 65% and 80% chord lines at an inboard and outboard station. The model is designed to be tested interactively under computer control in such a manner so as to optimize any one of eighteen possible aerodynamic (or structural) functions, while satisfying equality (or inequality) constraints with the remaining seventeen. These functions are to be measured "on line" by either the wind tunnel balance, potentiometers, wing pressure orifices or strain gages.

Simulations of the wing optimization procedure are presented using a highly simplified set of nonlinear algebraic equations to generate the aerodynamic functions. The simulations show that convergence may be obtained for various optimization problems, even when randomly generated testing type errors are included, provided however, that the various parameters in the optimization computer program have been properly tuned for the particular optimization problem.

FOREWORD

This research program was undertaken by the Convair Division of General Dynamics Corporation, San Diego, California, under Office of Naval Research Contract No. N00014-76-C-0742, ONR Tasks NR 212-224 and NR-213-139X. The ONR Scientific Officer was Dr. Robert Whitehead, Vehicle and Propulsion Programs, of the Technology Projects Division (Code 211). The principal investigator was Dr. Ely S. Levinsky. The work was accomplished during the period 15 April 1976 - 14 February 1977.

The present effort has relied heavily upon the support of many individuals, both within and without government service. The authors especially wish to express their appreciation for the cooperation, enthusiasm and technical support provided by members of the staff from Arnold Engineering and Development Center and the Arnold Research Organization Inc. (ARO) Propulsion Wind Tunnel. Their efforts continue to be essential to the success of the program and are being carried out under the direction of Major Kenneth B. Harwood (DYR) and Mr. Richard L. Palko (ARO). Thanks are also due to Mr. Ronald DeCamp, the AFTI-111 Program Manager (USAF FDL, FXS), and to the members of his staff, who provided valuable direction and support to the program and helped resolve various problems dealing with the model and balance. Finally, the authors wish to thank Dr. Robert Whitehead (ONR) who provided the overall leadership and goals for the program and who coordinated the requirements and activities of the various organizations.

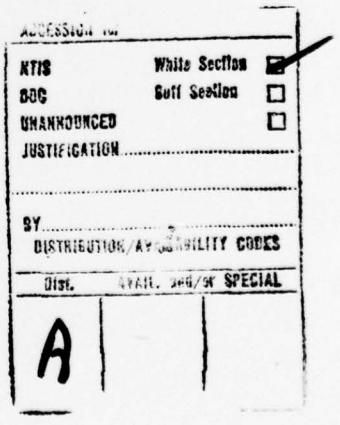

(This page intentionally left blank)

TABLE OF CONTENTS

LIST OF TABLES

TABLE 1 1 OVERALL SCHEDULE SOFT WING PROGRAM, PHASES I AND II REVISED

LIST OF FIGURES

LIST OF FIGURES

NOMENCLATURE

A_{ij}	actuator position (counts)
AR	aspect ratio
a	2D lift curve slope
b	full span of model
b_i	effective semispan of i th wing station
C_D	drag coefficient
C_{D_F}	friction drag coefficient of entire configuration
$C_{D_{IND}}$	induced drag coefficient
ΔC_{D_P}	additional profile drag coefficient
$\Delta C_{D_{RL}}$	additional compressibility drag coefficient
C_L	lift coefficient
C_L'	lift coefficient corrected for tail lift required to trim
C_M	pitching moment coefficient
C_P	pressure coefficient
C_{RB}	root bending moment coefficient ($= M_{RB}/q\,S\,b$)
CSC	creepless supercritical airfoil section
c	local wing chord (measured streamwise with $\Lambda = 16°$, also sound speed
c_i	average chord of i'th actuator
$\bar{c}$	mean aerodynamic chord
e	aerodynamic efficiency factor
F	Lagrangian function being minimized
g	vector of active constraints
H	Hessian matrix
H (x)	unit step function
K_k	step size factor used during simultaneous mode
ΔK_i	partial span lift factors
ℓ_t	tail arm
M	free stream Mach number (unless subscripted otherwise), also moment

MS	model scale
P_{L_i}	compressibility drag correction factor
q	free stream dynamic pressure (unless subscripted otherwise)
R	restoration criterion function
R_{i1}	leading edge radius of curvature
Re	Reynolds number based on $\bar{c}$
S	wing reference half area (unless subscripted otherwise); also vector of search directions
S_{ij}, S_α	search direction components for minimizing F
S_r	search direction vector for minimizing R
t	airfoil thickness or maximum thickness
W_{52}	TACT wing 52
x, z	axial and vertical positions
x_{GLOVE}	axial position of centroid of lift of fuselage and glove
α	angle of attack (degs)
α_t	tail incidence angle (degs)
γ	ratio of specific heats ($\gamma = 1.4$)
Δ	incremental value
δ_{ij}	actuator deflection angles (degs)
ϵ_t	tail downwash angle (degs)
η_{ij}	actuator aerodynamic effectiveness factors
θ_{ij}, θ_α	nondimensional transformed coordinates used in optimization program
θ_j	nondimensional actuator chords
Λ	sweep angle (degs)
λ	vector of Lagrange multipliers used in optimization program
σ	stress level

ϕ	objective (or merit) function being minimized
Ω	potentiometer resistance (ohms)
∇	gradient operator

SUBSCRIPTS

c	value beyond stall at which lift coefficient stops decreasing
i, j	indicies referring to actuator system i = 1 (inboard), 2 (outboard) j = 1 (L.E. radius), 2 (deflection about 15%c), 3 (deflection about 25%c), 4 (upper surface humping), 5 (deflection about 65%c), 6 (deflection about 80%c)
k	test point index during simultaneous mode
L	lower wing surface
MAX	maximum
MC	moment center
MIN	minimum
P	location of wing pivot, also pressure
RB	root bending
r	restoration direction
S.F.	safety factor
STALL	value at stall
TE_i	trailing edge value at station i
TW_i	wing twist at station i
t	tail
U	upper wing surface
$0L_i$	zero lift value for station i
α	$\partial/\partial\alpha$

SUSCRIPTS

δ	$\partial/\partial\delta$
∞	free stream

SUPERSCRIPTS

T	transposed matrix
*	nominal value, also best value

See Table 5.1 for common variables in the optimization computer program.

1.0 INTRODUCTION

The Self Optimizing Flexible Technology (SOFT) Wing program deals with the design, fabrication and testing of a SOFT Wing wind tunnel model and associated computer and control systems at AEDC Tunnel 16T. The program is being conducted by General Dynamics Convair Division (GDC) and the Arnold Engineering and Development Center (AEDC)/Aerodynamics Research Organization Inc. (ARO) on a cooperative basis. Funding is being provided by U.S. Navy (Office of Naval Research), and the U.S. Air Force (Flight Dynamics Laboratory and AEDC/ARO).

1.1 PROGRAM STATUS

In order to minimize the overall technical and financial risks and to remain within budgetary limits, the program has been incrementally funded and has been divided into two distinct phases:

(I) Model design, stress, flutter and aerodynamic analyses, computer programming and test simulation ~ GDC

(II) Model fabrication, calibration, test planning, test support and balance calibration ~ GDC
and
Control system, instrumentation, installation, computer program interface and testing ~ ARO

Specific tasks were to have been carried out during each phase of the program according to the schedule given in the original technical proposal (Ref. 1). The schedule has been subsequently revised as shown in Table 1.1. The decision to go-ahead with Phase (II) was made at the prefabrication conference, held at WPAFB, Ohio, on 14 October 1976, (Ref. 2). This meeting is labeled as meeting #4 under Task 4.2.8b in Table 1.1.

The status of the various Phase (II) tasks is currently as shown in Table 1.2. All Phase (II) tasks are either fully funded, or in the final stages of negotiation,

except for Tasks 4.2.6d and 4.2.8d dealing with the aerodynamic evaluation of the test data and the preparation and presentation of a final report. It is planned to submit a proposal for these tasks prior to the wind tunnel test, now set for July 14, 1977 as shown in Table 1.1. The pretest conference (meeting #5 under Task 4.2.8b) was held at GDC, San Diego, Calif, over the period 13-16 Dec. 1976 (Ref. 3). Details of the various Phase (II) activities may be obtained from the pretest report already submitted under Task 4.2.6c (Ref. 4).

The present interim technical report deals only with the Phase I effort, which was sponsored by the U.S. Navy (ONR). The report is scheduled under Task 4.1.7 (iii) of Table 1.1. Loads, stress and flutter data and final design drawings are being delivered under separate cover (Refs. 5- 7), in accordance with Task 4.1.7 (ii) of Table 1.1. Tapes and listings of the optimization computer program developed under Task 4.1.5 (i) were submitted previously to ARO during the pretest conference (Ref. 3).

1.2 PROGRAM DESCRIPTION AND BACKGROUND

The General Dynamics Convair SOFT Wing concept is a wing which adapts its shape conformally (continuous chordwise and spanwise variations of camber, thickness and twist) in a manner to maximize or minimize various merit functions (e.g., maximum load factor, minimum drag, maximum lift/drag ratio), while satisfying constraints (e.g., constant lift, trim, the avoidance of excessive buffet or flow separation, the avoidance of excessive structural stresses). The SOFT Wing thereby differs from other variable camber systems in that it not only employs mechanisms to conformally vary the geometry, but also automatically adapts its shape to each flight (or test) condition. Ideally, the wing shapes are optimum (within the limitations of the structural flexibility and articulation) and include all of the various viscous and inviscid flow effects.

Although the eventual application of the concept may be to real time flight conditions, the present program deals with the wind tunnel testing and optimization

of a 1/6'th scale semi-span SOFT Wing model representative of the AFTI-111 configuration. The test has been scheduled in AEDC tunnel 16T during the summer of 1977, and a test period of 128 hours occupancy is planned. Purposes of the investigation are as follows:

(i) to verify the structural integrity, flexibility and controllability of the model under transonic flow conditions,

(ii) to determine the suitability of the closed-loop computer control system,

(iii) to verify the convergence and stability characteristics of the optimization computer algorithms under conditions of transonic flow and with up to thirteen different control variables,

(iv) to arrive at optimum wing shapes for a given test condition, merit function and set of constraints, utilizing the maximum articulation capabilities of the model.

(v) to evaluate possible improvements in performance, maneuverability and load control which might accrue to the AFTI-111 aircraft through the utilization of a mission adaptive wing with either full model articulation or more limited articulation dictated by current AFTI-111 designs.

(vi) to demonstrate and use the General Dynamics Fort Worth (GDFW) stereophotographic system for measuring wing shape under airload conditions in the tunnel.

Recent test results obtained by GDFW in connection with the AFTI-111 variable camber, mission adaptive wing program, involving a wind tunnel model with interchangeable parts, have shown that the optimum leading edge and trailing edge camber and deflection are interdependent and sensitive to flight condition and static margin, (Ref. 8). The AFTI-111 tests seem to show that a large saving in wind tunnel test time might well have been achieved through use of a SOFT Wing type model. This would be especially true as the number of degrees of freedom and extent of articulation increase, and because the precision of control for the SOFT Wing permits essentially a continuous spectrum of settings.

Under a previous contract for the U.S. Navy (ONR), GDC has succeeded in fabricating and testing a two-dimensional flexible airfoil model which could be optimized in the tunnel in a manner similar to that planned for the present SOFT Wing model. The 2D model was tested under both low-speed[8] and transonic [10, 11] conditions, and employed five pair of hydraulic actuators to independently vary leading edge radius, leading edge incidence, lower surface humping, lower surface aft camber and trailing edge deflection. During the transonic tests (M=0.75) a link-up of analog and digital computers was used. The airfoil shape and angle of attack were controlled "on line" to minimize drag, subject to constraints on lift and trailing edge pressure, using the gradient projection optimization algorithm. Satisfactory convergence was found, even with flow separation; however, because of the intermittent blow-down type operation of the transonic test facility, a sequence of individual runs was required to complete a single optimization problem.

The new 3D SOFT Wing model employs twelve independent hydraulic actuator systems of similar design to those for the two-dimension model. The actuators are designed to perform the following variations:

A_{11} (nose radius, inboard station)

A_{12} (nose deflection about 15% chord line, inboard station)

A_{13} (nose deflection about 25% chord line, inboard station)

A_{14} (upper surface humping, inboard station)

A_{15} (trailing edge deflection about 65% chord line, inboard station)

A_{16} (trailing edge deflection about 80% chord line, inboard station)

A_{21} - A_{26} (same as A_{11} - A_{16}, except at outboard stations).

It is planned to employ similar computer controlled testing and optimization techniques with the new model as used for the 2-D investigations. Hence the new actuator systems, position readout instrumentation, control valves and computer link ups

are similar to those for the 2D model, except that the number of control channels has been increased to handle the larger number of independent control variables (13 including angle of attack). Other differences relate to the increased volume and pressure of the hydraulic system, to the incorporation of hydraulic shut-off valves to lock the actuator positions in the event of a failure of some component, and to the increased accuracy in positioning the actuators afforded by the new DAC and ADC components. The design, assembly and demonstration of the new control system (Task 4.2.2 of Table 1.1) is being performed by AEDC/ARO under Phase II, and will not be reviewed further herein, except to note that the 2D model is being used by ARO to check out the new control system prior to completion of the 3D model.

The forthcoming tests will use the computer elements of the AEDC closed-loop control system, which was developed in the Propulsive Wind Tunnel (PWT) Facility, and is described in References 12 and 13. Because of the continuous operation of tunnel 16T, it is planned to exercise continuous computer control of the model during wing optimization. Hence, under ideal circumstances, a single run in the wind tunnel would be sufficient to arrive at an optimum wing shape for a prescribed flight condition (Mach number and Reynolds number) and given merit function and constraints.

Because of the increased number of independent variables, and because of the greatly increased number and variety of the constraints for the 3D wing optimization problem, with respect to that for the 2D model, the optimization program allows the merit function to be optimized to be any one of eighteen functions (or combinations of functions) which are measured by either the wind tunnel balance, the model potentiometers, pressure orifices, or strain gages. Any, or all of the remaining seventeen functions may be specified as equality or inequality constraints. Among the new constraints which have been used in the program are inequality constraints which limit the maximum differential deflection between corresponding inboard and outboard systems (termed differential twist constraints) and inequality constraints on maximum rolling moment coefficient (for load control)

and on maximum wing root bending stress. In addition, equality constraints on pitching moment coefficient may be introduced via table lookup. This permits the optimization problem to account for effects of trim, without exceeding the maximum horizontal tail effectiveness, even through the tail incidence on the model is held fixed during the optimization. The new optimization problem allows up to fourteen independent variables consisting of the twelve actuators A_{ij}, $i = 1, 2; j = 1, 2, \ldots 6$, the tail incidence angle α_t and angle of attack α. Any one or several of the independent variables may be held fixed during an optimization problem, in order to simulate variable camber systems with reduced articulation, such as presently envisioned for the AFTI-111 (Ref. 8).

The new optimization program has been tested extensively for convergence in a series of simulated optimization problems. The aerodynamic characteristics used in the program were obtained from a set of nonlinear algebraic equations, termed "Pseudo Aerodynamic Module" (PAM), which were linked to the optimization program for the simulations. PAM provides aerodynamic coefficients as functions of the 14 independent variables, Mach number and Reynolds number. Emphasis in the PAM was placed on speed of computation and on a realistic representation of the nonlinearities expected in the test data, rather than on accuracy, in order to hold computational time in the simulations to an absolute minimum. Testing type errors and inaccuracies were added to PAM to further improve the realism of the simulations.

A summary of the design, including the support system, fuselage, leading edge and trailing edge actuation systems and instrumentation has been included in the next section. A brief summary of the stress, loads, and flutter considerations is given in Section 3, whereas the evaluation of a plastic, kinematic model of the SOFT Wing is found in Section 4. The mathematical basis for the optimization program, the defining equations in PAM, and results of test simulation computations carried out on the DEC 10 computer are presented in Section 5. Various aerodynamic computations already carried out and planned in the future for comparing the aerodynamic characteristics of various desired (target, AFTI-111 and TACT I airfoils

with the closest approximating (actual) SOFT Wing airfoils are found in Section 6.

TABLE 1 1 OVERALL SCHEDULE SOFT WING PROGRAM, PHASES I AND II REVISED DEC 31, 1976, FOR TACT TEST AT AMES, JULY 15 AEDC TEST DATE

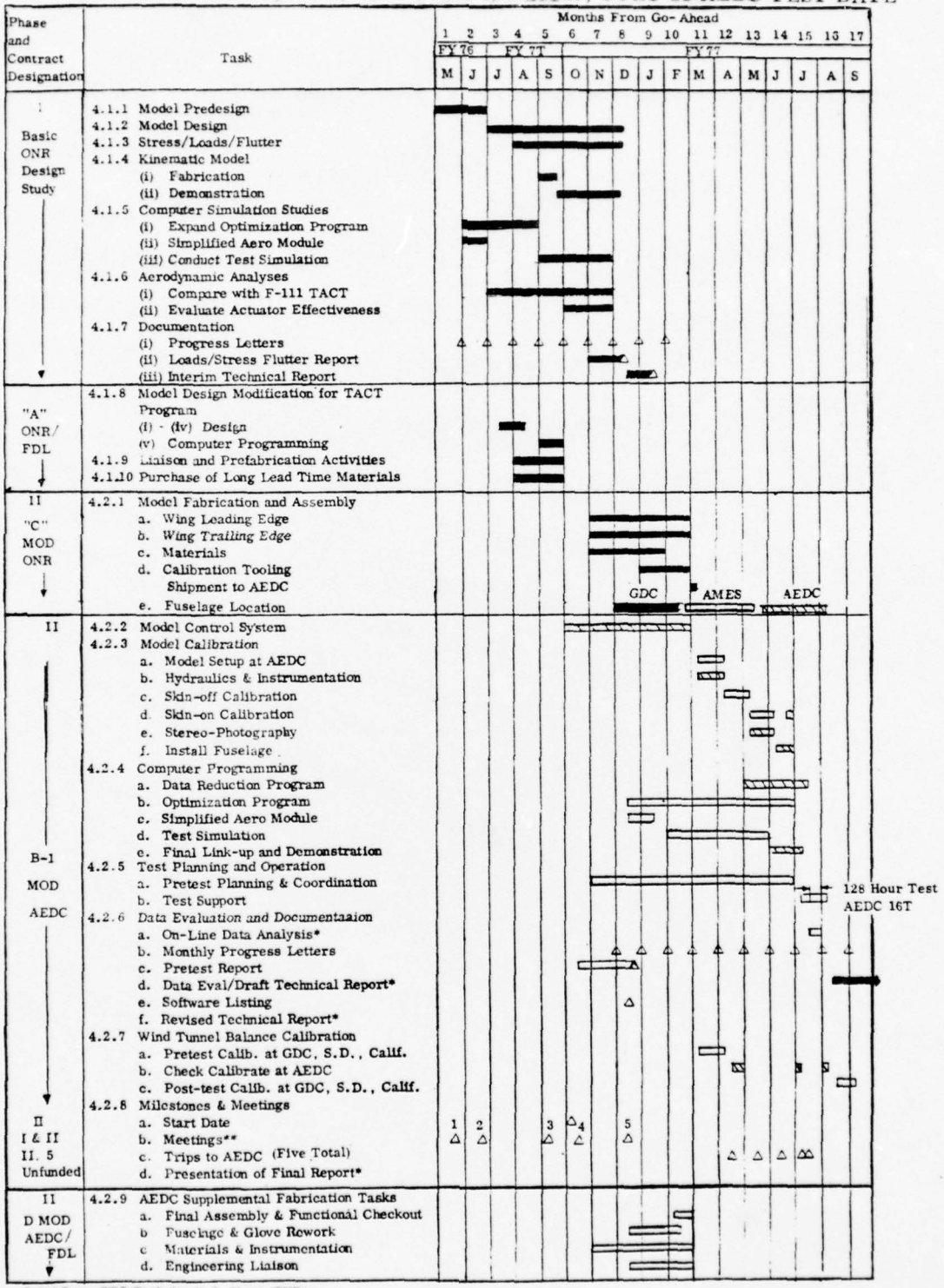

Solid Bar. GDC Task for U.S. Navy (ONR)
Open Bar. GDC Assist Task for AEDC (ARO Inc.)
Cross Hatched Bar Task to be performed solely by AEDC (ARO Inc.)

* Aspects dealing with post-test data evaluation and final report are presently unfunded.

** Meetings #1 - #5 are described in Section 2.0 under Task 4.2.8.b

TABLE 1.2 PHASE II TASKS STATUS SUMMARY

WIND TUNNEL TEST SET FOR 14 JULY - 31 JULY 1977				
TASK	RESPONSIBILITY	FUNDING TO GDC FROM	START DATE	SCHEDULED DELIVERY DATE
4.2.1 MODEL FABRICATION AND ASSEMBLY	GDC (SUBCONTRACTED)	USN (ONR) + USAF (FDL)	1 NOV '76	28 FEB '77
4.2.2 MODEL CONTROL SYSTEM	AEDC/ARO	-	1 OCT '76	28 FEB '77
4.2.3 MODEL CALIBRATION (EXCEPT 4.2.3 e)	AEDC (GDC ASSIST)	ARO	1 MAR '77	31 MAY '77
4.2.4 COMPUTER PROGRAMMING	(AEDC (GDC ASSIST)	ARO	13 DEC '76	30 JUNE '77
4.2.5 TEST PLANNING AND OPERATION	AEDC (GDC ASSIST	ARO	1 NOV '76	7 AUG '77
4.2.6 DATA EVALUATION AND DOCUMENTATION	AEDC AND GDC	ARO & USN (ONR)	1 NOV '76	7 AUG '77
4.2.7 BALANCE CALIBRATIONS	GDC	ARO	7 MAR '77	6 SEPT '77
4.2.9 SUPPLEMENTAL FABRICATION	GDC	ARO	1 NOV '76	28 FEB '77
4.2.3e STEREOPHOTOGRAPHY	GDFW	ARO	8 MAY '77	7 AUG '77

2.0 SUMMARY OF MODEL DESIGN

The wind tunnel model is a 1/6'th scale semi-span version of the F-111 TACT configuration with a SOFT Wing capability employing twelve remotely controllable hydraulic actuator systems, separable front and rear spars, and three flexible steel skin panels with sliding joints. The spar box and skin sections have been formed to correspond to the TACT W_{52} supercritical airfoil shapes (unloaded) at two control stations (0.348 b/2 and 0.913 b/2) for a given set of actuator positions, to be determined as part of the calibration. The wing and fuselage are designed for testing at sweep angles of 26° and 58°, with or without a horizontal tail at several fixed incidence angles. Additional sweep angles, viz., 16°, 45° and 65° may be set by making minor modifications to the fuselage glove section. However, trailing edge clearance problems will limit the maximum trailing edge deflection of the inboard actuators at sweep angles at or beyond 45°.

2.1 SUPPORT SYSTEM

The 3-D SOFT Wing model will be mounted horizontally from the east sidewall and will be installed as depicted in Figure 2.1. The model will be supported by the NASA Ames C-120-16.36 wind tunnel balance, to be procured by the Air Force FDL and modified and calibrated by GDC during the Phase II effort. The fuselage (shown in Figure 2.1) is metric and is mounted off a nonmetric image plate, which rotates with the fuselage. The gap, of approximately 1/4 inch, between the fuselage and the image plate shall be sealed with a fixed flexible seal designed to minimize any transmission of loads. The image plate is mounted off of a reflection plane which extends out approximately thirty inches from the sidewall. The gap between the rotatable image plate and the reflection plane shall be sealed with a sliding type seal designed to minimize any flow leakage. The reflection plane has been test calibrated by AEDC with a movable nose flap, and acts as a boundary layer diverter which is designed to channel the low energy boundary layer air between the reflection plane and the tunnel sidewall while causing only a minimal distortion to the flow pattern over the fuselage.

2.2 FUSELAGE

The fuselage assembly, shown in GDC drawing WT71-107010 #1, is the basic F-111 TACT 1/6'th scale fuselage and must be modified for the forthcoming test as depicted in GDC wind tunnel model drawing WT 76-1111-08. Revisions to the fuselage include

(i) provisions for internally mounting twelve hydraulic Moog valves,

(ii) provisions for internally mounting four individual and one (or more) manifolded blocking valves,

(iii) a modified trailing edge glove fairing which permits approximately 5° trailing edge deflection without fouling at the 58° sweep condition,

(iv) an extended leading edge fairing for testing with 58° wing sweep, provided the existing fairing is unavailable or unsuitable.

The model shall be tested tail on and with tail incidence angles chosen so as not to exceed balance pitching moment restrictions. Tail settings shall be made with existing tail brackets which give incidence angles of 0, -4, -10, and -25 degrees.

2.3 WING LEADING EDGE SECTION

The wing leading edge design consists of a front spar and six independently controlled double barreled hydraulic actuator systems as described in GDC drawing WT 76-111102, sheets 1 - 8. The actuator designations in the leading edge section are A_{11}, A_{12}, A_{13} (inboard) and A_{21}, A_{22} and A_{23} (outboard), which vary respectively nose radius, leading edge deflection about the 15% chord line, and leading edge deflection about the 25% chord line. The volumes, cross-sectional areas and longitudinal displacements of the hydraulic cylinders, and the maximum angular and longitudinal deflections of the wing elements are given in Table 2.1. The hydraulic cylinders for the A_{12}, A_{13} and A_{22}, and A_{23} systems are located inside the front spar section between 0.25c and 0.40c, whereas the cylinders for the A_{11} and A_{21} systems are located inside the nose section (forward of 0.15c).

Potentiometers for measuring and setting actuator position for the leading edge system are to be mounted as shown in Figures 2.2 - 2.4. Backup (spare) potentiometers are provided for each of the leading edge systems. For the A_{13} and A_{23} systems,

the potentiometers are linked between the piston and the front spar and measure piston displacement directly. For the A_{12} and A_{22} systems, the potentiometers are linked across the hinge line at the 15% chord to measure the rotation about this position. For the A_{11} and A_{21} actuators, the potentiometers are mounted between the actuator cylinder wall and the piston, and are designed to directly measure the nose extension, provided the nose skin always remains in contact with the push rod which is attached to the pistons. Experience with the kinematic model has shown that this may not be the case when the leading edge is deflected about the 15% chord hinge line, because of the sliding skin joint on the upper surface (see Section 4). Thus, deflecting down the leading edge could unport the nose skin from the push rod, due to the lengthening of the skin. This behavior, if uncorrected, would result in large nonlinear interactions between the A_{11} and A_{12} and between A_{21} and A_{22} actuators, including considerable backlash, and could complicate the optimization procedure for nose radius by requiring corrections to the calibrations of the A_{11} and A_{12} actuators as shown in Ref. 4, (Eqs. 3.1 and 3.2).

The leading edge skin is designed with a sliding joint (rearward facing lap) on the upper surface. The lap moves forward with increased deflection of the A_{12} and A_{13}, and A_{22} and A_{23} actuators. Care must be exercised when mounting the leading edge skin so that the lap does not import from the underlying surface so as to form a gap which could affect the data.

2.4 WING TRAILING EDGE SECTION

The wing trailing edge design consists of the main spar with four double barreled and two single barreled hydraulic actuator systems, as described in GDC drawings WT 76-111103, sheets 1 - 4. The actuator designations are A_{14}, A_{15} and A_{16} (inboard), and A_{24}, A_{25} and A_{26} (outboard), which vary respectively upper surface humping, trailing edge deflection about the 65% chord line, and trailing edge deflection about the 80% chord line. The volumes, cross-sectional areas, longitudinal displacements of the hydraulic cylinders, and the maximum angular and longitudinal deflections

of the wing elements are listed in Table 2.2.

The hydraulic cylinders for the A_{14} and A_{24} upper surface humping cylinders are circular in section and are designed to vary the spar thickness at the 60% chord position at two spanwise stations (SS 36.972 inches and 54.167 inches, corresponding to 62.3% b/2 and 91.3% b/2, respectively). The wing was designed to simulate the W_{52} spar depth at SS 36.972 with the A_{14} actuator nearly retracted, and the W_{52} spar depth at 54.167 inches with the actuator A_{24} extended. The upper rear wing panel has been stiffened with a spanwise stringer along the 60% chord line to extend the humping over a wider region of the span. Additional descriptions of the various airfoils to be approximated are given in Section 6.

The trailing skins are fabricated in two panels with sliding joints at the trailing edge, as shown in Figure 2.5. The trailing edge thickness has been increased by only 0.25%c from that of TACT wing W_{52} to 1.00%c, necessitating the use of fasteners which protrude outside the skin surface in the trailing edge region (Figure 2.5).

Potentiometers for measuring and setting actuator position for the trailing edge systems are shown in Figure 2.6 & 2.7. Backup potentiometers are provided for the A_{15}, A_{16}, A_{25} and A_{26}, actuators, but not for the A_{14} and A_{24} humping systems, because of space limitations. In the event of a potentiometer failure for either of these two systems, the blocking valves should lock the actuator at its last position. The potentiometers for A_{14} and A_{24} read the direct linear displacement of the pistons, and hence the change in spar box depth. The potentiometers for the A_{15} and A_{25} actuators are mounted off of the rear spar, and read the piston motion which is a direct measure of the rotation of the trailing edge about the 65%c hinge line. The potentiometers for the A_{16} and A_{26} actuators are linked across the hinge line at the 80% position and measure the trailing edge rotation about this hinge line.

TABLE 2.1 LEADING EDGE SYSTEMS

Actuator Symbol	Actuator Function	Maximum Deflection or Displacement Desired	No. of Cylinders	Area of each Cylinder (in^2)	Maximum Cylinder Stroke (in.)	Maximum Volumetric Displacement Per Cylinder (in^3)	Potentiometer Type and (Number)
A_{11}	Nose Radius (inb'd)	ΔRad=0.135 in. $\Delta c \simeq 0.04$ in.*	2	2.832 2.374	0.10 0.10	0.283 0.237	#141 (20014100) 3/16" Stroke 10 K Ω/in. Resiston (2)
A_{12}	Deflection about 0.15 c (inb'd)	-5° → 20°	2	6.316 5.225	0.96 0.75	6.06 3.92	#184, 1" Stroke 1 K Ω/in. Resiston (2)
A_{13}	Deflection about 0.25 c (inb'd)	-5° → 20°	2	6.316 5.225	0.45 0.40	2.842 2.090	#141 (20014100) (2) 7/16" Stroke 10 K Ω/in. Resiston
A_{21}	Nose Radius (outb'd)	ΔRad=0.023 in. $\Delta c \simeq 0.01$ in.*	2	1.912 0.994	0.10 0.10	0.191 0.994	Same as A_{11} (2)
A_{22}	Deflection about 0.15 c (outb'd)	-5° → 20°	2	3.244 1.275	0.62 0.41	2.011 0.523	Same as A_{12} (2)
A_{23}	Deflection about 0.15 c (outb'd)	-5° → 20°	2	3.244 1.275	0.18 0.19	0.584 0.242	#141 (200 14100) 1/4" Stroke (2) 10 K Ω/in. Resiston

* Δc Based on a quartic nose shape

TABLE 2.2 TRAILING EDGE SYSTEMS

Actuator Symbol	Actuator Function	Maximum Deflection or Displacement Desired	No. of Cylinders	Area of each Cylinder (in^2)	Maximum Cylinder Stroke (in.)	Maximum Volumetric Displacement Per Cylinder (in^3)	Potentiometer Type and (Number)
A_{14}	Upper Surface Humping (inb'd)	0.35% t/c (0.077 in.)	1	0.196	0.10	0.02	#055 F 1/2 Dia. 320° Electr. Angle 1K Ω Cond. Plastic (1)
A_{15}	Deflection about 0.65c	-10°→20°		5.220 3.550	0.410 0.640	2.14 2.27	Same as A_{12} (2)
A_{16}	Deflection about 0.80c (inb'd)	-10°→20°	2	5.220 3.550	0.375 0.610	1.96 2.17	Same as A_{13} (2)
A_{24}	Upper Surface Humping (outb'd)	0.7% t/c (0.11 inches)	1	0.196	0.075	0.015	Same as A_{14} (1)
A_{25}	Deflection about 0.65c (outb'd)	-10°→20°	2	2.630 1.150	0.325 0.400	0.855 0.460	Same as A_{13} (2)
A_{26}	Deflection about 0.80c (outb'd)	-10°→20°	2	2.630 1.150	0.325 0.190	0.855 0.218	Same as A_{13} (2)

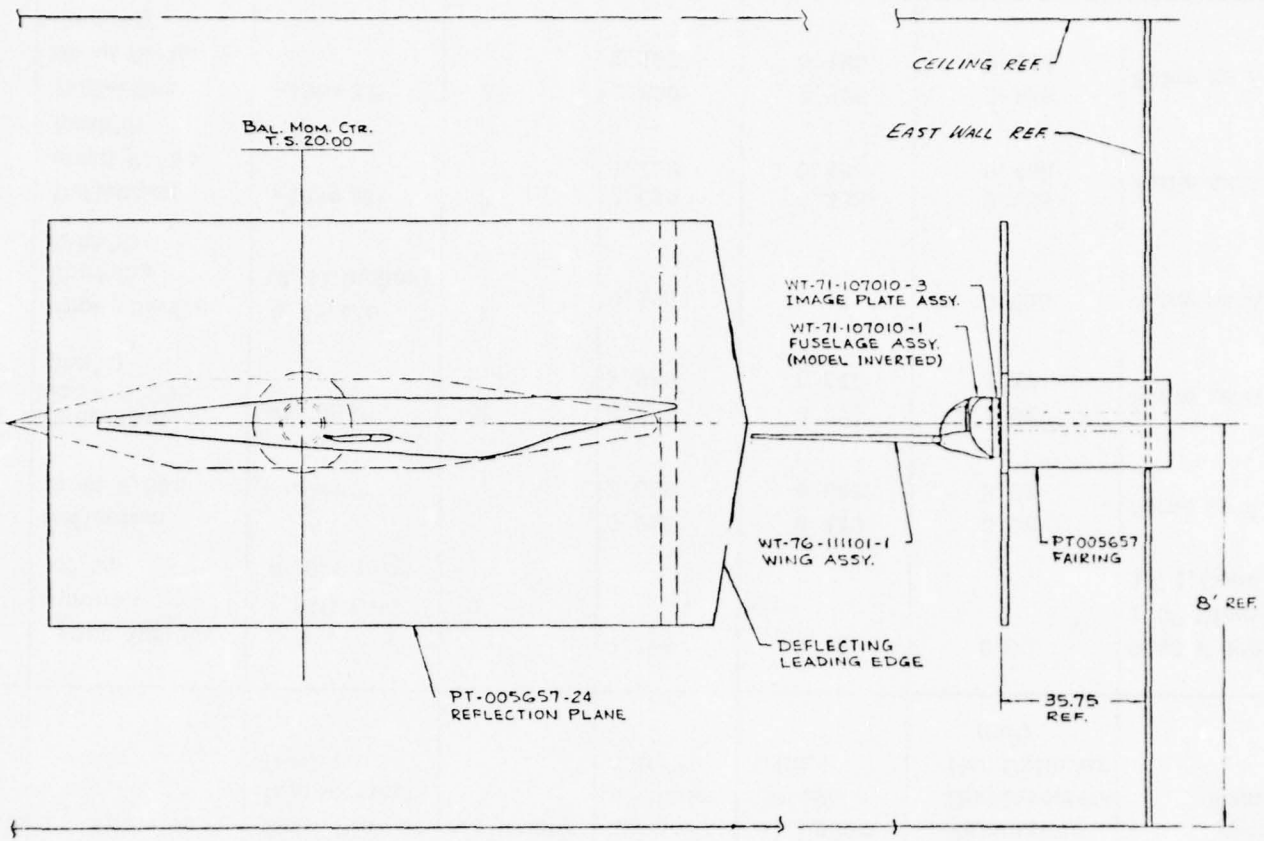

Figure 2.1 Model Installation in Tunnel 16T

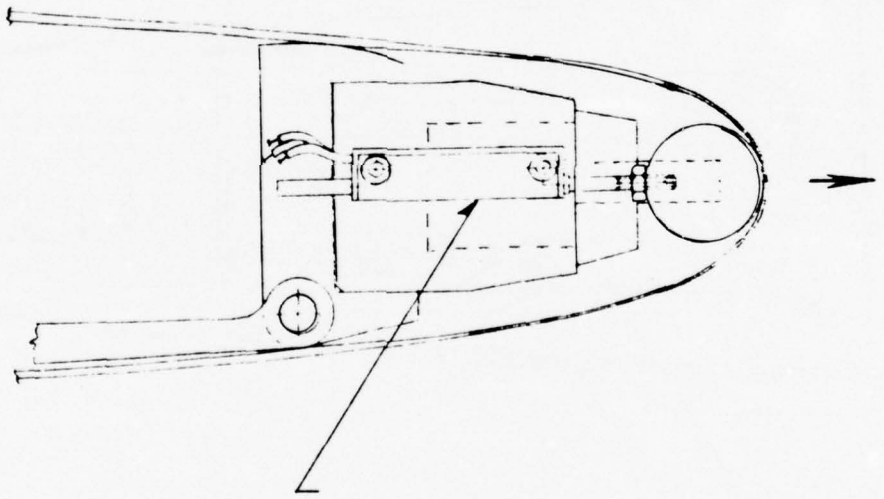

Figure 2.2 Potentiometer Link for L.E. Sharpness Actuators

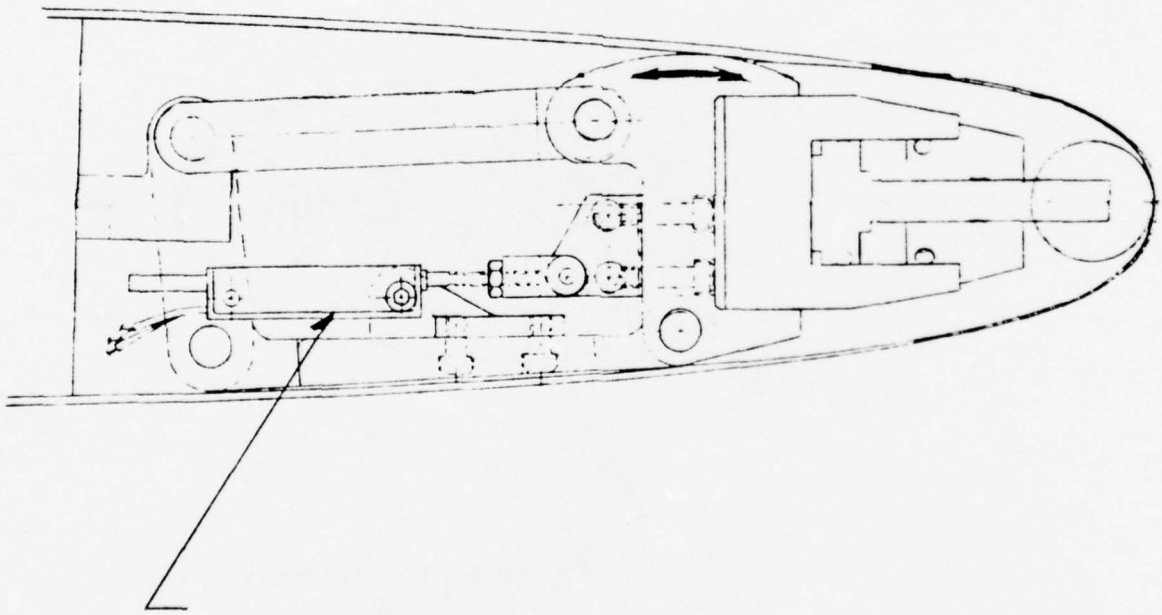

Figure 2.3 Potentiometer Link for 15% Chord L.E. Deflection Actuators

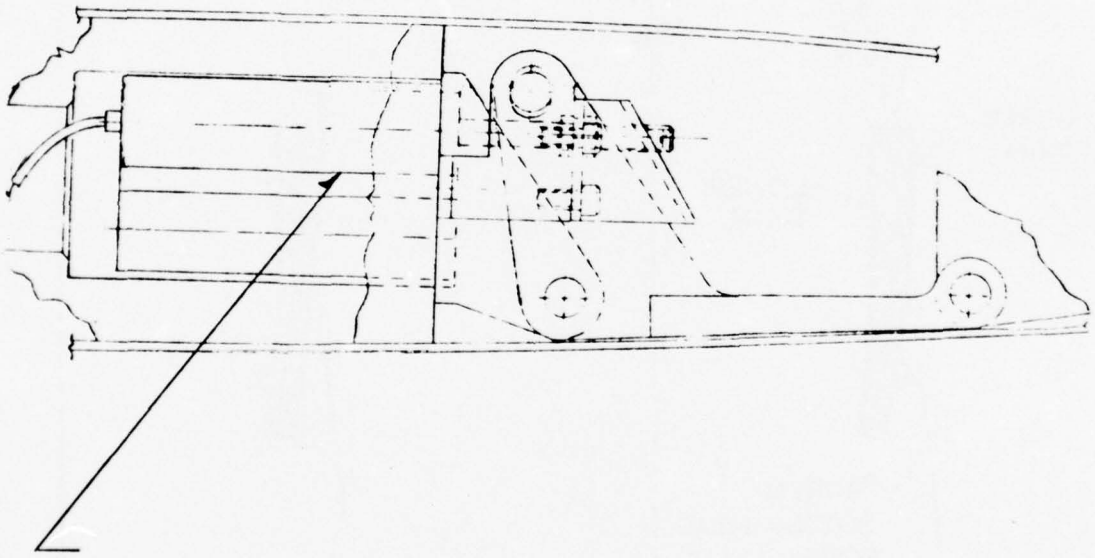

A_{13} and A_{23} Potentiometers

Figure 2.4 Potentiometer Link for 25% Chord L.E. Deflection Actuators

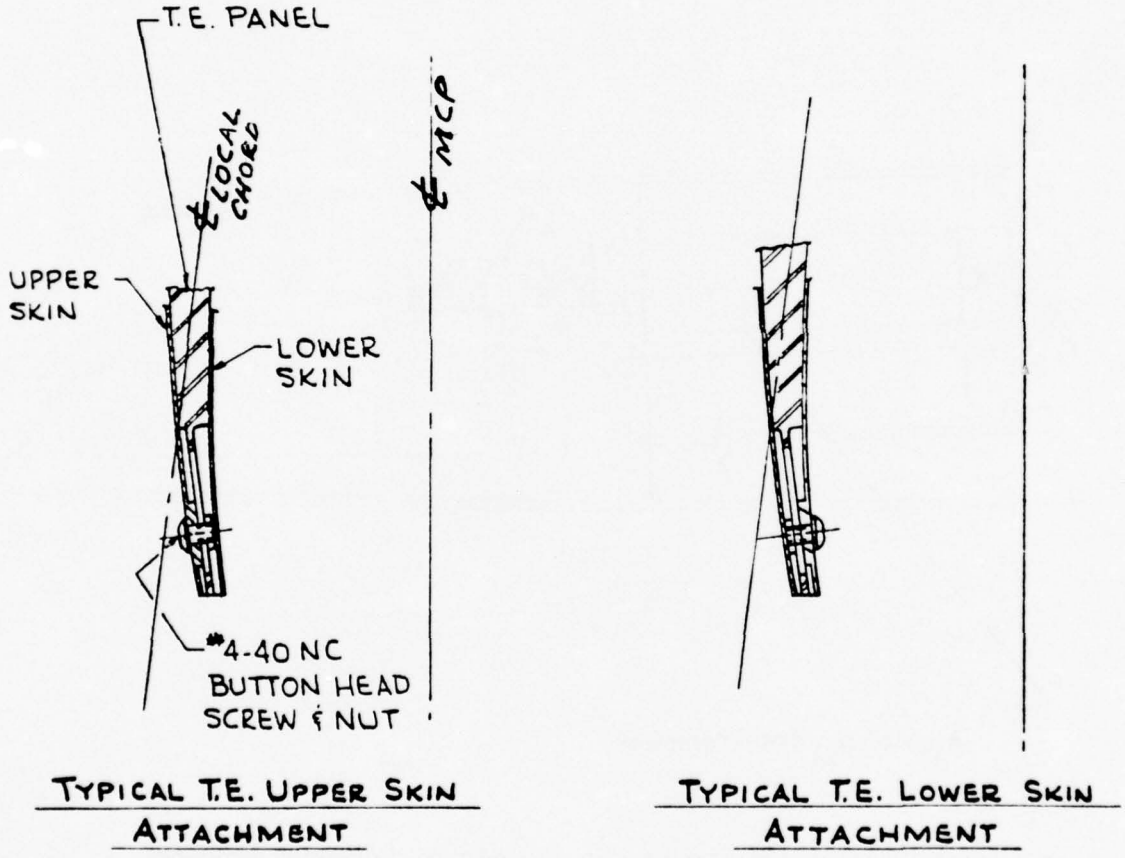

Figure 2.5 Wing T.E. Section Showing Sliding Joints

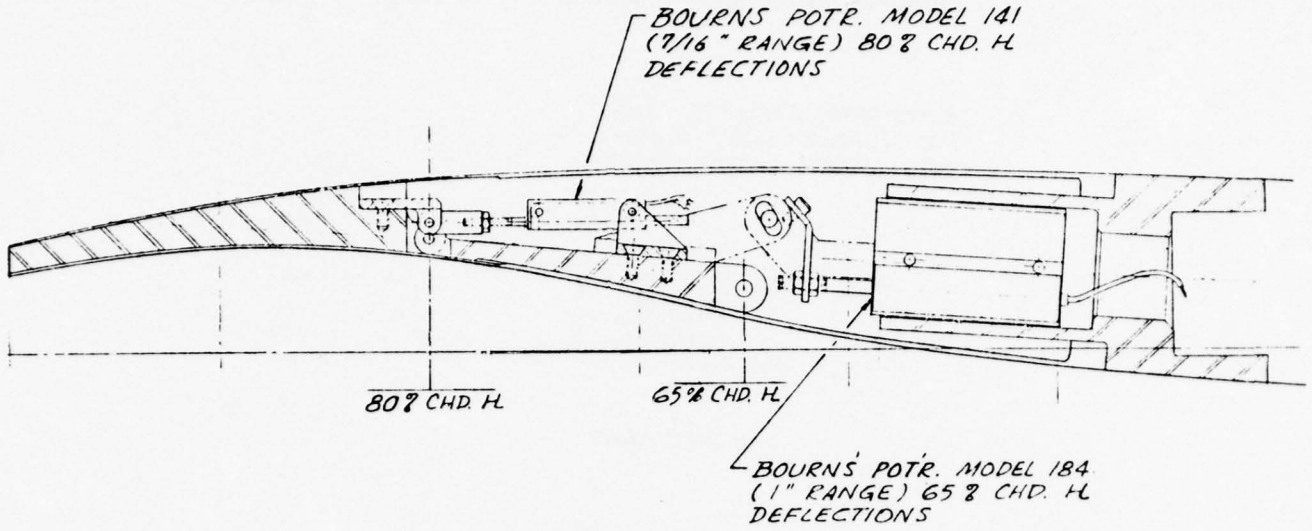

TYPICAL 65% & 80% H POT'R. INSTALLATION

Figure 2.6 Wing T.E. Section showing Potentiometers

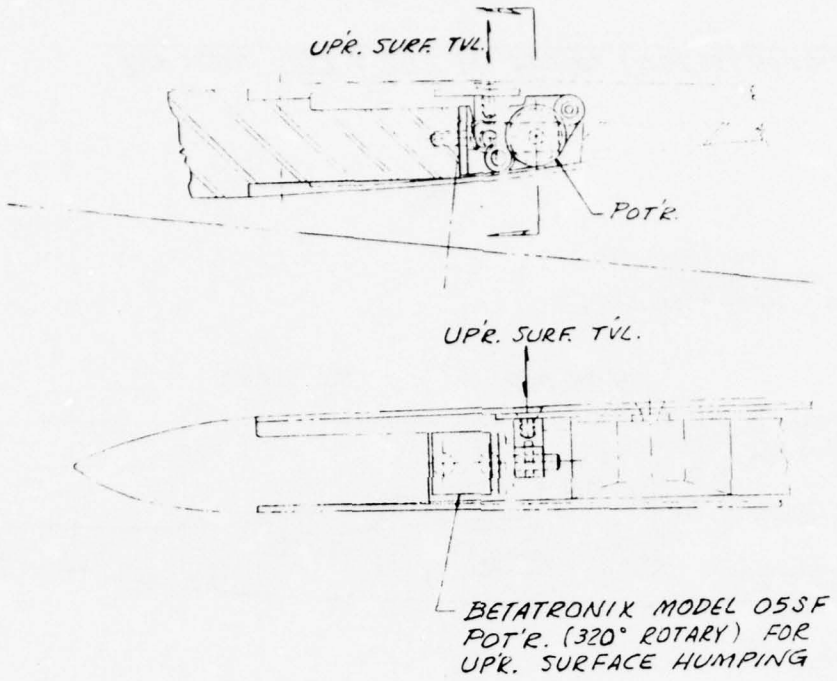

Figure 2.7 Upper Surface Humping Potentiometer Installation

3.0 SUMMARY OF STRESS, LOADS AND FLUTTER ANALYSES

Detailed stress, loads and flutter analyses carried out for the SOFT Wing design are given in References 5 and 6. Some of the basic assumptions and a summary of the results are presented below.

3.1 STRESS AND LOADS ANALYSES

The stress and loads analyses given in Reference 5 are based on a free stream dynamic pressure $q_\infty = 500$ PSF, and on wing pressure distribution data obtained from previous wind tunnel tests with a 1/6'th scale semispan F-111 TACT jet flap model (Reference 14). The loads taken for the stress analyses used the maximum differential pressure coefficient $C_{P_L} - C_{P_U}$ between the lower and upper wing surfaces measured at each tap on the wing. The data were compiled from six different runs covering wing leading edge sweep angles $\Lambda = 26°$ and $45°$, free stream Mach numbers $M_\infty = 0.85$, 0.90 and 0.95. The jet flap blowing coefficient and jet efflux angle were $C_\mu = 0.024$ and $\theta_j = 80°$, respectively. The angle of attack α for the various runs was selected as that which gave the maximum unstalled lift coefficient. Values of C_L ranged from 0.65 to 1.48. The resulting maximum values of $C_{P_L} - C_{P_U}$ are plotted in Figure 3.1, and were used to establish the wing pressure distributions, forces and moments for the stress analyses.

The design criteria called for a factor of safety S.F. = 4 based on ultimate, and S.F. = 3 based on yield. As seen from the S.F. summaries presented in Table 3.1 for the various model details, these criteria were met for the split spar design. The minimum S.F. for the spar is 5.71 (ultimate) and occurs 4 inches outboard of wing semispan station SS 14.7. On the other hand the summaries show that various actuator lever arms and brackets approach the S.F. = 4 limit very closely, with S.F. values ranging from 3.9 to 4.6 in ultimate being common. The page designations for the item or part listed in Table 3.1 are for Reference 5.

Because of added flexibility requirements, the skin panels were designed solely on the basis of yield, with a S.F. = 2 being considered acceptable. The S.F.'s given in Table 3.1 for the lower and upper skin panels, 1.9 and 2.0, respectively, should be considered approximate and are based on zero differential twist between inboard and outboard panels. Similar values have been predicted for the leading edge skin panels, but in this case the computations are even more unreliable, because of the combined effects of nose sharpness changes, leading edge deflection, and airload on the skin deformation, even without differential twist.

Because of the uncertainty of the stress levels in the leading edge and trailing edge skin panels, it is planned to implant approximately 50 strain gages in high stress locations on the outer surface of the skins during the pretest calibrations. These stress levels will be monitored during the calibrations of the actuators, and used to establish limits for actuator deflection (and differential twist) as described in Reference 4. Since the gages must be removed for the wind tunnel test, some uncertainty in maximum skin stress levels under airload conditions will remain. The test operation, as discussed in Reference 4, calls for making preliminary runs at gradually increasing values of q_∞, for reasons of verifying aerodynamic damping. It is planned to examine the skin panels after each run at increased q_∞, in order to look for evidence of yield.

3.2 FLUTTER ANALYSES

The flutter analysis of the SOFT Wing model, details of which are presented in Reference 6, was based on a highly simplified structural representation consisting of seven spanwise segments. The mass, geometry, torsional and bending stiffnesses for this representation, as well as coupled bending and torsional modal and frequency data are presented in Reference 6.

The aerodynamic damping computations were performed only for the $\Lambda = 26°$ sweep condition (judged most critical). The computer program was based on

Theodorsen's incompressible unsteady aerodynamic strip theory model and used a lift curve slope value $a = 2\pi$. The flutter equations were solved for flutter frequency and damping coefficient as a function of air density at a fixed sound speed c = 1160 ft/sec. The resulting incompressible flutter boundaries (zero damping coefficient) are plotted in Figure 3.2 versus q_∞. Also shown in Figure 3.2 are the compressible flutter boundaries (obtained with the Prandtl-Glauert factor) and the envelope of proposed test conditions.

Even though the test envelope is well within the compressible flutter boundary, various assumptions and uncertainties in the analysis dictate that the initial wind tunnel runs be made at q_∞ = 300 PSF, with q_∞ increasing in steps of 50 PSF to the design value of q_∞ = 500 PSF. It is planned to evaluate the level of aerodynamic damping coefficient at each value of q_∞ by taking dynamic data traces of the response of the model (wing tip acceleration) to step changes in actuator position, as discussed in Reference 4. It is also planned to verify the bending and torsional stiffness values used in the flutter computations by making static deflection measurements during model calibration (see Section 5.2.1 of Reference 4).

Computations were also made of the minimum skin thickness required to avoid panel flutter by the semi-empirical method given in Reference 15. The computations were made for the upper surface, rear panel, which was judged to be most critical, and showed that support was required at the 80% chord location. Because of the approximate nature of the panel flutter computations, the testing will be carried out with two strain gages on the upper skin panel from which RMS readings will be obtained on line during the test.

TABLE 3.1 SOFT WING SAFETY FACTOR SUMMARY FROM REF. 5

WIND TUNNEL FACILITY AEDC 16T TEST CONDITIONS q = 500 PSF

PAGE (Refs)	ITEM OR PART	MATERIAL	MATERIAL PROPERTIES		COMP. STRESS/LOADS		SAFETY FACTORS	
			ULTIMATE	YIELD	TENSILE	SHEAR	ULTIMATE	YIELD
30-34	WING PANEL SPAR (S.S. 18.76	17-4 PH H900	190 KSI	170 KSI	21.28 KSI	16.54 KSI	5.71	
	WT-76-111103-55 THRU-61 LEVER ARMS TO -65 PANEL	TRAILING EDGE ACTUATING SYSTEM						
39	PIN SHEAR	ALLEN DOWEL	156 KSI	——	——	15.92 KSI	10.1	
40	LEVER ARM SHEAR OUT	17-4 PH H-900	123 KSI	——	——	10.35 KSI	6.7	
41	-65/-63 PINS	ALLEN DOWEL	156 KSI	——	——	35.43 KSI	4.4	
	LUG SHEAR OUT	17-4PH H-900	123 KSI	——	——	12.72 KSI	7.6	
	LUG BENDING	"	195 KSI	170 KSI	49.02 KSI	——	3.9	3.5
42	-49 THRU -53 LEVER ARMS TO -69 PANEL PIN SHEAR	ALLEN DOWEL	156 KSI	——	——	29.69 KSI	5.3	
	LEVER ARM SHEAR OUT	17-4PH H900	123 KSI	——	——	29.15 KSI	4.2	
43	LEVER ARM TENSION	"	190 KSI	170 KSI	18.21 KSI	——	10.4	
43-44	BENDING OF -65, -69 & -25	17-4PH H900	"	"	——	——	NOT CRITICAL	
	-55 THRU -61 TO -25 PISTON PIN SHEAR & SHEAR OUT	SAME AS SHOWN ON PG'S			39 & 40			

TABLE 3.1 (Continued)

WIND TUNNEL FACILITY AEDC 16T TEST CONDITIONS q - 500 PSF

PAGE (Ref 5)	ITEM OR PART	MATERIAL	MATERIAL PROPERTIES		COMP. STRESS/LOADS		SAFETY FACTORS	
			ULTIMATE	YIELD	TENSILE	SHEAR	ULTIMATE	YIELD
46	BENDING -19	17-4PH H900	190 KSI	170 KSI	18.9 KSI	—	8.6	
	-9/LEVER ARM SHEAR OUT	"	123 KSI	—	—	27.36 KSI	4.5	
47	BENDING -9	"	190 KSI	170 KSI	26.7 KSI	—	7.1	
	-25/-71,-73,-75,-77 BRKT PINS	ALLEN DOWEL	156 KSI	—	—	22.06 KSI	7.1	
49	BKT. SHEAR OUT	17-4PH H900	123 KSI	—	—	16.11 KSI	7.6	
	BKT FLANGE SHEAR	"	"	—	—	28.04 KSI	4.9	
50	BKT ATTACH. SCREWS	#8-32 SCREWS	1985 lb	—	336 lb	307 lb	5.1	
51	-19 PISTON/-71,-81 BRACKETS BRKT SHEAR OUT	17-4PH H900	123 KSI	—	—	24.76 KSI	5.0	
52	BRKT FLANGE SHEAR	"	"	—	—	11.12 KSI	11.1	
	ATTACH. SCREWS	#8-32 SCREWS	1985 lb	—	185 lb	213 lb	10.9	
53	BENDING -19	17-4PH KSI	190 KSI	170 KSI	26.6 KSI	—	7.1	
	-9/-83,-85 BRKTS SHEAR OUT	"	123 KSI	—	—	24.03 KSI	5.1	
54	BRKT FLANGE SHEAR ATTACH. SCREWS & BENDING OF -9 PISTON	LESS THAN	SHOWN	ON PG'S	51, 52 &	53		

TABLE 3.1 (Continued)

WIND TUNNEL FACILITY: AEDC 16T TEST CONDITIONS: q = 500 PSF

PAGE (Ref 5)	ITEM OR PART	MATERIAL	MATERIAL PROPERTIES		CONT. STRESS/LOADS		SAFETY FACTORS	
			ULTIMATE	YIELD	TENSILE	SHEAR	ULTIMATE	YIELD
55	-63 TO -31/-33, -35/31 SUPPORTS PIN SHEAR	ALLEN DOWEL	156 KSI			25.41 KSI	6.1	
	-33 SHEAR OUT	17-4PH H900	123 KSI			24.02 KSI	5.1	
58	-65 TO -21/-23, -13/-15 SUPPORTS PIN SHEAR	ALLEN DOWEL	156 KSI			31.46 KSI	5.0	
	-21 SHEAR OUT	17-4 PH H900	123 KSI			28.25 KSI	4.3	
	-23 BENDING	"	190 KSI	170 KSI	28.75 KSI		6.7	
60	-37 PISTON SUPPORT -33 PINS	4340 HT 260	156 KSI			25.21 KSI	6.2	
	SPAR SHEAR OUT	17-4 PH H960	123 KSI			19.3 KSI	4.6	
61	-35 SUPPORT -31 PINS	4340 HT 260	156 KSI			19.2 KSI	8.1	
	SPAR SHEAR OUT	17-4 PH H960	123 KSI			12.05 KSI	9.7	
62	-25 SUPPORT -31 PINS	4340 HT 260	156 KSI			16.63 KSI	9.4	
	SPAR SHEAR OUT	17-4 PH H900	123 KSI			12.23 KSI	9.6	
63	-15 SUPPORT -47 PINS	4340 HT 260	156 KSI			18.28 KSI	8.5	
	SPAR SHEAR OUT	17-4 PH H900	123 KSI			16.56 KSI	7.4	

TABLE 3.1 (Continued)

WIND TUNNEL FACILITY AEDC 16 T TEST CONDITIONS q = 500 PSF

PAGE	ITEM OR PART	MATERIAL	MATERIAL PROPERTIES		CONT. STRESS/LOADS		SAFETY FACTORS	
			ULTIMATE	YIELD	TENSILE	SHEAR	ULTIMATE	YIELD
69	LEADING EDGE ACTUATING SYS PER WT-76-IN102							
	-75/-31 PIN SHEAR	ALLEN DOWELL	156 KSI	——	——	27.11 KSI	5.5	
	-77 SHEAR OUT	17-4 PH H900	123 KSI	——	——	18.97 KSI	6.5	
	-11 BENDING	17-4 PH H900	170 KSI	170 KSI	29.75 KSI	——	6.4	
71	BENDING -63	"	"	"	13.31 KSI	——	13.7	
73	-13/-33 PIN SHEAR	ALLEN DOWEL	156 KSI	——	——	11.79 KSI	13.0	
	-13 BENDING	17-4 PH H900	190 KSI	170 KSI	26.37 KSI	——	7.2	
	-91/-31 SHEAR PINS	ALLEN DOWEL	156 KSI	——	——	30.47 KSI	5.1	
	93/-97 "	"	"	——	——	26.37 KSI	5.9	
	-75/-77 "	"	"	——	——	20.78 KSI	7.4	
	-93/-73 "	"	"	——	——	22.55 KSI	6.3	
75	WT-76-IN103-97 PIN	17-4 PH H900	123 KSI	——	——	26.55 KSI	4.6	
	" -95 "	"	"	——	——	21.37 KSI	5.7	
	" -95 "	"	"	——	——	20.45 KSI	6.0	
	-27 SHEAR OUT	"	"	——	——	13.11 KSI	9.4	
	-97 "	"	"	——	——	12.34 KSI	10.0	
	-81 "	"	"	——	——	17.57 KSI	7.0	
	-71 "	"	"	——	——	11.93 KSI	10.5	

TABLE 3.1 (Concluded)

WIND TUNNEL FACILITY AEDC 16T TEST CONDITIONS $\bar{q}$ = 500 PSF

PAGE (Refs)	ITEM OR PART	MATERIAL	MATERIAL PROPERTIES		COMP. STRESS/LOADS		SAFETY FACTORS	
			ULTIMATE	YIELD	TENSILE	SHEAR	ULTIMATE	YIELD
77	PISTON RETAINER/ WING SPAR PINS WT-76-111103-13 RH	17-4 PH H900	123 KSI	—	—	10.22 KSI	12.0	
	" -21 "	"	"	—	—	13.53 KSI	9.1	
	" -97 "	"	"	—	—	11.21 KSI	11.0	
79-83	WT-76-111107-9 LOWER SKIN	17-4 PH H900	190 KSI	170 KSI	8737 KSI	—		1.9
84	ATTACH. SCREWS	#6-32 SCREWS	1250 lb	—	139 lb	—	11.6	
84-89	WT-76-111107-7 UPPER SKIN	17-4PH H900	190 KSI	170 KSI	8362 KSI	—		2.0
90	ATTACH SCREWS	#6-32 SCREWS	1250 lb	—	165 lb	—	7.6	
		#2-56 SCREWS	516 lb	—	36.5 lb	—	14.1	

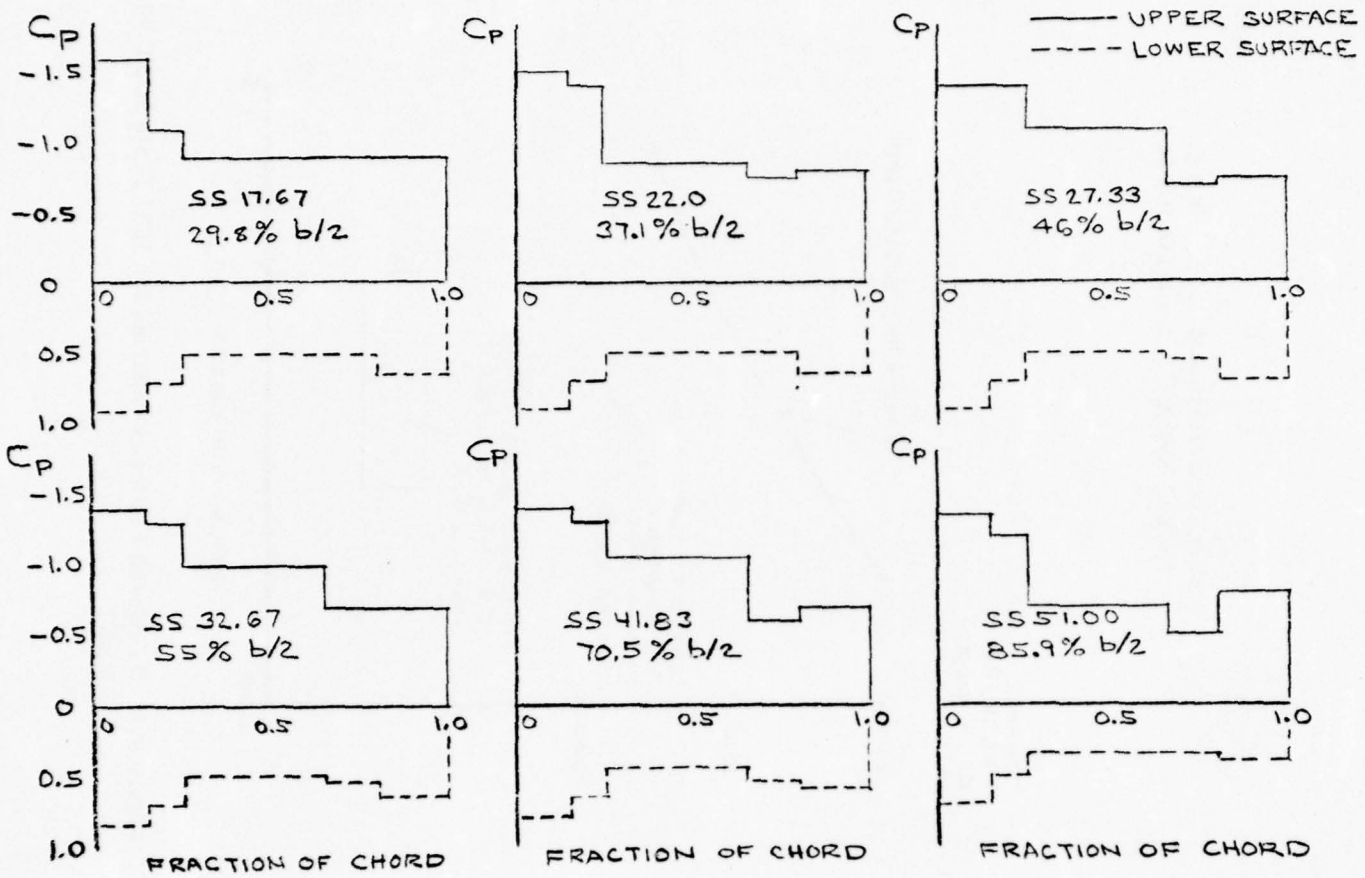

Figure 3.1 Envelopes of Maximum Pressure Coefficients for use in Stress Analyses

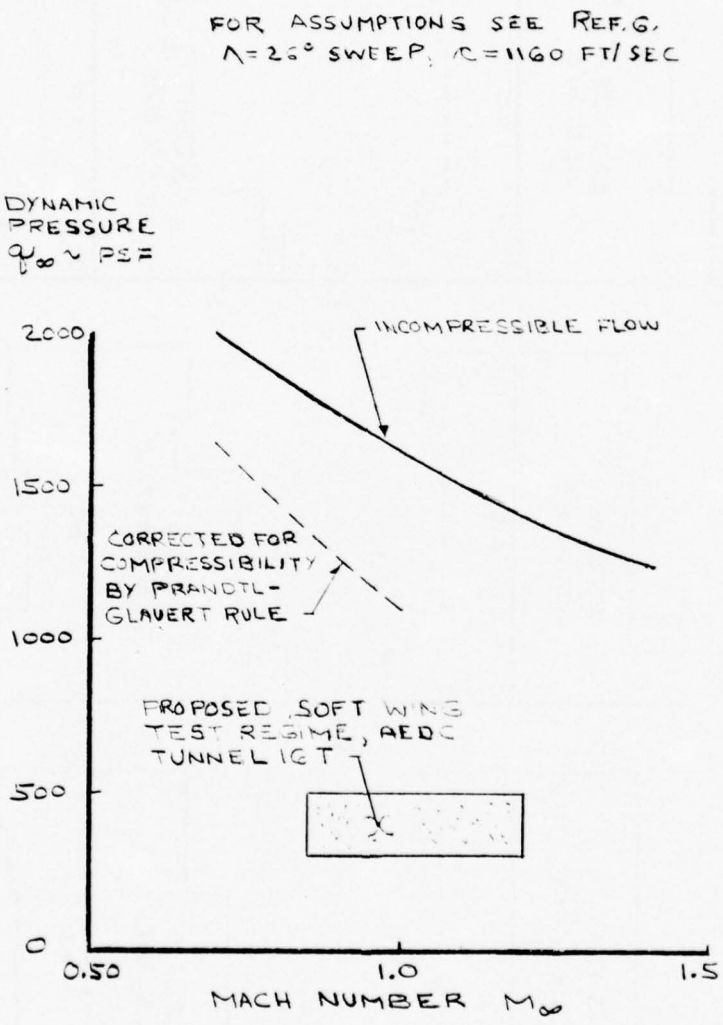

Figure 3.2 Calculated Flutter Boundaries for 16'th Scale SOFT Wing Model

4.0 EVALUATION OF KINEMATIC MODEL

A simplified kinematic model was designed and fabricated to illustrate the operation of the various actuation systems. The kinematic model was built in two separate parts, (i) leading edge, and (ii) trailing edge, as pictured in Figures 4.1 - 4.3. The kinematic models were built to the same scale as the wind tunnel model, but extended only over approximately 60% of the wing semispan, including the semispan stations at 34.8% b/2 and 91.3 % b/2 at which the airfoil sections are to be measured on the wind tunnel model. The kinematic model of the nose section was designed with hand operated actuators for varying leading edge radius (A_{11} and A_{21} actuators), leading edge deflection about the 15% chord line (A_{12} and A_{22} actuators) and leading edge deflection about the 25% chord line (A_{13} and A_{23} actuators). The trailing edge kinematic model was designed with hand operated actuators for deflecting the trailing edge about the 65% chord line (A_{15} and A_{25}) actuators and about the 80% chord position (A_{16} and A_{26} actuators). The upper surface humping mechanisms (A_{14} and A_{24} actuators) were omitted from the design to save on cost, and because their operation should be relatively straight forward and not require a physical demonstration. Separate actuators were designed at the inboard and outboard stations of the kinematic model to permit differential deflection across the span of the kinematic model for each of the five actuator systems. This should illustrate the skin deformation and maximum stress areas due to differential actuator deflection over that portion of the skin simulated by the kinematic model.

The skin panels of the kinematic model were fashioned from plexiglass sheet stock which were laminated together to approximate the thickness distribution of the steel skins on the wind tunnel model. Slip joints were placed on the upper surface of the leading edge section and at the trailing edge. Thus, the skin deflections and stress distributions would be similar to those produced on the wind tunnel model with similar actuator deflections. In principal, at least, the absolute actuator force and stress levels expected on the wind tunnel model may also be estimated from the kinematic model through EI scaling (see References 10 and 16). Lack of time and difficulties

in measuring skin radius of curvature to sufficient accuracy prevented this aspect of the program from being accomplished.

An evaluation of the functionality of the kinematic model has been given in Reference 16. The kinematic model was also transported to Wright Patterson AFB, Ohio, and demonstrated at the SOFT Wing Prefabrication Meeting held there on 14 October 1976. The kinematic model was also displayed and exercised at the SOFT Wing Pretest Conference held at GDC on 13 December 1976. A summary of the evaluations is given below.

4.1 LEADING EDGE UNIT

Operation of the leading edge unit has shown that the inboard and outboard actuators may be deflected through the positions given in Table 4.1 without wrinkling or deforming the nose skin, provided the same angular deflections are maintained inboard and outboard, i.e., zero differential twist or camber. However, considerable crinkling and warping of the nose shape was observed whenever the total inboard deflection angle (as given by $A_{12} + A_{13}$) differed from the total outboard deflection angle (as given by $A_{22} + A_{23}$) by as much as 10°.

TABLE 4.1 LEADING EDGE DEFLECTIONS

INBOARD	
A_{13} (Deg)	A_{12} (Deg)
20	0
20	10
20	20
10	0
10	10
10	20
0	0
0	10
0	20

OUTBOARD	
A_{23} (Deg)	A_{22} (Deg)
20	0
20	10
20	20
10	0
10	10
10	20
0	0
0	10
0	20

A second potential difficulty encountered in the nose region stemmed from the bending of the rod which is pushed into the nose of the airfoil by the A_{11} and A_{21} nose sharpness actuators. Although the rod is much stiffer in the kinematic model (made of aluminum) in relation to the skin than in the wind tunnel model, considerable bending of the rod in the chordwise direction was observed where it is unsupported by the actuators. The nose sharpness push rod in the wind tunnel model will be supported in additional locations and stiffened considerably to prevent chordwise bending from occurring.

A third difficulty, which was observed, dealt with the unporting of the nose sharpness push rod from the nose skin when the A_{12} and A_{22} actuators are displaced to deflect the nose about the 15% chord position while holding the A_{11} and A_{21} nose sharpness actuators fixed. If uncorrected, this would make the variation of nose radius highly nonlinear with regard to the displacement of the A_{11} and A_{21} actuators, lead to a sizable back lash zone over which leading edge radius does not vary with actuator position, and lead to interactions between the A_{11} and A_{21} actuators and the A_{12} and A_{22} systems. Aerodynamic loads on the skin might pull the nose skin up tightly around the push rod under the conditions of high lift and high tunnel dynamic pressure, making the actual variation of nose radius dependent on these tunnel parameters as well as upon the A_{11}, A_{21}, A_{12}, and A_{22} actuators.

One possible method of avoiding the difficulty may be to program the A_{11} and A_{21} actuators to displace linearly with the position of the A_{12} and A_{22} systems. This would require additional programming changes to both the optimization program and to the controller, as shown in Reference 4. However, a final decision in regard to this interaction will not be made until the wind tunnel model has been calibrated and the same effects observed.

4.2 TRAILING EDGE UNIT

Initial operation of the trailing edge unit has shown that the inboard and outboard actuators may be deflected through the positions shown in Table 4.2 without wrinkling either

the upper or lower skin. In contrast to the observations made with regard to the leading edge, no crinkling or undue warpage of the skin was produced even with a 10° difference in deflection angle between the inboard and outboard systems, although a bulge was noted at the trailing edge for this condition. and excessive stress may be introduced in the skin panels across the spanwise gap between the inboard and outboard actuators. It is planned to implant strain gages on the skin of the wind tunnel model in the gap region to check the stress levels produced, and to increase the span of the gap between the actuators, should this prove necessary.

TABLE 4.2 TRAILING EDGE DEFLECTIONS

INBOARD	
A_{15}	A_{16}
20	0
20	10
20	20
10	0
10	10
10	20
0	0
0	10
0	20

OUTBOARD	
A_{25}	A_{26}
20	0
20	10
20	20
10	0
10	10
10	20
0	0
0	10
0	20

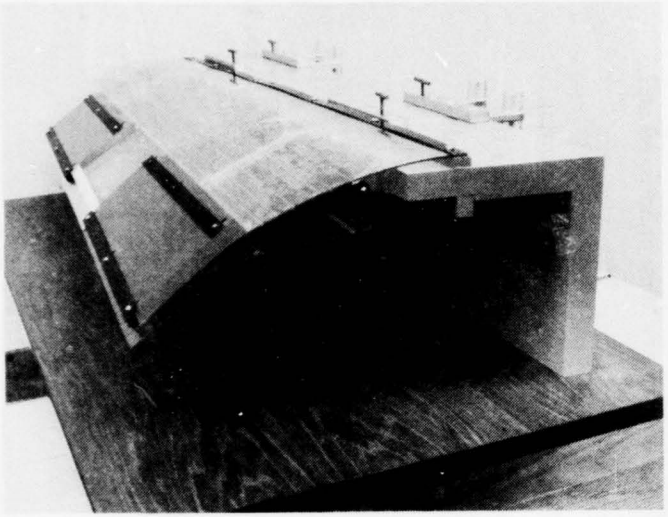

Figure 4.1 Kinematic Model of Trailing Edge

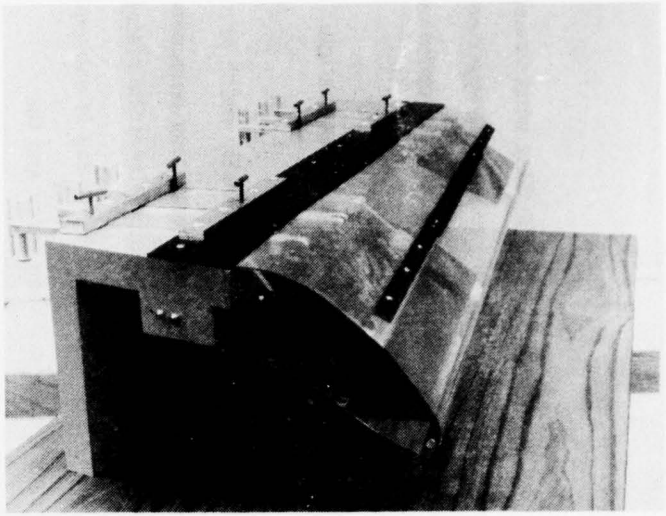

Figure 4.2 Kinematic Model of Leading Edge

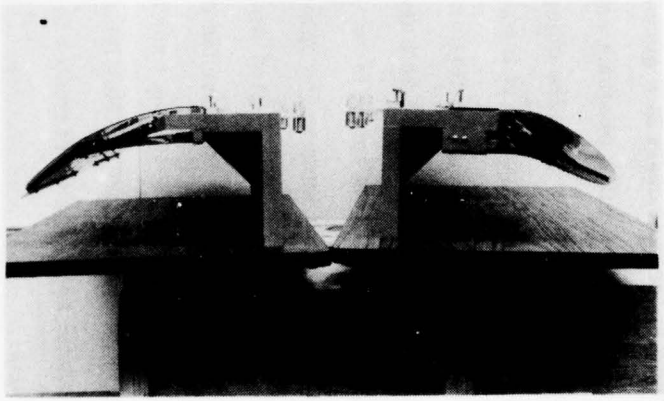

Figure 4.3 Leading Edge and Trailing Edge Kinematic Models

5.0 COMPUTER SIMULATION STUDIES

The optimization computer program plays a central role in the SOFT Wing wind tunnel testing technique being planned at AEDC, in that the optimization program determines how to change the actuator settings and angle of attack in order to achieve the optimum value of a specified aerodynamic function subject to given constraints. The relation of the optimization program to the SOFT Wing wind tunnel testing operation is shown in the flow chart in Figure 5.1.

The optimization program has controlling parameters which specify which aerodynamic parameter is to be the objective function and which of the remaining parameters are to be subject to equality or inequality type constraints. The output from the optimization program is an array of actuator settings and angle of attack. The wing is subsequently positioned according to these settings. Wind tunnel data are then taken and the results reduced to coefficient form, e.g. C_L, C_D, C_M, etc. These reduced wind tunnel data are then input to the optimization program, so that it can evaluate the effect of its previously predicted settings. New settings are then calculated and output in an attempt to optimize the objective function.

The SOFT Wing testing technique is basically a nonlinear programming optimization procedure in which the optimization computer program views the wind tunnel as an analog computer for evaluating the following mathematical functions:

$$\left.\begin{aligned} C_L &= C_L\,(A_{ij}, \alpha) \\ C_D &= C_D\,(A_{ij}, \alpha) \\ C_M &= C_M\,(A_{ij}, \alpha) \\ \sigma_{RB} &= \sigma_{RB}\,(A_{ij}, \alpha) \\ C_{P_{TE_{1,2}}} &= C_{P_{TE_{1,2}}}\,(A_{ij}, \alpha) \\ &\text{etc.,} \end{aligned}\right\} \qquad (5.1)$$

where these and other possible aerodynamic parameters are defined in the Nomenclature Section. Thus the wind tunnel system consisting of the airstream, test section, support system, model, control system, instrumentation and data reduction package, is considered simply as a physical function generator with which the optimization program interacts. The advantages of using the wind tunnel as a function generator rather than making analytical computations of the aerodynamic parameters during the optimization, as done in References 17 - 19, stems from the improved accuracy and speed of the wind tunnel over any known flow field computational procedure. This will be especially true under conditions of viscous, turbulent, transonic flow and for complicated three dimensional geometries representative of aircraft. The disadvantages of using the wind tunnel stem from wall type interactions and scale effects, which may make the results difficult to apply to the flight of full scale aircraft, to the restrictions imposed by limits of model articulation and to instrumentation errors.

Section 5.1 presents the mathematical basis for the optimization computer program to be used during the forthcoming test. Section 5.2 presents a highly simplified set of algebraic equations used to calculate the aerodynamic coefficients during computer simulation studies of the optimization procedure. These algebraic equations, termed "Pseudo Aerodynamic Module," replace the entire wind tunnel system when conducting test simulations with the optimization program. Section 5.3 presents a number of sample results from the simulations illustrating the effects of various parameters in the optimization program on convergence rate. As a result of the simulation studies it was concluded that all optimization problems to be attempted during the wind tunnel test should be first simulated by using the Pseudo Aerodynamic Module, in order to establish the proper values for the various optimization parameters prior to the test.

5.1 OPTIMIZATION PROGRAM

The present section describes the mathematical basis for the optimization computer program, and presents the input parameters which define the wing optimization

problem to be solved and control the rate of convergence. Additional programming details are given in Reference 4.

5.1.1 Mathematical Basis

The optimization program uses the gradient projection method for numerically solving the constrained optimization problems arising from wing optimization. In conjunction with this procedure, transformations of variables are used to enforce independent variable constraints, and restoration steps are required to restore equality constraints that have become unsatisfied due to nonlinearities.

The actuator readings A_{ij}, tail incidence angle α_t and wing angle of attack α, which constitute the independent variables in the physical coordinates, are represented internally in the program as the vector θ, where

$$A_{ij} = (XMAX) \sin^2(\theta_n) \tag{5.2}$$

$$\alpha_t = 2(ATMAX) \sin^2\theta_{13} - ATMAX \tag{5.3}$$

and

$$\alpha = 2(AMAX) \sin^2\theta_{14} - AMAX \tag{5.4}$$

Here the subscripts i, j and n have the correspondance

i	1	1	1	1	1	1	2	2	2	2	2	2
j	1	2	3	4	5	6	1	2	3	4	5	6
n	1	2	3	4	5	6	7	8	9	10	11	12

whereas XMAX, ATMAX and AMAX are parameters which specify the maximum actuator readings, maximum (and minimum) tail incidence angles, and maximum (and minimum) wing angles of attack.

The optimization procedure used by the optimization computer program is based upon the gradients of the objective function and the equality constraint functions. The independent variables are changed so that the objective function decreases in a modified steepest descent direction. The direction is modified by projecting the negative gradient of the objective function onto the tangent planes of the equality constraints. In this way the independent variables are changed so that the design moves along a linear projection of the constraints. If g is a row vector of the equality constraint functions, all of whose components are zero when the equality constraints are satisfied, ϕ is the objective function to be minimized, F is the Lagrangian function, and

$$C = \begin{cases} +1 \text{ if } \phi \text{ is to be minimized} \\ -1 \text{ if } \phi \text{ is to be maximized} \end{cases} \tag{5.5}$$

then the search direction used is

$$S = -(C \nabla \phi + \nabla g \wedge) = -\nabla F \tag{5.6}$$

where
$$\wedge = -C (\nabla g^T \nabla g)^{-1} \nabla g^T \nabla \phi \tag{5.7}$$

and
$$F = C\phi + g\wedge \tag{5.8}$$

The independent variables are changed by adding

$$\Delta\theta = KS \tag{5.9}$$

where K is the step magnitude which is selected to optimize the Lagrangian function (5.8) in the direction S.

Although the gradient projection method gives the search direction S, it does not yield the magnitude of the step size to be taken. This must be found by taking a series of steps K_k in the search direction and then determining which step size minimizes F. Since all independent variables are incremented simultaneously during this process, this operation has been termed the "simultaneous mode" portion of an optimization run. That portion of the optimization procedure during which the

independent variables are perturbed individually and then reset to their basic position, in order to generate the components of the gradient matrices $\wedge\phi$ and ∇g, has been termed the "incremental mode" portion of the optimization run (See also Refs. 4, 9, 10 and 11).

Eleven values of K are used during the simultaneous mode. They are selected as follows:

$K_1 = 0$

K_2 = the smallest value such that one of the components of $\Delta\theta$ is two times the standard deviation of error in that component.

$$K_k = K_{k-1} + (1.4)^{k-2} K_2 \qquad k = 3, 4, \ldots, 11$$

If K^* denotes the particular K_k at which the Lagrangian is minimal then the new independent variables for the next incremental mode are

$$\theta_{new} = \theta_{old} + K^* S_{old} \tag{5.10}$$

and the process is repeated if no restoration is required. The accomplishment of Equation 5.10 during the wind tunnel test requires that all actuators and wing angle of attack (tail incidence angle will be held fixed), be reset with a high degree of precision to avoid compromising convergence.

The process of finding K^* during the simultaneous mode operation is called a one dimensional search. For each new step K_k of the one dimensional search, all constraint functions are checked. If any equality constraint (or activated inequality constraint) drifts too far from being satisfied, then the one dimensional search is aborted. If any inequality constraint becomes violated beyond a prescribed limit during the one dimensional search, the search is also aborted. In the event of an abort, the point which had the lowest value for equation (5.8) but did not cause the abort is taken as the optimal point for the one dimensional search.

The components of the vector DEV (see Section 5.1.2) specify the absolute values of the maximum deviations permitted for all constraints without aborting the

the one dimension search. The components of the vector TOL (Section 5.1.2) specify the tolerance to which the constraints must be satisfied prior to searching in the optimization direction S.

Restoration is the process of finding a point θ at which all equality and activated inequality constraints are satisfied within TOL. As noted above, the one dimensional search can result in a point θ at which one or more constraints have drifted beyond TOL, due to the nonlinear nature of the aerodynamic functions (dependent variables). When this occurs, a restoration run must be carried out. The search direction which will accomplish this (in the linear sense) is

$$S_r = \nabla g \, (\nabla g^T \nabla g)^{-1} g \tag{5.11}$$

As in the optimization case, a one dimension search must be made to determine the K^* such that the restoration criterion function

$$R = gg^T \tag{5.12}$$

is minimized. However, in the case of restoration with linear dependent variables the theoretical stepsize for minimizing R is $K^* = 1$. Therefore the candidate stepsizes are selected as follows for restoration:

k	1	2	3	4	5	6	7	8	9	10	11
K_k	0	.1	.5	.8	.9	.95	**1.0**	1.05	1.1	1.2	2.0

Figure 5.2 summarizes the flow of the mathematical operations just described. Each time a new point θ is determined, all inequality constraints are checked to determine whether they are still satisfied. If some are not, then those that are not are activated, which means they are added to the set of equality constraints which must be kept satistied by the operations described in the preceeding section. Similarly, those equality constraints which are the result of an activated inequality constraint on a previous step must be checked to determine whether they can be removed from the set ot equality constraints. The condition for removal is that the current search

direction must be interior to the region defined by the inequality. Mathematically, this condition for constraint ℓ is,

$$(\nabla F)^T \nabla g_\ell \leq 0. \tag{5.13}$$

If this condition holds the equality constraint g_ℓ is deactivated.

A procedure which is employed to improve the convergence rate of the gradient projection method is the Davidon-Fletcher-Powell (DFP) variable metric method. This procedure differs from the gradient projection method previously described by the inclusion of a scaling matrix H and by formulas for updating H. For this method, equations (5.6) and (5.7) become

$$S = -H(C\nabla\phi + \nabla g \Lambda) \tag{5.14}$$

$$\Lambda = -C(\nabla g^T H \nabla g)^{-1} \nabla g^T H \nabla \phi \tag{5.15}$$

The matrix H is initially the identity matrix in which case equations (5.14) and and (5.15) reduce to equations (5.6) and (5.7). When two consecutive minimization iterations occur (without an intervening restoration) second derivative information can be computed by differencing first derivative values:

$$\Delta(\nabla F) = \nabla F_{new} - \nabla F_{old} \tag{5.16}$$

If

$$\Delta\theta = -K^* H \nabla F \tag{5.17}$$

then the update formula for H is

$$H_{new} = H_{old} + \frac{\Delta\theta\,\Delta\theta^T}{\Delta\theta^T \Delta(\nabla F)} - \frac{H_{old}\,\Delta(\nabla F)\,\Delta(\nabla F)^T H_{old}}{\Delta(\nabla F)^T H_{old}\,\Delta(\nabla F)} \tag{5.18}$$

For nonquadratic functions F, there is no guarantee that H_{new} will be an improvement over H_{old}, consequently H_{new} must be checked for validity. Since H must be positive definite, it must have positive diagonal elements. A check for positive

diagonals is performed, and if any negative values are found the H_{new} is reset to the identity. The other conditions for which H_{new} is reset to the identity are when $K^* = K_1$ in the one dimensional search, and whenever a restoration is performed.

5.1.2 Input Parameters

Prior to attempting a particular wing optimization problem, either in the wind tunnel or in a simulation, the problem to be solved must be specified. This is accomplished by inputing to the program an ordered list of up to 18 aerodynamic functions such as shown in Equation 5.1. These functions are recognized by the program as the array FX(I) of dimension I. To specify which of the 18 functions is to be optimized, the variable IOBJ must be set to an integer value from 1 to 18.

To define equality and inequality constraints the array CAN(I), I = 1, 18 must be set. If CAN (I) = 0, then function I is not used at all. If CAN(I) = 1, then function I is an equality constraint. Finally, if CAN(I) = -1, then function I is an inequality constraint.

The vector of values T(I), I = 1, 18 are the target value for the constraints. For equality constraints, FX(I) =T(I) is the mathematical condition constraining the optimum. For inequality constraints FX(I) ≥ T(I).

The angle of attack α is bounded by the variable AMAX which is nominally set at 20 degrees: $|\alpha| \leq$ AMAX.

The actuator positions are bounded by the variable XMAX which is nominally set at 1000 counts: $0 \leq A_{ij} \leq$ XMAX.

The initial positions of the actuators and the initial angles of the tail and wing are specified by the vector AVE (N), where the correspondance between N and the independent variables is as given in the table subsequent to Equation 5.4.

During the wind tunnel test all independent variables may not be used (active). Thus α_t, corresponding to N = 13, will be fixed on the model during an optimization, since the model does not have a self trimming tail. Also, various actuators will be deactivated to simulate the reduced articulation of the AFTI-111 aircraft

(See Table 6.1 of Reference 4). Finally various actuators may fail during the course of the wind tunnel test (blockage valves in the model should permit testing with the remaining actuators, should either the A_{11}, A_{14}, and A_{21} or A_{24} systems fail). To provide for the deactivation of an independent variable the array DA(N) is used. If DA(N) = 0, then AVE (N) is the frozen value of independent variable number N.

The vector DA(N) is also used to specify the magnitude of the perturbations during the incremental mode operation. If DA(N) $\neq$ 0, then independent variable N is perturbed by DA(N), the direction of the perturbation being away from the closest boundary (see Reference 4).

ZNL (I) is the vector with components equal to the one standard deviation noise levels (testing errors) for the measured values of the independent variables I $\leq$ 14 and the 18 function values for I = 15, 16, ...32. The ZNL vector is utilized in determining the size of the K_2 step during the simultaneous mode portion of an optimization run, as discussed in connection with Equations 5.9 and 5.10. The ZNL vector is also used to introduce effects of testing type errors into the analytical simulations, as will be shown in Section 5.3.

As noted previously in Section 5.1.1 in describing the one dimensional search and restoration procedures, TOL(I) is the tolerance for each of the 18 aerodynamic function values which are equality or activated inequality constraints. The constraint FX(I) is assumed satisfied, or restored, if

$$\left|FX(I) - T(I)\right| \leq TOL(I) \tag{5.19}$$

DEV(I) is the tolerance used during the one dimensional search to determine whether an equality or inequality constraint becomes violated. This is taken larger than TOL(I) to avoid restricting progress of the one dimensional search while at the same time, not allowing the constraints to be violated by too much. If either

$$\left|FX(I) - T(I)\right| > DEV(I) \text{ (for equality constraints} \tag{5.20}$$

or $\quad FX(I) - T(I) + TOL(I) < 0$ (for inequality constraints) (5.21)

then the one dimensional search is aborted.

CMAX specifies the number of times cycled through the incremental mode. In the presence of noise (testing errors), redundant perturbations of the independent variables are taken and the results are averaged together to improve the accuracy of the gradient components.

A summary of all input parameters is included in the dictionary of common variables listed in Table 5.1.

5.1.3 Tabular Input for Simulating a Self-Triming Tail

As noted previously, the optimizations to be carried out with the present model must be made with the horizontal tail held fixed, since a variable tail incidence mechanism was not incorporated in the model. Hence, the constraint on trim

$$C_M = 0$$

can not be implemented directly.

An approximate method of implementing the trim constraint has been presented in Reference 20. The method introduces two inequality constraints to insure that sufficient tail trim control is available for all wing shapes reached during the optimization, viz., that

$$C_M(\alpha, \alpha_t^*, A_{ij}) \leq C_M(\alpha, \alpha_t^*, A_{ij}^*) - C_{M_{MIN}}(\alpha, \alpha_t, A_{ij}^*) \tag{5.22}$$

and $$-C_M(\alpha, \alpha_t^*, A_{ij}) \leq C_{M_{MAX}}(\alpha, \alpha_t, A_{ij}^*) - C_M(\alpha, \alpha_t^*, A_{ij}^*) \tag{5.23}$$

Here $C_M(\alpha, \alpha_t^*, A_{ij})$ is the pitching moment coefficient as measured during the wing optimization runs at a fixed tail incidence $\alpha_t = \alpha_t^*$ and at variable α and A_{ij}'s. $C_M(\alpha, \alpha_t^*, A_{ij}^*)$ is the pitching moment variation with α recorded during a preliminary run at fixed tail angle α_t^* and with the actuators held fixed at the nominal

positions $A_{ij} = A_{ij}^*$. $C_{M_{MIN}}(\alpha, \alpha_t, A_{ij}^*)$ represents the variation with α of the minimum pitching moment coefficient as recorded during a series of preliminary runs at different tail incidence angles α_t and at the nominal actuator settings A_{ij}^*. $C_{M_{MAX}}(\alpha, \alpha_t, A_{ij}^*)$ represents the corresponding variation for the maximum pitching moment coefficient.

The coefficients $C_{M_{MIN}}(\alpha, \alpha_t, A_{ij}^*)$ and $C_{M_{MAX}}(\alpha, \alpha_t, A_{ij}^*)$ must be input in tabular form. The tables are designated in the optimization program as

$$\text{ALP(I)} = \alpha$$
$$\text{CMMIN(I)} = C_{M_{MIN}}(\alpha, \alpha_t, A_{ij}^*)$$
$$\text{CMNOM(I)} = C_M(\alpha, \alpha_t^*, A_{ij}^*)$$
$$\text{CMMAX(I)} = C_{M_{MAX}}(\alpha, \alpha_t, A_{ij}^*)$$
$$\text{LTAB} = \text{number of I (points in ALP array).}$$

It is assumed that the tables are functions of the independent variable array ALP. A separate set of tables is generally required for each Mach number.

When using the tabular form of the trim constraint, it is meaningful to correct C_L for the change in lift which would have occurred had the tail been self trimming. The correction, as derived in Reference 20, is

$$\Delta C_{L_{TRIM}} = \left(\frac{\ell_t}{\bar{c}}\right)^{-1} C_M(\alpha, \alpha_t^*, A_{ij}) \tag{5.24}$$

and depends upon the ratio of the tail arm ℓ_t to the mean aerodynamic cord $\bar{c}$ and the measured C_M. The latter coefficient depends upon the longitudinal position of the center of gravity (or moment reference center x_{MC}). Moving the C.G. forward makes C_M more negative and detracts from C_L, whereas moving the C.G. aft has the opposite effect. Hence, the optimization procedure may be used to investigate effects of static margin on wing optimization.

The corrected lift coefficient

$$C_L' = C_L + \Delta C_{L_{TRIM}} \tag{5.25}$$

must then be used as one of the eighteen aerodynamic functions in FX(I).

5.2 PSEUDO-AERODYNAMIC MODULE

Computer simulations are required to check the convergence of the optimization procedure prior to testing, because of the various nonlinearities and testing inaccuracies which could seriously compromise convergence. This is especially true under transonic conditions and with a large number of independent variables, since these effects tend to increase the sensitivity of the computed optimum search directions S to testing errors, and make the restoration and the holding of constraints increasingly difficult.

In order to carry out computer simulations of the interactive testing operation, it was necessary to link the optimization program with a set of equations for calculating the aerodynamic functions ordinarily supplied by the wind tunnel data reduction system (see Equation 5.1). These equations, termed "Pseudo-Aerodynamic Module" (PAM) are a set of nonlinear, algebraic relations for the aerodynamic functions of Equation 5.1 in terms of the twelve actuator positions A_{11}, A_{12}, ... A_{26}, tail incidence angle α_t, angle of attack α, Mach number M and Reynolds number Re. Because of the numerous times that the PAM subroutine must be called upon during an optimization problem, it was impractical from a computer time standpoint to perform even the most simplified type of flow field analysis. Hence emphasis in PAM was placed on computational speed and on a realistic approximation of the form of the nonlinear features expected in the aerodynamic test data, rather than on accuracy. Random errors were also added to the ouput from PAM to simulate testing inaccuracies. The free stream Mach number M in PAM must be taken as subsonic, viz., $M < 1$.

The following expressions constitute PAM as currently programmed, and are based somewhat on thin airfoil theory with empirical corrections for three dimensional and compressibility effects. Numerical values for the various coefficients were chosen to correspond with the 1/6'th scale SOFT Wing wind tunnel model.

5.2.1 Relation Between Actuator Readings and Geometric Deflections

$(R/c)_{11} = 0.01\,(3-2\,A_{11}/1000)$ (inb'd L.E. radius)

$\delta_{12} = 25\,(A_{12}/1000 - 1/5)$ (inb'd L.E. deflection, degs, 15%c)

$\delta_{13} = 25\,(A_{13}/1000 - 1/5)$ (inb'd L.E., degs, 25%c)

$(t/c)_{14} = 0.09 + 0.01\,(2A_{14}/1000 - 1)$ (inb'd upper surface humping)

$\delta_{15} = 30\,(A_{15}/1000 - 1/3)$ (inb'd T.E. deflection, degs, 65%c)

$\delta_{16} = 30\,(A_{16}/1000 - 1/3)$ (inb'd T.E. deflection, degs, 80%c)

$(R/c)_{21} = 0.005(3 - 2\,A_{21}/1000)$ (outb'd L.E. radius)

$\delta_{22} = 25\,(A_{22}/1000 - 1/5)$ (outb'd L.E. deflection, degs, 15%c)

$\delta_{23} = 25\,(A_{23}/1000 - 1/5)$ (outb'd L.E. deflection, degs, 25%c)

$(t/c)_{24} = 0.06 + 0.01\,(2\,A_{24}/1000 - 1)$ (outb'd upper surface humping)

$\delta_{25} = 30\,(A_{25}/1000 - 1/3)$ (outb'd T.E. deflection, degs, 65%c)

$\delta_{26} = 30\,(A_{26}/1000 - 1/3)$ (outb'd T.E. deflection, degs, 80%c)

5.2.2 Aerodynamic Coefficients

(i) Section Zero Lift Angle

$$\alpha_{0L_i} = -\frac{57.3}{2\pi}\,\Delta(C_{L\delta})_i - \alpha_{TW_i} \qquad , i = 1, 2$$

$$\Delta(C_{L\delta})_i = 2\Big[(\sin\theta_2 - \theta_2)\sin\delta_{i2} + (\sin\theta_3 - \theta_3)\sin\delta_{i3} + \eta_{i5}(\sin\theta_5 + \theta_5)\sin\delta_{i5} + \eta_{i6}(\sin\theta_6 + \theta_6)\sin\delta_{i6}\Big] \qquad i = 1, 2$$

$$\theta_j = \cos^{-1}\left[1 - 2\,c_j/c\right]$$

where $\alpha_{TW_1} = -3.15°$, $\alpha_{TW_2} = -6.7°$,

$c_2/c = 0.15$, $c_3/c = 0.25$, $c_5/c = 0.35$, $c_6/c = 0.20$

and

$$\eta_{15} = \eta_{16} = \eta_{25} = \eta_{26} = 1.$$

(ii) Wing Lift Curve Slope

$$C_{L_\alpha} = \frac{\pi AR}{1 + \left\{1 + [1 - (M \cos \Lambda)^2](AR/2 \cos \Lambda)^2\right\}^{1/2}}$$

where the values $AR = 5.83$, $\Lambda = 16°$ and $M = 0.85$ were input for the simulations.

(iii) Section Stall Parameters and Section Lift Coefficient

$$C_{L_{MAX_i}} = 0.8 + 0.3 (R/c)_{i1}^{1/3} + 4 (c_2/c)^{1/2} \sin \delta_{i2} + 4 (c_3/c)^{1/2} \sin \delta_{i3}$$

$$+ \eta_{i5} (\sin \theta_5 + \theta_5) \sin \delta_{i5} + \eta_{i6} (\sin \theta_6 + \theta_6) \sin \delta_{i6}$$

$$\alpha_{STALL_i} = \alpha_{0L_i} + 57.3 C_{L_{MAX_i}}/C_{L_\alpha}$$

$$C_{L_i} = C_{L_\alpha}\left[1 - H\left(\frac{\alpha}{\alpha_{STALL_i}} - 1\right)\right] \sin(\alpha - \alpha_{0L_i})$$

$$+ H\left(\frac{\alpha}{\alpha_{STALL_i}} - 1\right) C_{L_\alpha} \sin(\alpha_{STALL_i} - \alpha_{0L_i}) \left[1 - H\left(\frac{\alpha}{\alpha_{c_i}} - 1\right)\right]$$

$$- \Delta C_{L_i}\left[1 - \cos 90\left(\frac{\alpha - \alpha_{STALL_i}}{\alpha_{c_i} - \alpha_{STALL_i}}\right)\right] H\left(\frac{\alpha}{\alpha_{STALL_i}} - 1\right)\left[1 - H\left(\frac{\alpha}{\alpha_{c_i}} - 1\right)\right]$$

$$+ 1.8 \sin(\alpha - \alpha_{0L_i}) \cos(\alpha - \alpha_{0L_i})\ H\left(\frac{\alpha}{\alpha_{c_i}} - 1\right)$$

where

$$\alpha_{c_i} = \alpha_{STALL_i} + \left[100\,(R/c)_{i1}\right]^2$$

$$\Delta C_{L_i} = \sin(\alpha_{c_i} - \alpha_{0L_i})\left[C_{L_\alpha} \frac{\sin(\alpha_{STALL_i} - \alpha_{0L_i})}{\sin(\alpha_{c_i} - \alpha_{0L_i})} - 1.8 \cos(\alpha_{c_i} - \alpha_{0L_i})\right]$$

and $H(x)$ is the unit step function, $H = 0$, $x < 0$, $H = 1$, $x \geq 0$.

(iv) Component and Total Lift Coefficient

a. Wing

$$C_{L_{WING}} = \Delta K_1\ C_{L_1} + \Delta K_2\, C_{L_2}$$

with $\Delta K_1 = 0.41$ and $\Delta K_2 = 0.24$

b. Glove

$$C_{L_{GLOVE}} = (1 - \Delta K_1 - \Delta K_2)\, C_{L_\alpha} \sin\alpha \cos\alpha$$

c. Tail

$C_{L_{\alpha_t}}$ is given by the same expression as C_{L_α}, except use $AR_t = 2.12$ and $\Lambda_t = 57°$ instead of the corresponding wing values.

The downwash angle ϵ_t (in degrees) is

$$\epsilon_t = \frac{90\,(C_{L_{WING}} + C_{L_{GLOVE}})}{(0.785\,\pi)^2\,AR}\left[1 + \sqrt{1 + (0.785\,b/\ell_t)^2}\right]$$

where the span to tail arm ratio $b/\ell_t = 2.5$.

$$C_{L_t} = C_{L_{\alpha_t}} \sin(\alpha_t - \epsilon_t)\left[1 - H\left(\frac{\alpha + \alpha_t - \epsilon_t}{\alpha_{STALL_t}} - 1\right)\right]$$

$$+ C_{L_{\alpha_t}} \sin(\alpha_{STALL_t})\, H\left(\frac{\alpha + \alpha_t - \epsilon_t}{\alpha_{STALL_t}} - 1\right)$$

$$- \Delta C_{L_t}\left[1 - \cos 90\left(\frac{\alpha + \alpha_t - \epsilon_t - \alpha_{STALL_t}}{\alpha_{c_t} - \alpha_{STALL_t}}\right)\right] H\left(\frac{\alpha + \alpha_t - \epsilon_t}{\alpha_{STALL_t}} - 1\right)$$

$$\times\left[1 - H\left(\frac{\alpha + \alpha_t - \epsilon_t}{\alpha_{c_t}} - 1\right)\right]$$

$$- \Delta C_{L_t}\, H\left(\frac{\alpha + \alpha_t - \epsilon_t}{\alpha_{c_t}} - 1\right)$$

where

$$\alpha_{STALL_t} = 12\,\frac{(\alpha + \alpha_t - \epsilon_t)}{|\alpha + \alpha_t - \epsilon_t|} \quad \text{(in degs)}$$

$$\alpha_{c_t} = 14\,\frac{(\alpha + \alpha_t - \epsilon_t)}{|\alpha + \alpha_t - \epsilon_t|} \quad \text{(in degs)}$$

and $\Delta C_{L_t} = C_{L_{\alpha_t}} \sin(4°) \frac{(\alpha + \alpha_t - \epsilon_t)}{|\alpha + \alpha_t - \epsilon_t|}$

d. Total Lift

$$C_L = C_{L_{WING}} + C_{L_{GLOVE}} + \left(\frac{S_t}{S}\right)\left(\frac{q_t}{q}\right) C_{L_t}$$

where $S_t/S = 0.25$ and $q_t/q = 0.9$

(v) Profile and Induced Drag Components

$$\Delta C_{D_{P_i}} = \frac{4\pi^2}{60} \left| \frac{\alpha - \alpha_{0L_i}}{57.3} \right|^3 \quad , \; i = 1, 2$$

$$\Delta C_{D_{P_t}} = \frac{4\pi^2}{60} \left| \frac{\alpha + \alpha_t - \epsilon_t}{57.3} \right|^3$$

$$C_{D_{IND_{WING}}} = \frac{C_{L_\alpha}^2 \left[\Delta K_1 \sin(\alpha - \alpha_{0L_1}) + \Delta K_2 \sin(\alpha - \alpha_{0L_2}) + C_{L_{GLOVE}} \right]^2}{\pi AR\, e}$$

$$C_{D_{IND_t}} = C_{L_t} \left[\frac{C_{L_t}}{\pi AR_t e} + \sin \epsilon_t \right]$$

where the aerodynamic efficiency e of both the wing and tail surfaces has been set equal to 0.9.

(vi) Wing Compressibility Drag

$$\Delta C_{D_{RL_i}} = P_{L_i} \left\{ \frac{1}{10} (M_{MAX_i} - 1.05)^{1/2} H(M_{MAX_i} - 1.05) \left[1 - H(M_{MAX_i} - 1.45) \right] \right.$$

$$\left. + (M_{MAX_i} - 1.2)^2 H(M_{MAX_i} - 1.45) \right\} \quad , i = 1, 2$$

where

$$P_{L_1} = 10 \left| 10 (t/c)_{14}^2 + 100 (R/c)_{11}^2 - \frac{1}{4} \left(\frac{\alpha_{0L_1} + \alpha_{TW_1}}{57.3} \right) \right|$$

$$P_{L_2} = 10 \left| 16.7 (t/c)_{24}^2 + 200 (R/c)_{21}^2 - \frac{1}{4} \left(\frac{\alpha_{0L_2} + \alpha_{TW_2}}{57.3} \right) \right|$$

and

$$M_{MAX_i} = \left(\frac{2}{\gamma - 1} \right)^{1/2} \left[(1 + \frac{\gamma - 1}{2} M^2)(\frac{\gamma M^2}{2} C_{P_{MIN_i}} + 1)^{-\left(\frac{\gamma - 1}{\gamma} \right)} - 1 \right]^{1/2}$$

Here $C_{P_{MIN_i}}$ is the minimum pressure coefficient reached on the i'th section of the wing, and is taken as the more negative value of the following two expressions, but not less than the third expression, which is related to the vacuum pressure coefficient.

$$C_{P_{MIN_i}} \leq - \frac{1}{\sqrt{1 - M^2}} \left[2 (t/c)_{i4} + 10 (R/c)_{i1} + 0.35 C_{L_\alpha} \sin (\alpha - \alpha_{0L_i}) \right]$$

or

$$C_{P_{MIN_i}} \leq - \frac{1}{\sqrt{1 - M^2}} \left\{ \frac{0.2 \left[C_{L_\alpha} \sin(\alpha - \alpha_{0L_i}) \right]^2}{(t/c)_{i4} + 5 (R/c)_{i1}} - \sin\theta_3 \sin\delta_{i3} - \sin\theta_2 \sin\delta_{i2} \right\}$$

but

$$C_{P_{MIN_i}} \geq \frac{1.5}{\gamma M^2}$$

(vii) Total Drag Coefficient

$$C_D = C_{D_F} + C_{D_{IND\ WING}} + \Delta K_1 (\Delta C_{D_{P_1}} + \Delta C_{D_{RL_1}})$$

$$+ \Delta K_2 (\Delta C_{D_{P_2}} + \Delta C_{D_{RL_2}}) + \frac{S_t}{S} \frac{q_t}{q} (\Delta C_{D_{P_t}} + C_{D_{IND_t}})$$

where $C_{D_F} = 0.016335$ is the overall skin friction coefficient (includes wing, fuselage and tail).

(viii) Pitching Moment Coefficient

The pitching moment coefficient about the wing pivot C_{M_P} (see sketch below) was taken as

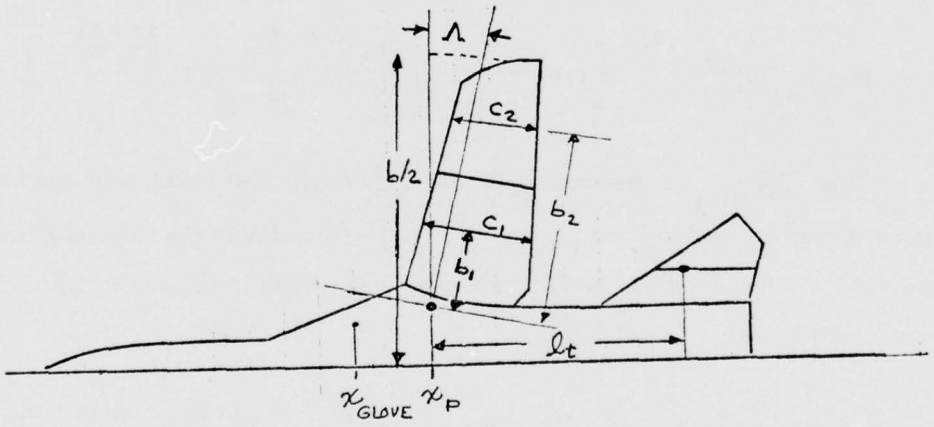

$$C_{M_P} = \sum_{i=1}^{2} \left[(c_i/\bar{c}) \left(\frac{C_{L_\alpha}}{2\pi}\right) (\Delta C_{M_\delta})_i - C_{L_i} (b_i/\bar{c}) \sin \Lambda \right] \Delta K_i$$

$$+ C_{L_{GLOVE}} \left[x_P/\bar{c} - x_{GLOVE}/\bar{c} \right]$$

$$- \frac{S_t}{S} \frac{q_t}{q} \frac{\ell_t}{c} \left[C_{L_t} \cos\alpha + C_{D_t} \sin\alpha \right]$$

where

$$\Delta C_{M_{\delta_i}} = -2(.03)(\sin\theta_2 - \theta_2)\sin\delta_{i2} - 2(.05)(\sin\theta_3 - \theta_3)\sin\delta_{i3}$$
$$-2\eta_{i5}(.17)(\sin\theta_5 + \theta_5)\sin\delta_{i5} - 2\eta_{i6}(.20)(\sin\theta_6 + \theta_6)\delta_{i6}$$

$c_1/\bar{c} = 1.0$, $c_2/\bar{c} = 0.82$, $b_1/\bar{c} = 0.525$, $b_2/\bar{c} = 1.589$,

$x_{P}/\bar{c} = 0$, $x_{GLOVE}/\bar{c} = -0.875$, $\ell_t\,\bar{c} = 2.32$, $S_t/S = 0.25$, $q_t/q = 0.9$

and

$$C_{D_t} = 0.0055 + \Delta C_{D_{P_t}} + C_{D_{IND_t}}$$

(ix) Buffet

$$C_{P_{TE_i}} = \frac{1}{10}\left(1 - 3\Delta C_{D_{P_i}} - 3\Delta C_{D_{RL_i}}\right)$$

(x) Root Bending Moment

$$C_{RB} = \frac{1}{AR}\sum_{i=1}^{2}(b_i/\bar{c})\,C_{L_i}\,\Delta K_i$$

and

$$M_{RB} = 214,668\,(MS)^3\;C_{RB}\;q_\infty \quad \text{(inch lbs)}$$

where MS is the model scale, (MS = 1 for the full scale aircraft).

5.2.3 Sample Computations with PAM

Sample computations were made with PAM, to examine the realism of the calculated nonlinearities and of the individual effects of the various actuators, and to generate the pitching moment tables described in Section 5.1.3 for making simulation runs. The computations included the parametric variation of each of the twelve actuators about the nominal value, in addition to tail incidence angle and angle of attack, according to the following table:

NOMINAL POSITION

A_{11}	A_{12}	A_{13}	A_{14}	A_{15}	A_{16}	A_{21}	A_{22}	A_{23}	A_{24}	A_{25}	A_{26}	α_t
500	200	200	500	333	333	500	200	200	500	333	333	5°

PERTURBATIONS FROM NOMINAL

ΔA_{11}	ΔA_{12}	ΔA_{13}	ΔA_{14}	ΔA_{15}	ΔA_{16}	ΔA_{21}	ΔA_{22}	ΔA_{23}	ΔA_{24}	ΔA_{25}	ΔA_{26}	$\Delta\alpha_t$
-500	-200	-200	-500	-333	-333	-500	-200	-200	-500	-333	-333	-3°
0	0	0	0	0	0	0	0	0	0	0	0	-1
500	200	200	500	333	333	500	200	200	500	333	333	0
	400	400		667	667		400	400		667	667	1
												3

Because of space limitations, only a limited number of parametric variations listed in the above table have been included herein. Representative plots showing the effects of the A_{13}, A_{14}, A_{15} and A_{21} actuators on the variations of C_L with α, C_D with C_L, and C_M with C_L are shown in Figures 5.3(a) - 5.6(c). Similar parametric plots for the A_{11} actuator and for α_t were given previously in Reference 21. The shapes of the nonlinearities in the stall region shown in the figures appear sufficiently similar to test data to make simulations carried out with PAM a meaningful test of effects of nonlinearities on convergence.

The pitching moment tables were generated from the same nominal actuator positions, except A_{14} and A_{24} = 200 instead of 500 counts and α_t = 0° instead of 5°. The calculations were carried out with tail incidence angles α_t between -24° and 12°, and for angle of attack α between 0° and 16°. The results may be plotted as shown in Figure 5.7, from which tabulated pitching moment data given in Table 5.2 were prepared. These data are to be used in simulations involving inequality constraints on tail trim control, as discussed in Section 5.1.3.

5.3 COMPUTER SIMULATIONS

An extensive set of simulations involving the optimization computer program in conjunction with PAM were run on the DEC 10 computer. The majority of the runs, which were reported originally in Reference 22 and are summarized in Tables 5.3 and 5.4, dealt with effects of cycling, testing errors, the size of the perturbations in the incremental mode (DA's), etc., on convergence for problems dealing with either minimizing C_D or maximizing C_L. A summary of the "standard" values used for the components of DA, DEV and TOL, and a list of the "standard" testing errors is found in Table 5.5. The inequality constraints were on trailing edge pressure (buffet constraint) and on differential actuator deflection (twist constraint) as follows:

$$C_{P_{TE_1}} \geq 0, \quad C_{P_{TE_2}} \geq 0$$

$$|A_{1j} - A_{2j}| \leq 200, \quad j = 2, 3, 4, 5$$

Equality constraints were enforced on pitching moment (trim) and on lift coefficient, as shown in Tables 5.3 and 5.4. The tail incidence angle α_t was taken as a free independent variable to be optimized, hence the constraint on C_M could be satisfied without recourse to the approximate procedure given in Section 5.1.3.

Representative results from these runs are presented in Figures 5.8 to 5.12. Thus, Figures 5.8-5.10 illustrate the effect of cycling (averaging) and the choice of the random number (seed) for generating testing errors on convergence for the minimum C_D problem. Figure 5.8 depicts the minimum value of C_D obtained for sets of runs with 1, 2 and 3 cycles. Six cases are shown for each set, corresponding to different seed values in starting the random number generator. Although the runs with standard testing errors consistently gave higher values of $C_{D\,MIN}$ than those without testing errors, it was somewhat surprising that the lowest values of $C_{D\,MIN}$ were found for the two cycle case, rather than for three cycles, as was expected. This result is illustrated in Figure 5.9 which shows average values of $C_{D\,MIN}$ for 1, 2, and 3 cycles

with standard testing errors and without testing errors. The variations of C_L, C_D and C_M during typical runs from the series are shown in Figure 5.10.

Figures 5.11 and 5.12 deal with maximizing C_L. All constraints are the same as shown in Figure 5.8, except that the C_L constraint has been replaced by a constraint on C_D, viz., $C_D = 0.11$, corresponding to a sustained maneuver condition for the F-111 TACT aircraft at M = 0.90. Figure 5.11 shows the effect of cycling on convergence. The maximum C_L with testing errors is again obtained from the two-cycle case, but is somewhat below that found without testing errors.

The study shown in Figure 5.12 was carried out to investigate effects of the size of testing errors and of the size of the actuator perturbations during the incremental mode on convergence. Thus, all runs were made with twice the standard testing errors given in Table 5.5 For the 1 cycle case, convergence was poor, and was helped somewhat by increasing the size of the actuator perturbations. Increasing the number of cycles to 2, 3, and 4 gave similar results to that observed previously.

However, the uppermost curve in Figure 5.12 shows that good convergence was eventually obtained by changing the number of cycles and actuator perturbation sizes in combination. This was accomplished by controlling the DEC-10 "interactively" from a video terminal and monitoring the resultant convergence properties. This "interactive" capability has been added to the optimization program and will also be available during the wind tunnel test, because of the similarity between the hardware at AEDC and at GD/Electronics Division at which the DEC-10 is located. A detailed discussion of the "interactive" operation of the optimization program has been included in Reference 4.

Prior to the transfer of the computer program to AEDC/ARO (on Dec. 16, 1976), several additional simulations were performed with α_t held fixed (frozen), and also with other actuators frozen, to simulate more closely the testing at AEDC. Run 215 in Figure 5.13 deals with minimizing C_D. The equality and inequality constraints, tolerances, etc., are identical to those for the previous runs with α_t variable, except that the equality constraint $C_M = 0$ has been dropped and replaced by the

inequality constraints stated by Equations 5.22 and 5.23. The required tabulated values were taken from Table 5.2.

As seen from Figure 5.13, reasonable convergence was demonstrated with zero testing errors, with the solution giving a considerable lower value of $C_{D\,MIN}$ ($\simeq$ 0.043) than had been obtained for the trimmed zero testing error case ($C_{D\,MIN}$ $\sim$ 0.049 from Figures 5.8 and 5 9). As seen also in Figure 5.13, the pitching moment coefficient drifts to the positive maximum limit after the fifth iteration, and remains at this bound for the duration of the run. The trace of C_M during the run in relation to the bounding values from the tables may also be seen from Figure 5.14. It is surprising that C_M becomes bounded positively rather than negatively, since a positive C_M may be thought of as adding additional drag. This anomaly may be due to the position of the C.G. (assumed at the pivot), and further simulations should be carried out to verify the cause for the positive C_M.

Similar optimization runs with standard testing errors have prove unsuccessful to date. The runs have indicated an inability to satisfy constraints. A possible cause of the difficulty is the value of TOL = .003 used in satisfying the pitching moment tables, which may be too small in the presence of testing errors. Additional simulations and fine tuning of the program parameters are required for this condition.

Runs involving maximizing C_L with α_t frozen and with pitching moment tables introduced to limit the maximum and minimum C_M values were also attempted, but were unsuccessful. These runs must also be simulated successfully prior to attempting them in the wind tunnel.

The optimization computer program was modified prior to shipment to AEDC/ARO for up to a maximum of twenty dependent functions and constraints. It was also demonstrated in a series of interactive runs that various actuators, which might not be present in the full scale AFTI-111, could be readily locked out. These modifications included freezing the upper surface humping and/or leading edge sharpness systems, not deflecting about the 25% chord position, and testing without differential twist along the leading edge. Although the optimization program may be

used with C_L (corrected for tail trim lift according to Equations 5.25), demonstrations of the equivalence between optimizing on C'_L (corrected) with the tail held fixed, and on C_L with a self trimming tail, were not obtained. It is recommended that this equivalence be established by making additional simulations prior to testing at AEDC with the tabulated pitching moment constraints and with C_L replaced by C'_L.

TABLE 5.1 DICTIONARY OF COMMON VARIABLES IN THE OPTIMIZATION COMPUTER PROGRAM


```
ABORT=WHEN NONZERO THIS FLAG ABORTS ITERATIONS OF
      GRADIENT PROJECTION ALGORITHM.
ALP = ARRAY OF ANGLE OF ATTACK VALUES FOR TRIM CORRECTION
      TABLES.
AMAX= MAXIMUM ALLOWED ALPHA
ATMAX=MAXIMUM ALPHA TAIL (CURRENTLY NOT USED)
AVE = NOMINAL AVERAGE
C   = MULTIPLIER FOR EQUALITY CONSTRAINTS - EITHER 0 OR 1.
      TO DEACTIVATE OR ACTIVATE THE CONSTRAINT
CAN = CANDIDATE FLAGS FOR CONSTRAINTS. =+1 FOR EQUALITY
      CONSTRAINT, = 0 FOR NOT ACTIVE, =-1 FOR INEQUALITY
CMAX= NUMBER OF CYCLES FOR GRADIENT EVALUATION
CMMAX=CM TABLE FOR TRIM CORRECTION FOR ALPHA = AMAX
CMMIN=CM TABLE FOR TRIM CORRECTION FOR ALPHA = ATMIN
CMNOM=CM TABLE FOR TRIM CORRECTION FOR ALPHA = NOMINAL
DA  = SIZE OF PERTURBATION FOR INCREMENTAL MODE
DACT= INDICATOR USED IN DEACT TO SIGNAL A CONSTRAINT
      WAS DEACTIVATED.

DEV = DEVIATION TOLERANCE FROM EQUALITY CONSTRAINT
FIRST=FLAG TO SIGNAL GRADIENT COMPUTATION ONLY ON FIRST
      ITERATION.
FX  = ARRAY OF REDUCED COEFFICIENTS CORRESPONDING TO
      ACTUATOR SETTINGS IN X ARRAY.
FXOPT=OPTIMUM FUNCTION VALUE FROM 1-D SEARCH
G   = CONSTRAINT VECTOR
GG  = GRAD OF G
GL  = GRAD OF LAGRANGE FUNCTION
GPHI= GRAD OF PERFORMANCE FUNCTION PHI
H   = HESSIAN
ICMAX=INTEGER EQUIVALENT OF CMAX
ICOR= DISK FILE NUMBER FOR CORRECTIONS TO PARAMETERS
      OR FILE IDIS
ICOU= COUNTER FOR DATA POINT RETRIEVAL.
IDIS= FILE NUMBER OF PROBLEM DEFINING FILE
IOBJ= INDEX OF OBJECTIVE FUNCTION. (=OBJ)
IOUT= OUTPUT FILE NUMBER
IS  = NUMBER OF POINTS
ISS = INDEX OF OPTIMAL POINT FROM 1-D SEARCH
ISWO= SWITCH FOR PROBLEM DEFINITION. =1 FOR MIN CD
                                     =2 FOR MAX CL
ITRA= ITERATION NUMBER FOR GRADIENT PROJECTION
ITTY= TELETYPE FILE NUMBER (=5)
LTAB= LENGTH OF TRIM CORRECTION TABLES (ALP, CMMIN, ETC.)
MAXD1=MAXIMUM DIMENSION OF DATA POINTS (=8)
MAXD2=MAXIMUM DIMENSION OF STATES (=20)
MAXD3=MAXIMUM DIMENSION OF CONSTRAINTS (=18)
NC  = NUMBER OF ACTIVE EQUALITY CONSTRAINTS.
NCON= TOTAL NUMBER OF CONSTRAINTS PROGRAMMED.
NITER=NUMBER OF COMPLETE ITERATIONS OF GRADIENT PROJECTION
      ALGORITHM.
NIV = NUMBER OF INDEPENDENT VARIABLES.
NIV1= NIV-1
NIV2= NIV-2
NPRO= ITERATION NUMBER OF LAST GRADIENT PROJECTION ITERATION
      ON WHICH NO PROGRESS WAS MADE.
NOIS= INDICATOR WHICH WHEN NONZERO INDICATES A NOISE RUN
NWDS= NUMBER OF WORDS ON PROBLEM DEFINING FILE
N1D = NUMBER OF 1-DIMENSIONAL SEARCH STEPS (=11)
OBJ = OBJECTIVE FUNCTION INDEX
RESTO=RESTORATION SEARCH INDICATOR
S   = SCALING FACTORS
SD  = SEARCH DIRECTION
SEED= RANDOM NUMBER GENERATOR SEED
T   = TARGET VALUES
TH  = INDEPENDENT VARIABLE IN ANGULAR COORDINATES
TOL = TOLERANCE OR RESTORATION CRITERION.
X   = ARRAY OF ACTUATOR SETTINGS FOR GRADIENT COMPUTATION
XMAX= MAXIMUM EXCURSION OF ACTUATORS (=1RAD, COUNTS)
ZK  = STEP SIZE ARRAY FOR ONE DIMENSIONAL SEARCH.
ZL  = LAGRANGE MULTIPLIERS
ZLAG= LAGRANGE FUNCTION VALUES FROM 1-D SEARCH.
ZNL = NOISE LEVELS
```

TABLE 5.2 PITCHING MOMENT TABLES OBTAINED WITH PSEUDO-AERODYNAMIC MODULE (PAM)

ALP(I)	CM MIN (I)	CM NOM (I)	CM MAX (I)
-2	-0.176	0.020	0.310
0	-0.140	0.044	0.336
2	-0.120	0.068	0.364
4	-0.090	0.092	0.390
6	-0.060	0.115	0.418
8	-0.030	0.137	0.450
10	-0.005	0.157	0.480
12	+0.025	0.175	0.510
14	0.070	0.188	0.550
16	0.190	0.244	0.650

LTAB = 10

$\alpha_t^* = 0$

$A_{ij}^* =$ 500, 200, 200, 500, 333, 333, 500, 200, 200, 200, 333, 333

ij = 11, 12, 13, 14, 15, 16, 21, 22, 23, 24, 25, 26

TABLE 5.3 RUN LOG - DEC-10 OPTIMIZATION RUNS

RUN NO.	1976 DATE	OPTIMUM VARIABLE	EQUALITY CONSTRAINTS	INEQUALITY CONSTRAINTS	TESTING ERRORS	CYCLES	Δ'S	TOL	DEV	MAX ITER.	REMARKS
1	8/26	C_D	$C_L=0.50$, $C_M=0$	$C_{P_{TE_{1,2}}}$ $\|\Delta Y\|_{2,3,5,6}$	Zero	1	$\Delta Y=4$	Too Small	Scalar	10	Premature abort, $C_D = 0.0524$
2	8/26	√	$C_L=0.25$, $C_M=0$	√ √	√	√	√	√	√	20	Convergence, $C_D=0.03356$
3	8/30	√	√ √	√ √	√	√	√	√	Vector	11	Corrected deactivation, Premature abort, $C_D=0.0302$
4	8/31	√	√ √	√ √	Standard	√	√	√	√	20	C_M Tol too small. Δ's too small, $C_D=0.0463$
5	9/2	√	√ √	√ √	√	√	STD	STD	STD	9	Premature abort. Error found in abort crit, $C_D=0.0402$
6	9/2	√	√ √	√ √	√	√	√	√	√	9	Modified abort crit with inequalities $C_D=0.0394$
7	9/3	√	√ √	√ √	Zero	√	√	√	√	9	PT 1 optimal, $C_D=0.0303$
8	9/3	√	√ √	√ √	STD	3	√	√	√	20	PT 1 optimal, $C_D=0.0303$
9	9/3	√	√ √	√ √	√	√	√	√	√	20	No deactivation if restore constraints. Conv'ged $C_D=0.0304$
10	9/3	√	√ √	√ √	√	√	√	√	√	20	Doesn't use aborted points as optimum. Conv'ged, $C_D=0.0311$
11	9/3	√	√ √	√ √	√	2	√	√	√	20	Conv'ged, $C_D=0.0311$
12	9/3	√	√ √	√ √	√	1	√	√	√	14	PT 1 Opt. , $C_D=0.0322$
13	√	√	$C_L=0.5$ √	√ √	√	√	√	√	√	20	PT 1 Opt. , $C_D=0.0558$
14	√	√	√ √	√ √	√	2	√	√	√	20	Conv'ged $C_D=0.0526$
15	√	√	√ √	√ √	√	3	√	√	√	20	Conv'ged $C_D=0.0541$
16	√	√	√ √	√ √	Zero	1	√	√	√	6	PT 1 Opt. , $C_D=0.0566$ Δ's may be too large
17	√	√	√ √	√ √	√	√	Reduced by 1/10	√	√	11	PT 1 Opt. , Poor grad., $C_D=0.0566$
101	9/7	√	√ √	√ √	√	√	√	√	√	14	PT 1 Opt. , $C_D=0.053$ Elimated noise in α & α_T.
102-107	√	√	√ √	√ √	STD	1	STD	√	√	VAR	Study of Effects
108-113	√	√	√ √	√ √		2		√	√	VAR	of Random Noise &
114-119	√	√	√ √	√ √		3		√	√	VAR	Cycling on Convergence

TABLE 5.4 DEC-10 OPTIMIZATION RUNS WITH INTERACTIVE RECOVERY MODE

RUN NO.	1976 DATE	OPTIMUM VARIABLES	EQUALITY CONSTRAINTS	INEQUALITY CONSTRAINTS	TESTING ERRORS	CYCLES	Δ's	TOL	DEV	MAX ITER.	REMARKS
201	9/13	$C_{D_{MIN}}$	C_L= 05, C_M=0	$C_{P-TE_{1,2}}$ $\|\Delta Y\|$ 2,3,5,6	Zero	1	1/10 STD	STD	STD	33	Same as 101 up to iteration 9, Then deviates for unknown reason. $C_{D_{MIN}}$ = 0.0494
202	9/13	√	√ √	√ √	√	√	√	√	√	53	Same as 101 & 102 up to iteration 9. Then deviates for unknown reason. $C_{D_{MIN}}$ = 0.0492
203	9/13	$C_{L\ MAX}$	C_D= 0.11, C_M=0	√ √	√	√	√	√	√	177	Exercised recovery mode. $C_{L_{MAX}}$ = 0.858
204	9/14	$C_{D_{MIN}}$	C_L= 0.5, C_M=0	√ √	√	√	√	√	√	49	Same as 201 up to iteration 16. Then deviates for unknown reason. $C_{D_{MIN}}$ = 0.506
205	9/23	√	√ √	√ √	√	√	√	√	√	?	Same as 203 up to iteration 16. After this use interactive recov. $C_{D_{MIN}}$ = 0.0498
206	9/23	$C_{L_{MAX}}$	C_D= 0.11, C_M=0	√ √	√	√	STD	√	√	50	$C_{L_{MAX}}$ = 0.8945 — Study of cycling
207	√	√	√ √	√ √	STD	√	√	√	√	√	$C_{L_{MAX}}$ = 0.8319 — & testing errors
208	√	√	√ √	√ √	√	2	√	√	√	√	$C_{L_{MAX}}$ = 0.8796 — on $C_{L_{MAX}}$
209	√	√	√ √	√ √	√	3	√	√	√	√	$C_{L_{MAX}}$ = 0.8315 — Problem
210	√	√	√ √	√ √	2xSTD	1	√	√	√	20	$C_{L_{MAX}}$ = 0.63 "
210C	√	√	√ √	√ √	√	1	2xSTD	√	√	15	$C_{L_{MAX}}$ = 0.68 "
210CC	√	√	√ √	√ √	√	1	4xSTD	√	√	7	$C_{L_{MAX}}$ = 0.68 "
211	√	√	√ √	√ √	√	2	STD	√	√	22	$C_{L_{MAX}}$ = 0.712 "
211C	√	√	√ √	√ √	√	√	2xSTD	√	√	4	" = 0.71 "
211CC	√	√	√ √	√ √	√	√	4xSTD	√	√	2	" = 0.70 "
212	√	√	√ √	√ √	√	3	STD	√	√	23	" = 0.725 "
212C	√	√	√ √	√ √	√	√	2xSTD	√	√	2	" = 0.733 "
213	√	√	√ √	√ √	√	4	STD	√	√	11	" = 0.5563 "
214	√	√	√ √	√ √		√	√	√	√	5	$C_{L_{MAX}}$ = 0.623 — Same as 213 but different seed
214C	√	√	√ √	√ √	√	5	√	√	√	2	" = 0.627 "
214CC	√	√	√ √	√ √	√	3	√	√	√	2	" = 0.627 "
CCC	√	√	√ √	√ √	√	√	2xSTD	√	√	25	" = 0.742 "
CCCC	√	√	√ √	√ √	√	√	√	√	√	25	" = 0.847 "

TABLE 5.5 PARAMETERS FOR USE IN RUNS WITH TESTING ERRORS

VARIABLE	Y_{11}	Y_{12}	Y_{13}	Y_{14}	Y_{15}	Y_{16}	Y_{21}	Y_{22}	Y_{23}	Y_{24}	Y_{25}	Y_{26}	α_T	α
DA	40	20	20	40	20	20	40	20	20	40	20	20	.20	.20
1σ's	2	2	2	2	2	2	2	2	2	2	2	2	.02	.02

FUNCTIONS	C_L	C_D	C_M	$C_{P_{TE1}}$	$C_{P_{TE2}}$	C_{RB}	$\lvert Y_{13}-Y_{22}\rvert$	$\lvert Y_{13}-Y_{23}\rvert$	$\lvert Y_{15}-Y_{25}\rvert$	$\lvert Y_{16}-Y_{26}\rvert$
TOL	.01	1.5×10^{-3}	3×10^{-3}	5×10^{-3}	5×10^{-3}		10	10	10	10
DEV	.04	.0060	.012	.02	.02	.002	20	20	20	20
1σ's	.001	3×10^{-4}	3×10^{-4}	5×10^{-4}	5×10^{-4}	5×10^{-5}	2	2	2	2

TOL = 10 (1σ) DEV = 4 TOL

TOL = 5 (1σ) DEV = 2 TOL

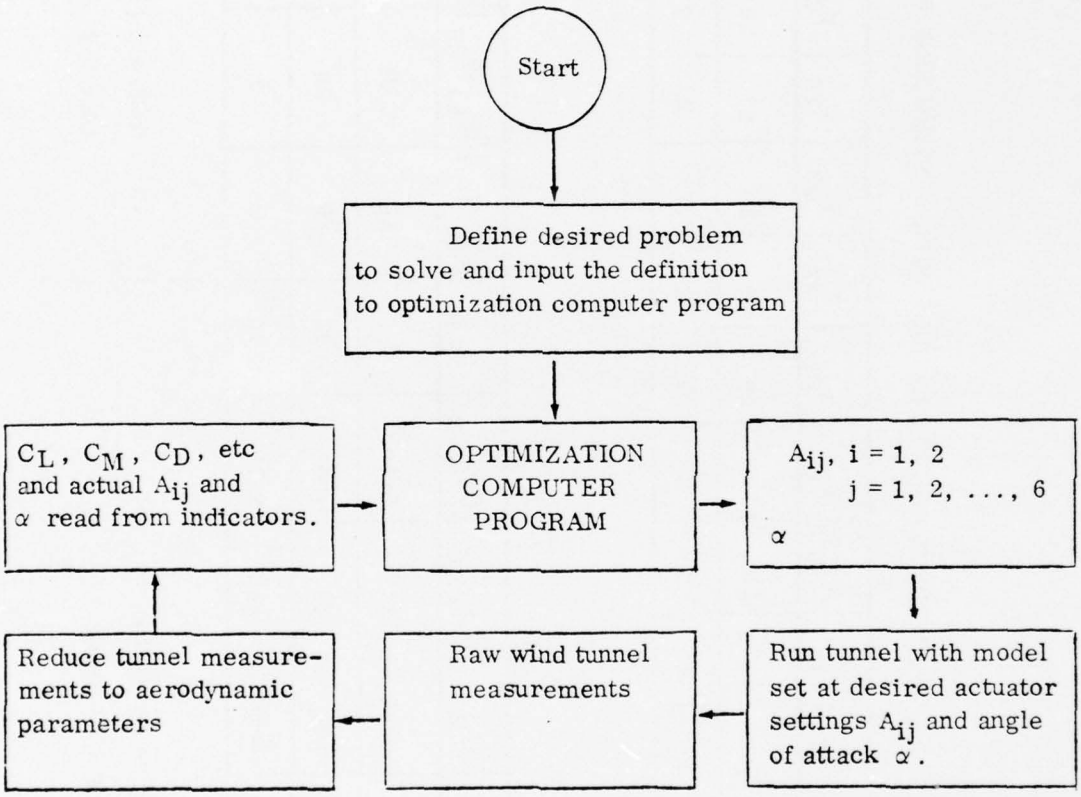

Figure 5.1 Flowchart of wind tunnel operation as controlled by the optimization computer program

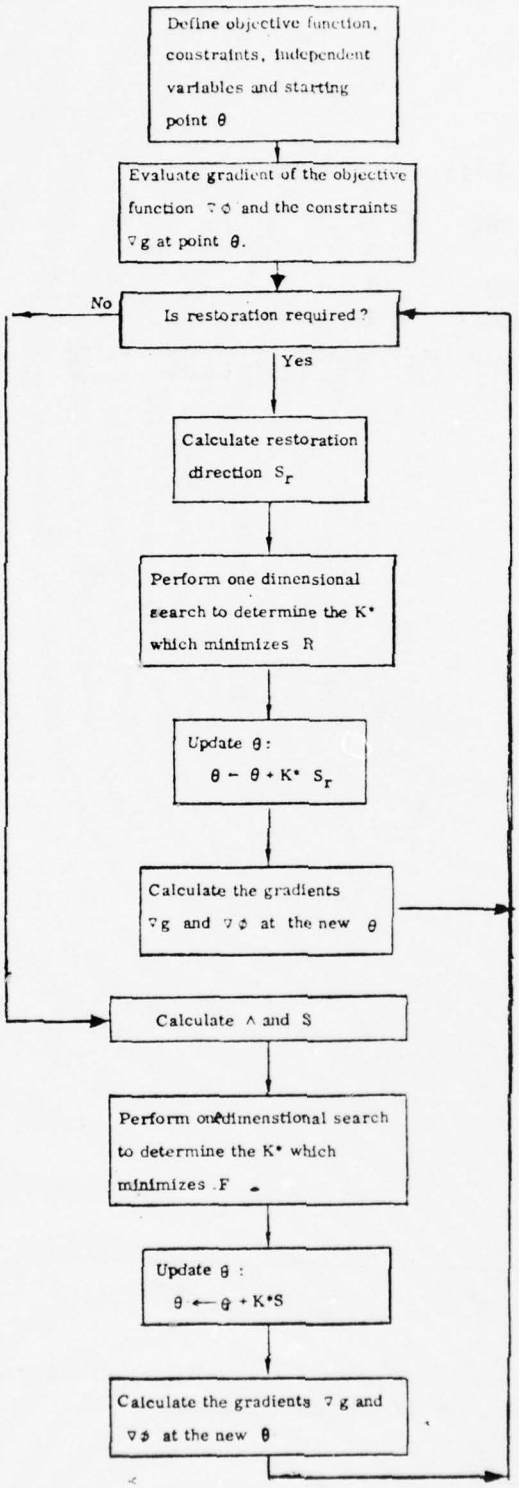

Figure 5.2 Flowchart of the Mathematical Optimization Procedure

LEGEND

Symbol	ΔA_{13}	δ_{13} (Degs)
□	-200	-5
○	0	0
△	200	5
+	400	10

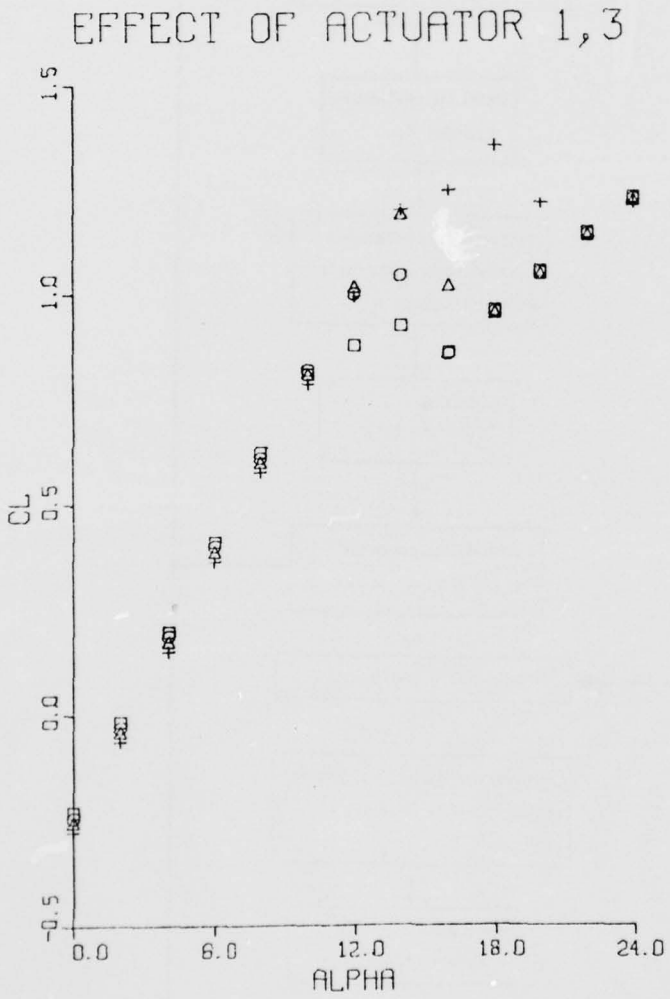

Figure 5.3a Effect of Inboard Leading Edge Deflection on Lift Curve, Pseudo Aerodynamic Module

LEGEND

Symbol	ΔA_{13}	δ_{13} (Degs)
□	-200	-5
○	0	0
△	200	5
+	400	10

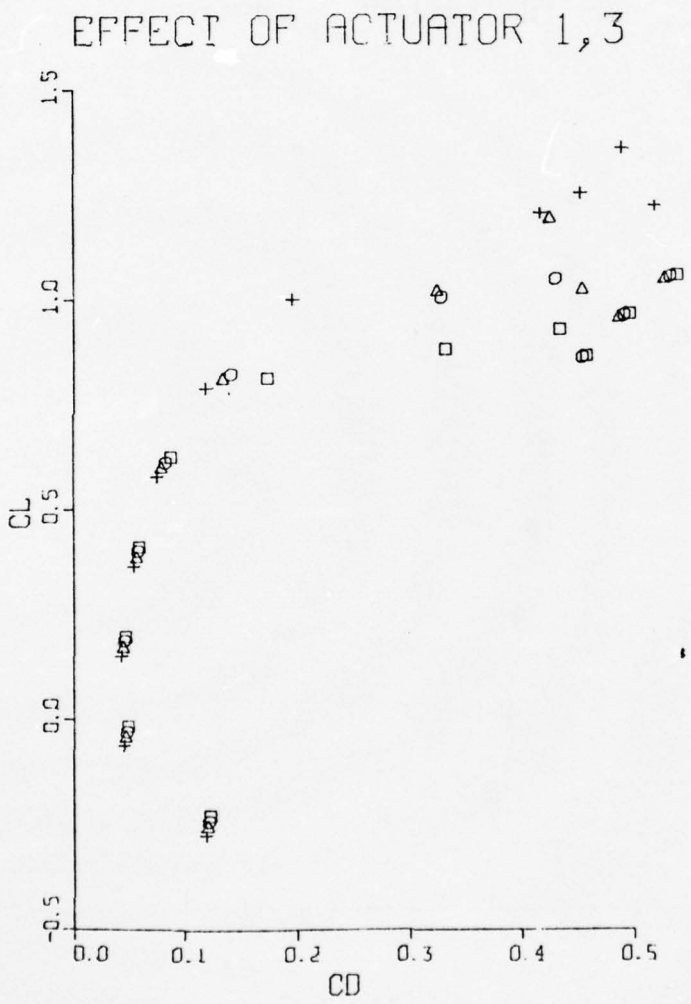

Figure 5.3b Effect of Inboard Leading Edge Deflection on Drag Polar, Pseudo Aerodynamic Module

LEGEND

Symbol	ΔA_{13}	δ_{13} (Degs)
□	-200	-5
○	0	0
△	200	5
+	400	10

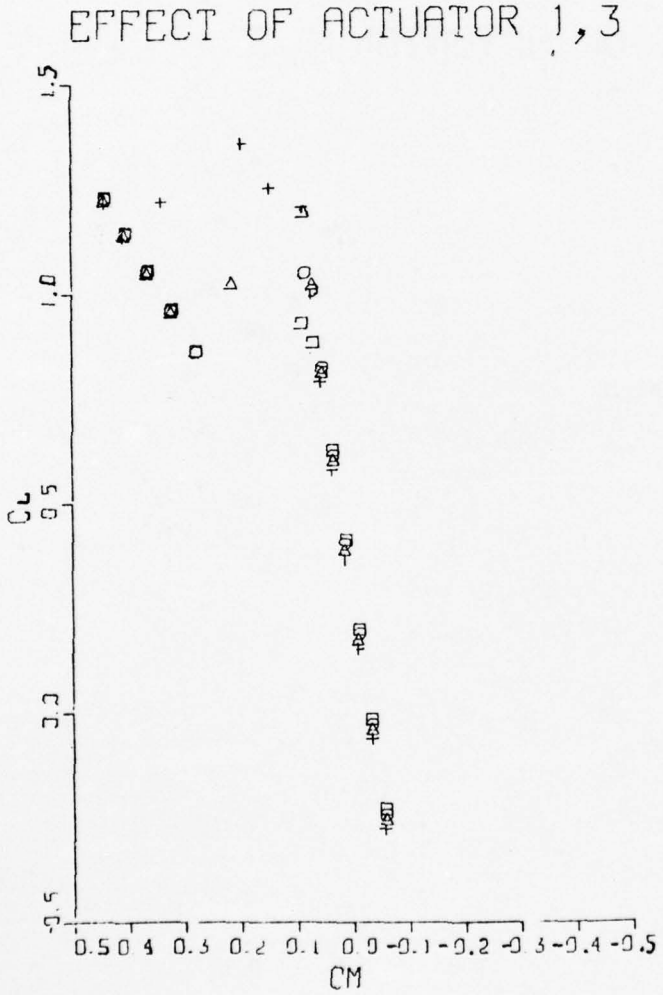

Figure 5.3c Effect of Inboard Leading Edge Deflection on Pitching Moment, Pseudo Aerodynamic Module

LEGEND

Symbol	ΔA_{14}	$(t/c)_{14}$
⊡	-500	0.08
⊙	0	0.09
△	500	0.10

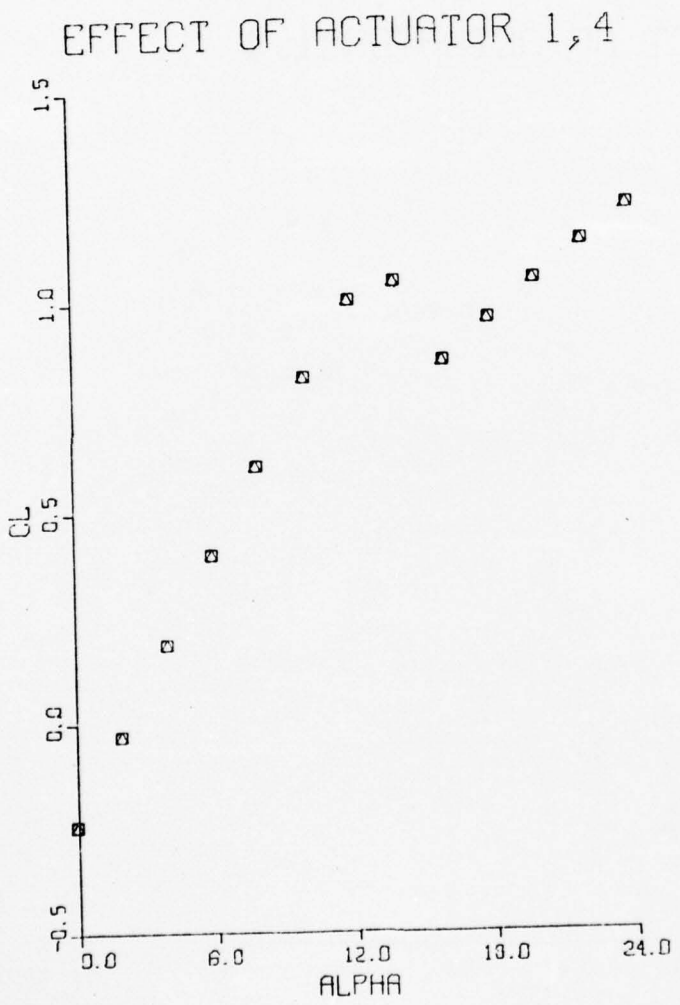

Figure 5.4a Effect of Inboard Upper Surface Humping on Lift Curve, Pseudo Aerodynamic Module

LEGEND

Symbol	ΔA_{14}	$(t/c)_{14}$
⊡	-500	0.08
⊙	0	0.09
△	500	0.10

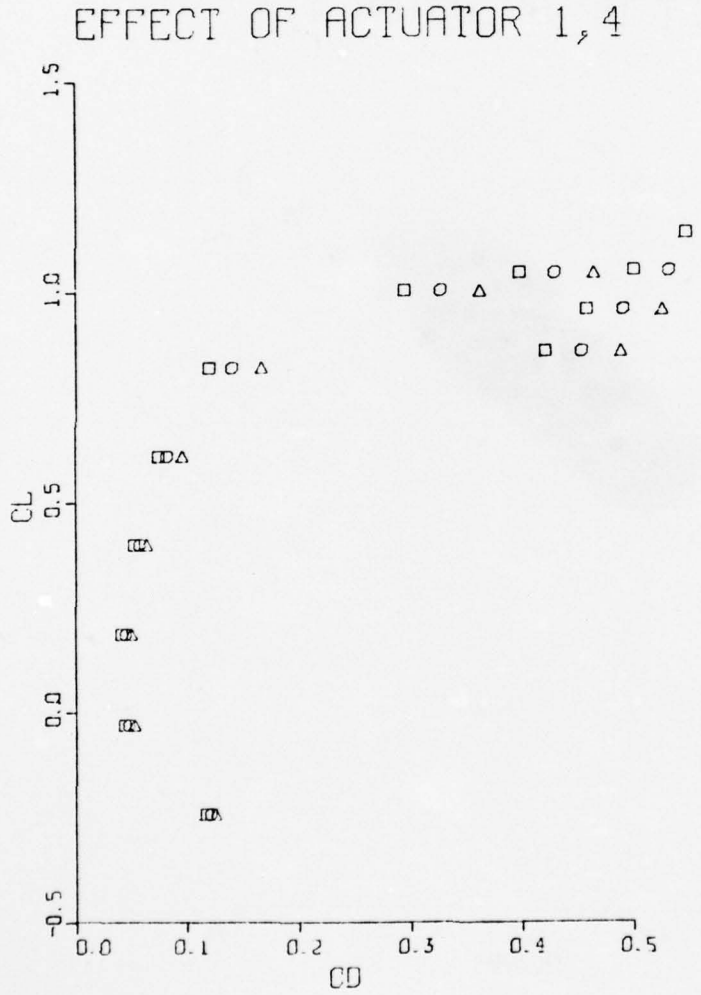

Figure 5.4b Effect of Inboard Upper Surface Humping on Drag Polar, Pseudo Aerodynamic Module

LEGEND

Symbol	ΔA_{14}	$(t/c)_{14}$
⊡	-500	0.08
⊙	0	0.09
△	500	0.10

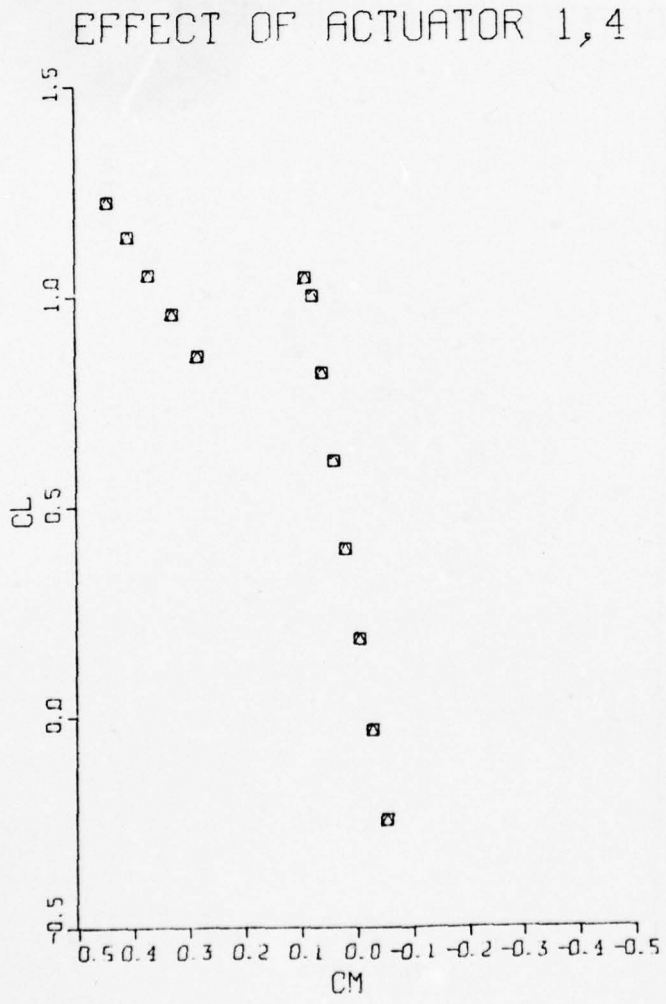

Figure 5.4c Effect of Inboard Upper Surface Humping on Pitching Moment, Pseudo Aerodynamic Module

LEGEND

Symbol	ΔA_{15}	δ_{15} (Deg)
⊡	-333	-10
⊙	0	0
△	333	10
+	667	20

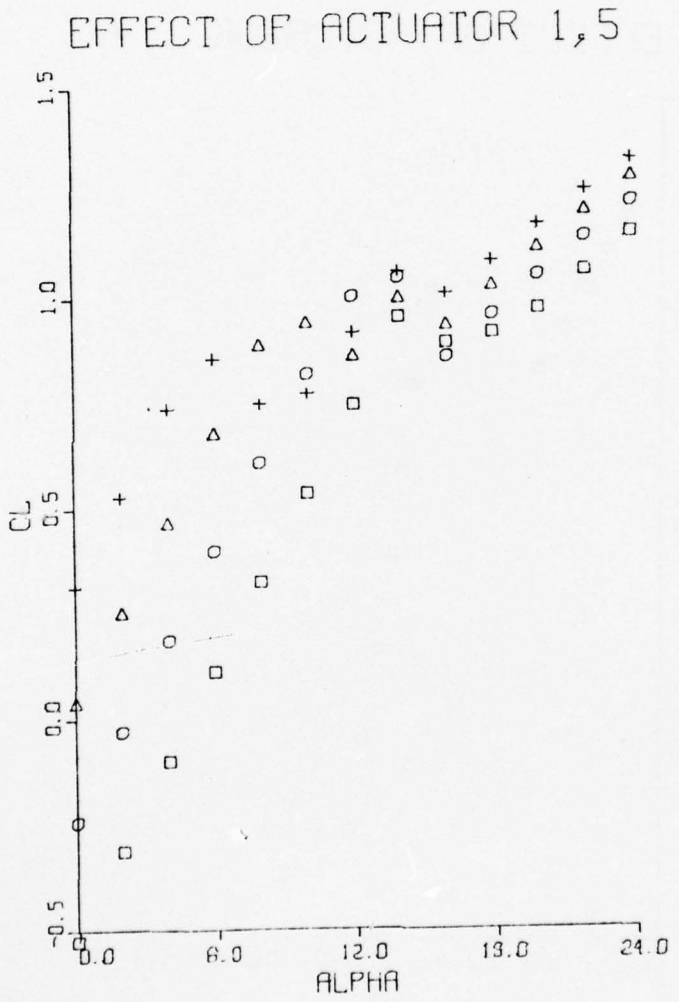

Figure 5.5a Effect of Inboard Trailing Edge Deflection of Lift Curve, Pseudo Aerodynamic Module

LEGEND

Symbol	ΔA_{15}	δ_{15}
⊡	-333	-10
⊙	0	0
△	333	10
+	667	20

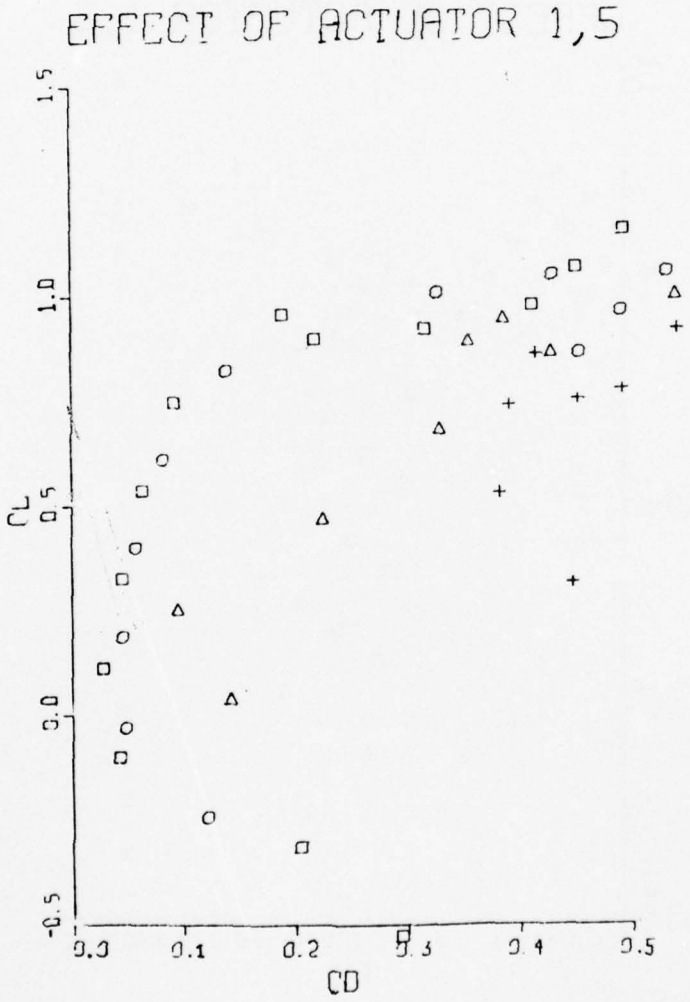

Figure 5.5b Effect of Inboard Trailing Edge Deflection on Drag Polar, Pseudo Aerodynamic Module

LEGEND

Symbol	ΔA_{15}	δ_{15}
⊡	-333	-10
⊙	0	0
△	333	10
+	667	20

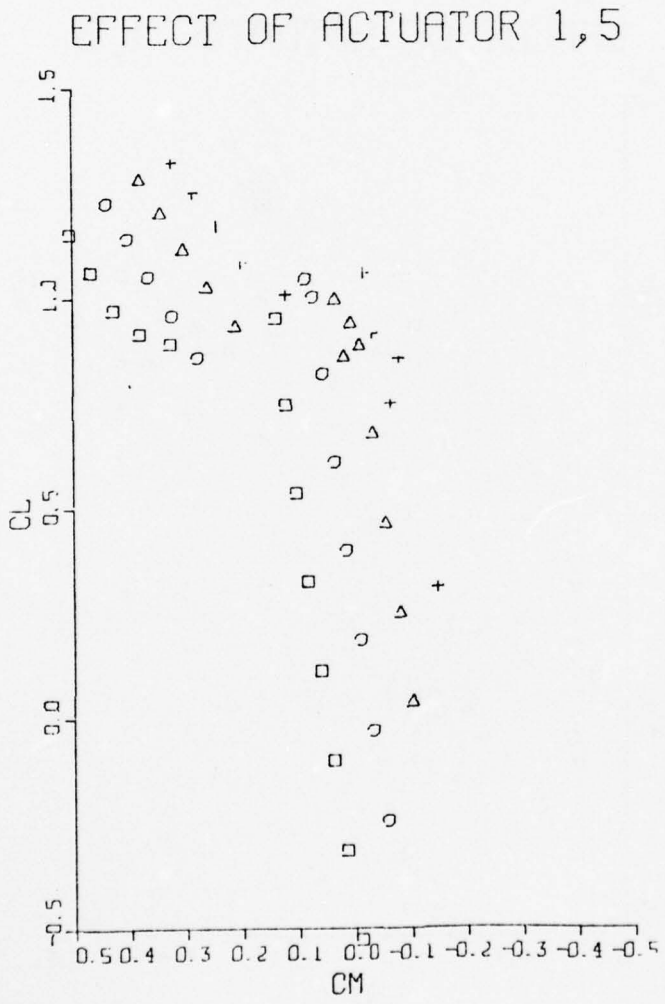

Figure 5.5c Effect of Inboard Trailing Edge Deflection on Pitching Moment, Pseudo Aerodynamic Module

LEGEND

Symbol	ΔA_{21}	$(R/c)_{21}$
△	-500	0.005
○	0	0.010
□	500	0.015

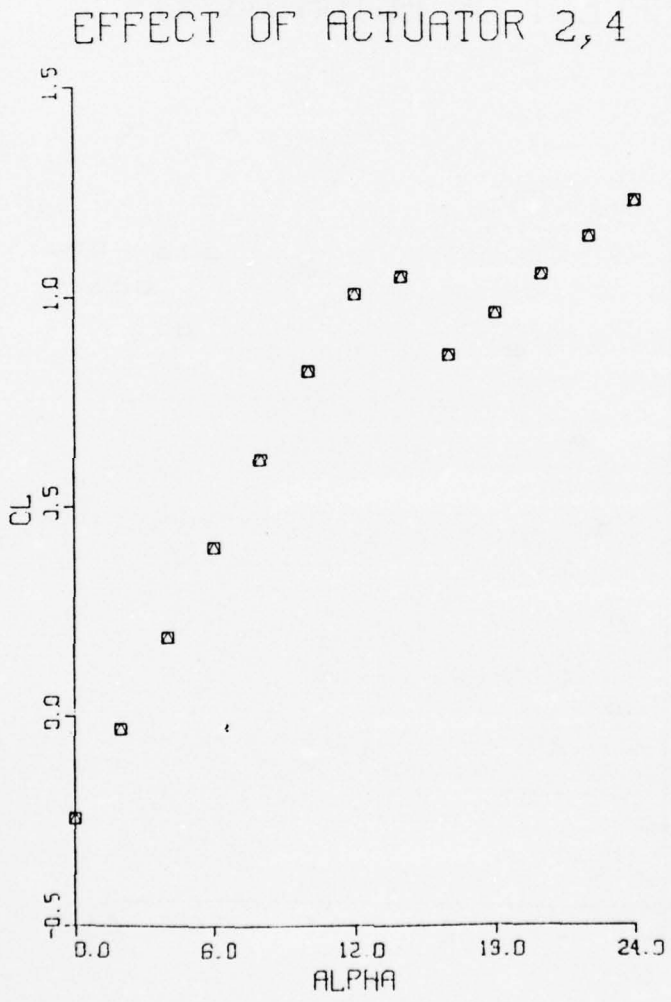

Figure 5.6a Effect of Outboard Leading Edge Radius on Lift, Pseudo Aerodynamic Module

LEGEND

Symbol	ΔA_{21}	$(R/c)_{21}$
△	-500	0.005
⊙	0	0.010
□	500	0.015

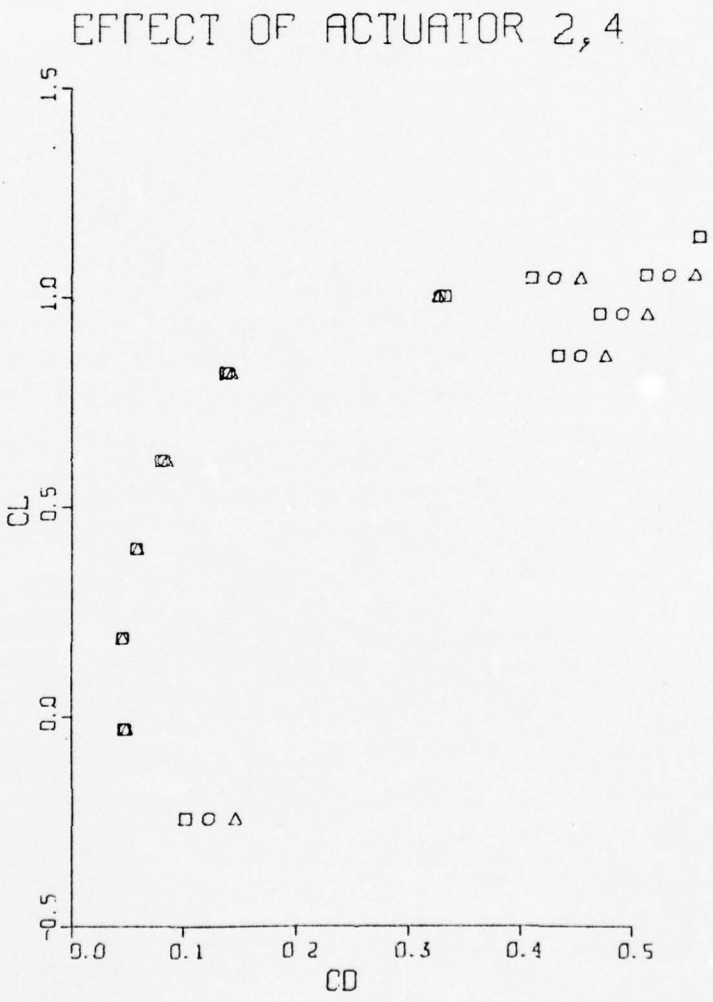

Figure 5.6b Effect of Outboard Leading Edge Radius on Drag Polar, Pseudo Aerodynamic Module

LEGEND

Symbol	ΔA_{21}	$(R/c)_{21}$
△	-500	0.005
⊙	0	0.010
⊡	500	0.015

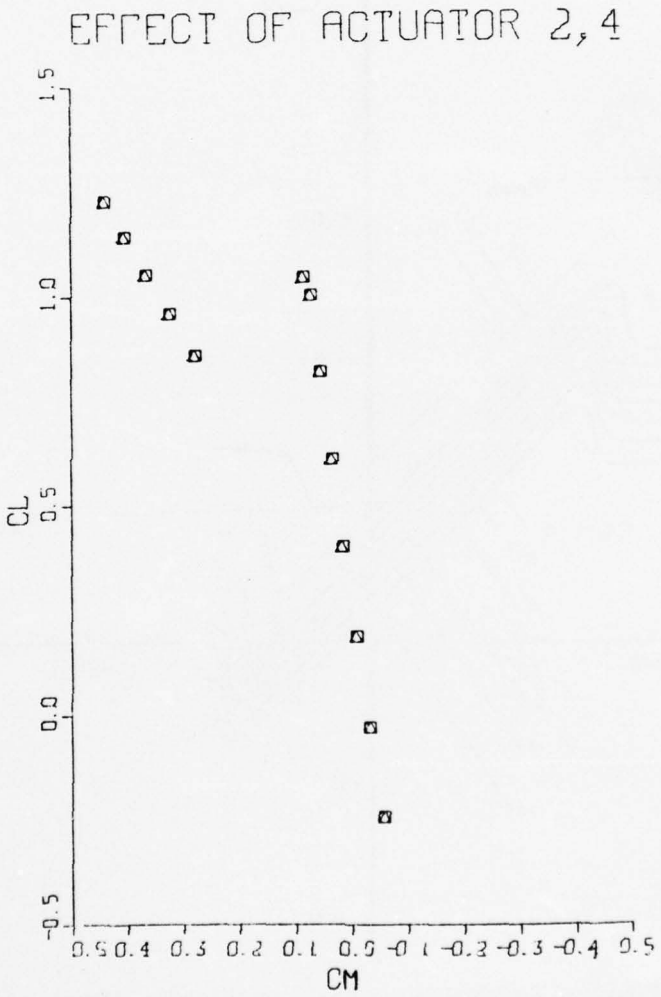

Figure 5.6c Effect of Outboard Leading Edge Radius on Pitching Moment, Pseudo Aerodynamic Module

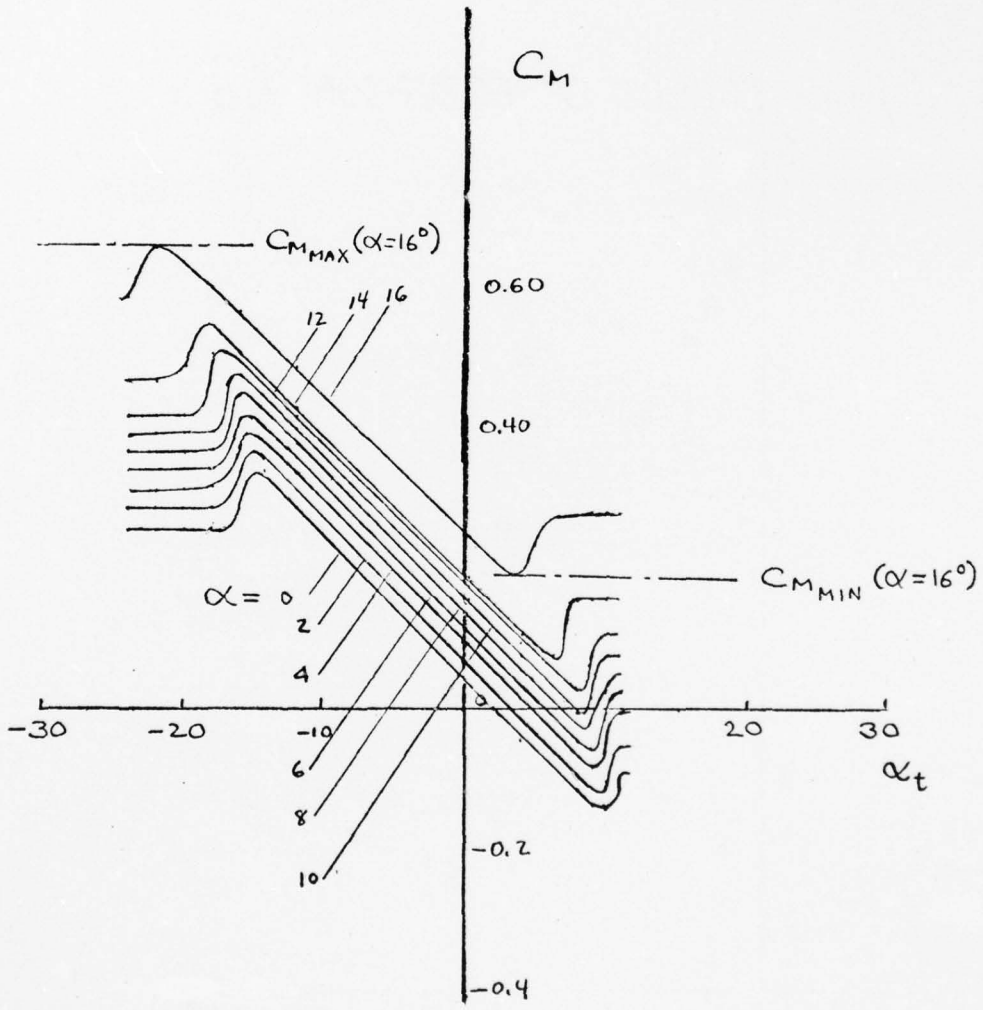

Figure 5.7 Effect of Tail Incidence Angle on Pitching Moment at Various Angles of Attack, from Pseudo Aerodynamic Model

AD-A039 085 GENERAL DYNAMICS SAN DIEGO CALIF CONVAIR AEROSPACE DIV F/G 1/3
SELF OPTIMIZING FLEXIBLE TECHNOLOGY WING PROGRAM, SEMISPAN WIND--ETC(U)
FEB 77 E S LEVINSKY, R H SCHAPPELLE N00014-76-C-0742
UNCLASSIFIED CASD-NSC-77-001 ONR-CR212-224-3 NL

2 OF 2
ADA039085

END
DATE FILMED
5-77

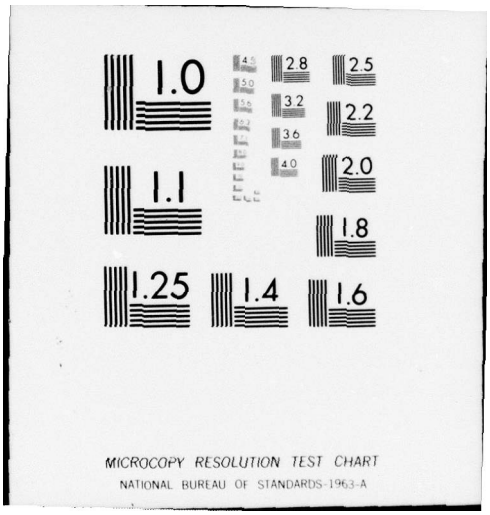
1.0
1.1
1.25
1.4
1.6
1.8
2.0
2.2
2.5
2.8
3.2
3.6
4.0
MICROCOPY RESOLUTION TEST CHART
NATIONAL BUREAU OF STANDARDS-1963-A

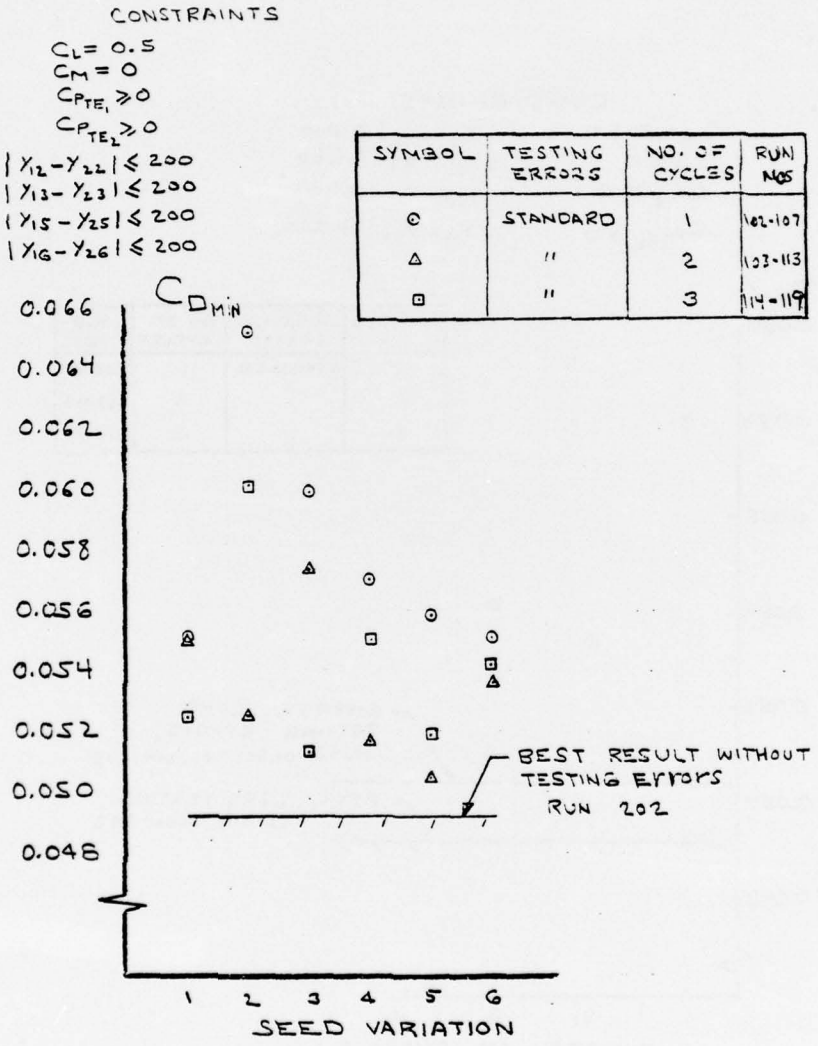

Figure 5.8 Effect of Seed Variation and Cycles on Convergence for Minimizing C_D

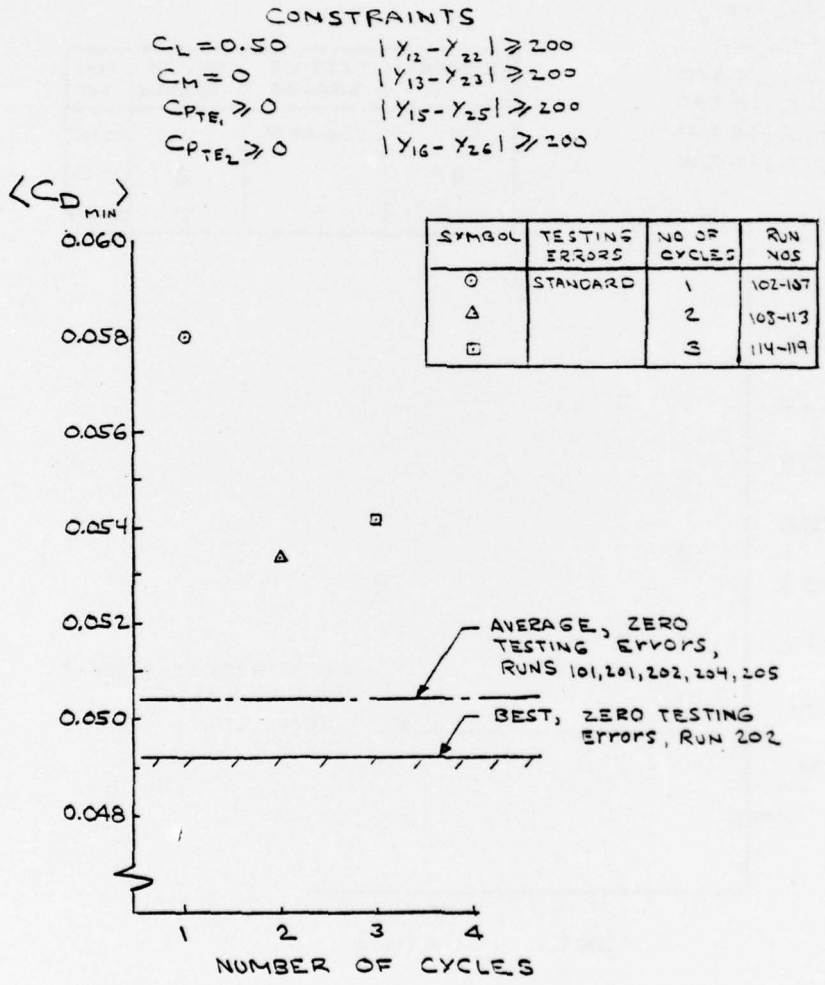

Figure 5.9 Effect of Number of Cycles on Average Value of Minimum C_D with Standard Testing Errors

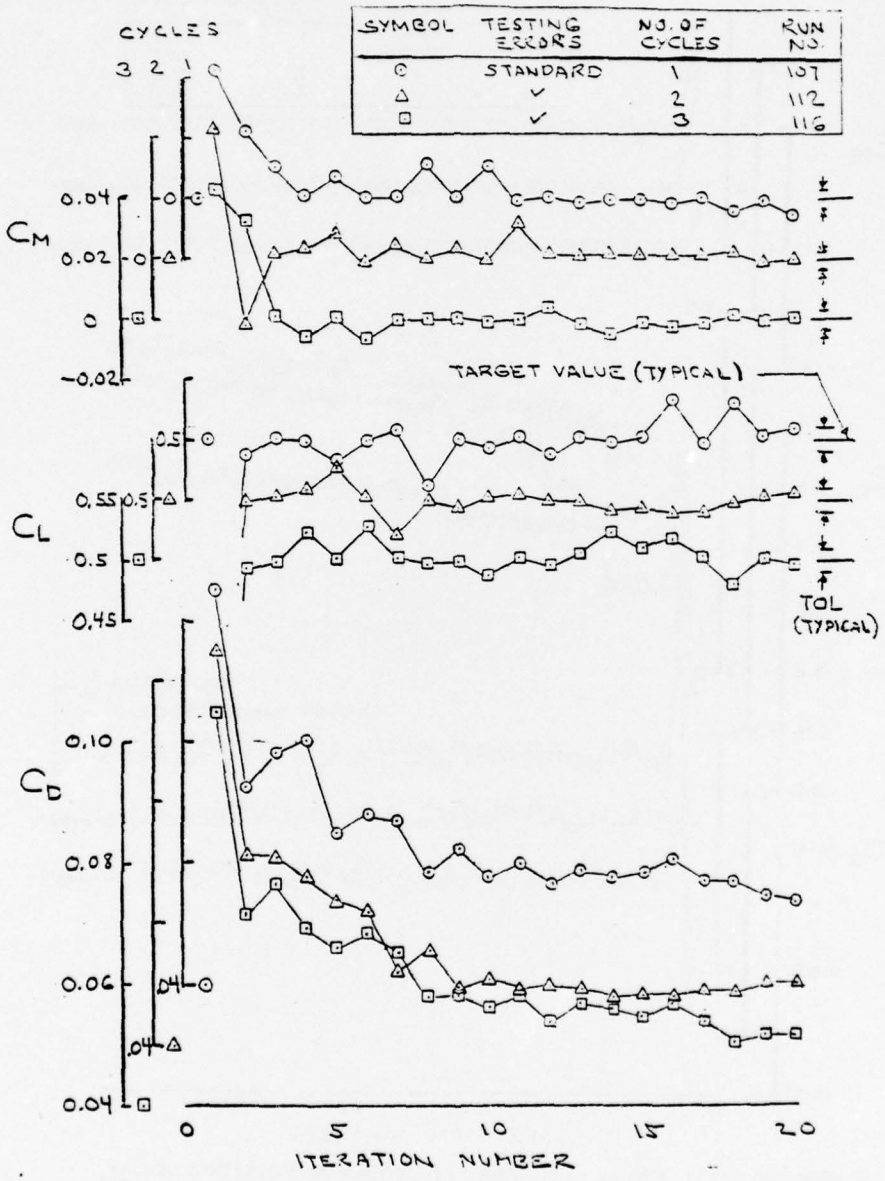

Figure 5.10 Effect of Number of Cycles on Variation of C_M, C_L and C_D During Iterations while Minimizing C_D

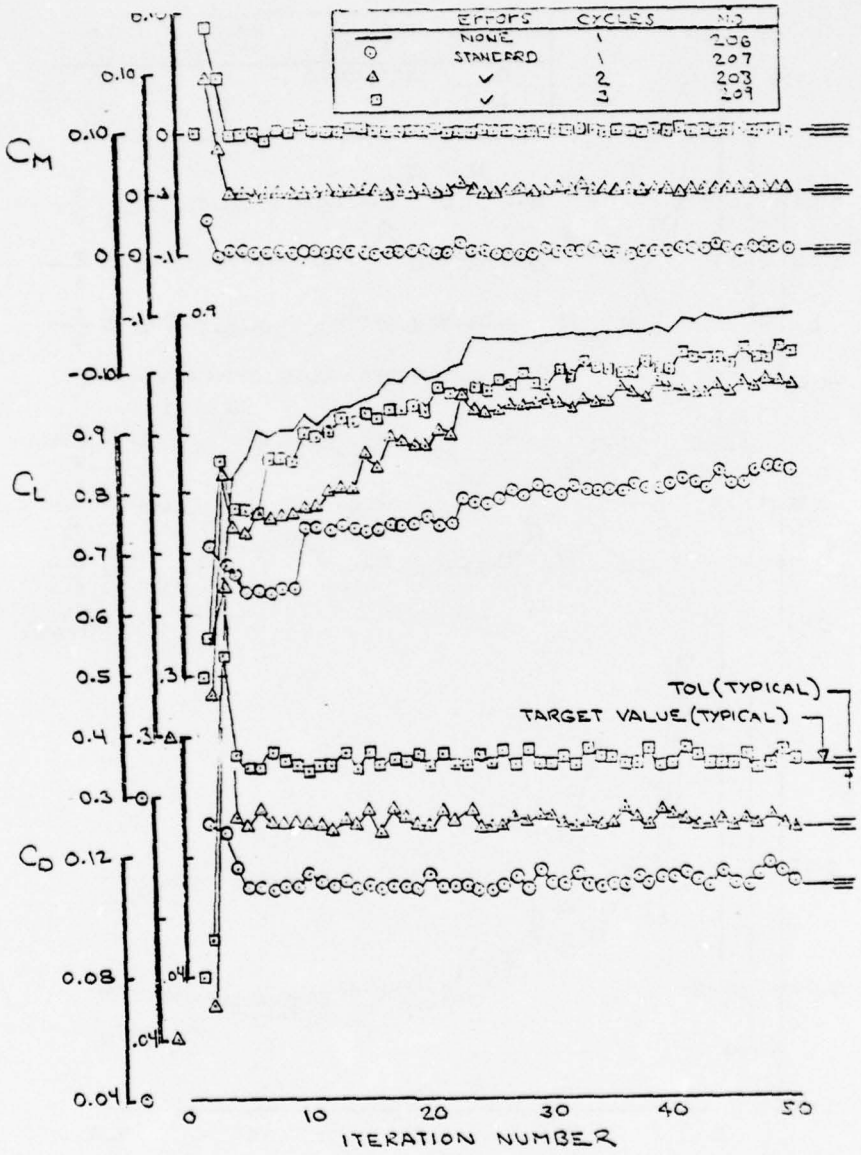

Figure 5.11 Effect of Number of Cycles on Variation of C_M, C_L and C_D During Iterations while Maximizing C_L

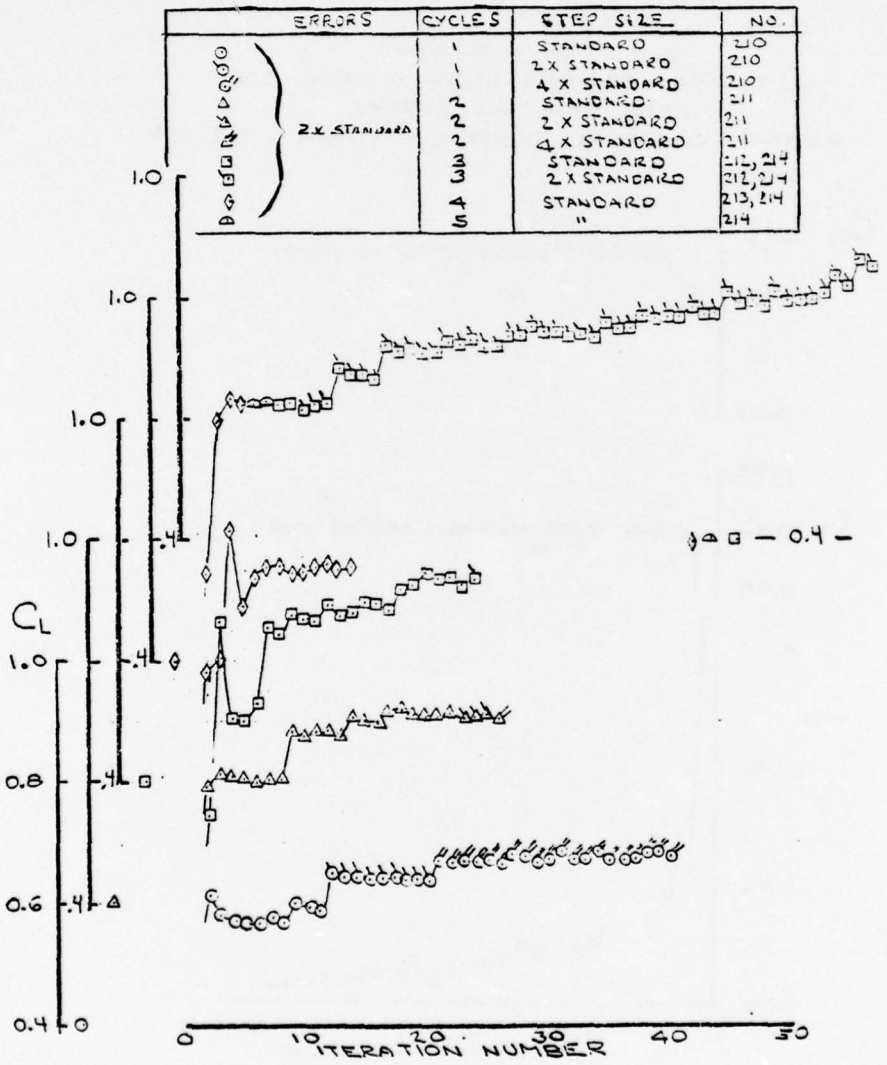

Figure 5.12 Effect of Cycling and of Perturbation Step Size on Convergence for Maximizing C_L with twice the Standard Testing Errors

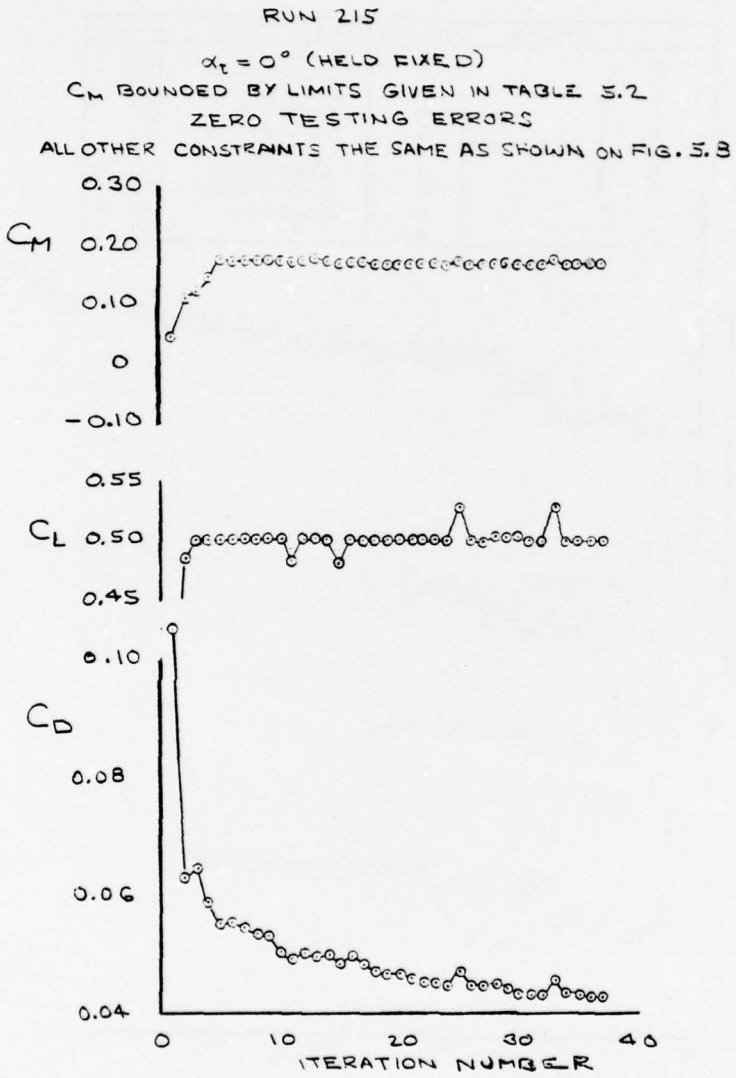

Figure 5.13 Convergence of Drag Minimization with Tabular Pitching Moment Constraints During Run 215

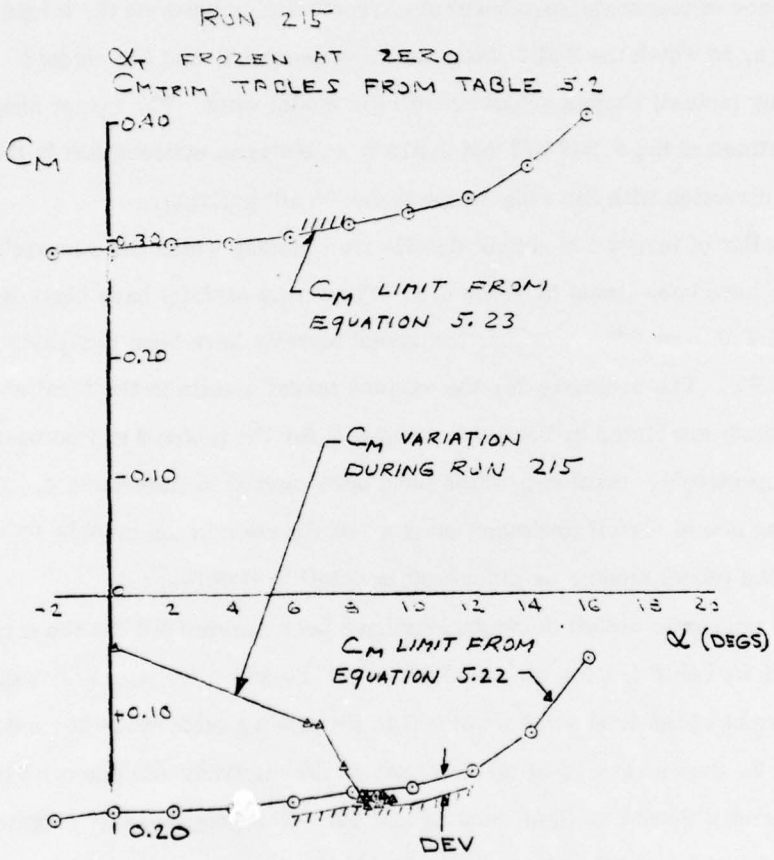

Figure 5.14 Variation of Pitching Moment with Relation to Tabular Bounds During Run 215

6.0 AERODYNAMIC ANALYSES

The purpose of the aerodynamic analyses has been to evaluate the relative correspondence of transonic aerodynamic characteristics between the target airfoil shapes, to which the SOFT Wing has been designed, and the closest approximating (actual) shapes achieved with the model wing. The target shapes have been defined at the 0.348 b/2 and 0.913 b/2 semispan stations and in the streamwise direction with the wing swept at the $\Lambda = 16°$ position.

The list of target and actual airfoils from among which the comparisons will be made have been listed in Table 6.1. The target airfoils have been designated by the prefix TACT or CSC, whereas the actual airfoils have been designated with the prefix SOFT. The ordinates for the various target airoils in the local chord plane (untwisted) are listed in Tables 6.2 and 6.3 for the inboard and outboard span stations, respectively. Section profiles have been plotted in Reference 4. The corresponding actual airfoil ordinates must await the completion of skin-on calibration of the wind tunnel model, as discussed in detail in Reference 4.

The transonic airfoil computations have been carried out for the target airfoil shapes in Table 6.1 for the condition $M = 0.80$ and $\alpha = 0°$ (corresponding to the component of the free stream normal to the leading edge at $\Lambda = 26°$ and $M = 0.89$). An available F. Bauer version of the Jameson nonlinear transonic potential theory program was used (based on Reference 23 and 24). The program was supplied to GDC by Mr. Ray Hicks of NASA (ARL), and includes boundary layer displacement effects in combination with relaxation methods to solve the finite difference equations.

To save on computer time, and because only a relative comparison of aerodynamic characteristics is to be made, only the first iteration in the relaxation procedure was taken and no boundary layer displacement effects were included. Figure 6.1, based on previous inviscid computations which were made with the same computer program for the airfoils presented in Reference 10, shows that the initial iteration approximates lift coefficient to within $\delta C_L \simeq 0.05$, at least for the three airfoils presented.

The single-iteration inviscid Bauer program computations of C_L, C_D and C_M for the target airfoil shapes are listed in Table 6.4. The correspondence between the calculated chordwise pressure distributions for the TACT W_{52} and creepless supercritical CSC airfoil sections (airfoils 1 and 3 inboard, and 2 and 4 outboard) has been indicated in Figures 6.2 and 6.3.

Following the determination of the actual airfoil shapes it is planned to perform the comparitive computations of C_L, C_D, C_M and C_P distribution versus chord. A newer faster version of the Bauer program, recently received from NASA (ARL), may be used for the actual airfoil computations (and possibly to further evaluate the accuracy of the single-iteration inviscid approximation). However, the "fast" Bauer program has as yet not been converted to run at GDC on the CDC CYBER 70 (or at GDE on the DEC 10).

TABLE 6.1 LIST OF AIRFOILS FROM AMONG WHICH COMPUTATIONS AND COMPARISONS WILL BE MADE WITH ONE-ITERATION INVICID BAUER PROGRAM

Status 0-not run 1-run completed	Case No.	Mach No.	Angle of Attack	Inboard Airfoil 0.348 b/2	Outboard Airfoil 0.913 b/2
1	1	0.80	0°	TACT, W_{52}	
1	2				TACT, W_{52}
1	3			CSC - (t/c=0.0958)	
1	4				CSC - (t/c=0.06122)
0	5			SOFT-1A (Matches #1)	
0	6				SOFT-2A (Matches #2)
0	7			SOFT-1B (Matches #3)	
0	8				SOFT-2B (Matches #4)
1	9-1			TACT, W_{52} (TE #5)	
1	9-2				TACT, W_{52} (TE #5)
1	9-3			TACT, W_{52} (TE #6)	
1	9-4				TACT, W_{52} (TE #6)
1	9-5			TACT, $W_{52}(\delta_{LE}=5°)$	
1	9-6				TACT, $W_{52}(\delta_{LE}=5°)$
1	9-7			TACT, $W_{52}(\delta_{LE}=10°)$	
1	9-8				TACT, $W_{52}(\delta_{LE}=10°)$
1	9-9			TACT, $W_{52}(\delta_{LE}=15°)$	
1	9-10				TACT, $W_{52}(\delta_{LE}=15°)$
0	10-1			SOFT-1C (Matches #9-1)	
0	10-2				SOFT-2C (Matches #9-2)
⋮	⋮			⋮	⋮
0	10-9			SOFT 1G (Matches #9-9)	
0	10-10				SOFT-2G (Matches #9-10)

TABLE 6.2 UNTWISTED ORDINATES, INBOARD TARGET AIRFOILS ~ INCHES (1/6'TH)

CASE	1		3		9-1		9-3		9-5		9-7		9-9	
%	z_u	z_L	z_u	z_L	z_u	z_L	z_u	z_L	z_u	z_L	z_u	z_L	z_u	z_L
0	0	0	0	0	SAME AS CASE #1	SAME AS CASE #1	SAME AS CASE #1	SAME AS CASE #1	-.2546	-.2546	-.5094	-.5094	-.7640	-.7640
.0222	.1394	-.1418							-.1108	-.3920	-.3607	-.6419	-.6111	-.8923
.0444	.1940	-.1987	.1511	-.1749					-.0511	-.4437	-.2961	-.6887	-.5411	-.9338
.0666	.2342	-.2406							-.0062	-.4810	-.2464	-.7211	-.4870	-.9618
.0888	.2666	-.2750							.0311	-.5105	-.2042	-.7458	-.4399	-.9815
.1110	.2939	-.3043	.2394	-.2527					.0628	-.5354	-.1680	-.7662	-.3991	-.9973
.1665	.3478	-.3622							.1281	-.5820	-.0917	-.8017	-.3114	-1.0215
.2775	.4244	-.4417							.2275	-.6386	-.0304	-.8357	-.1636	-1.0326
.5549	.5471	-.5676							.3982	-.7165	.2495	-.8652	.1003	-1.0144
1.1098	.6883	-.7209	.6120	-.6009					.6133	-.7959	.5383	-.8710	.4632	-.9460
1.6647	.7837	-.8206							.7491	-.8552	.7145	-.8898	.6799	-.9245
2.2196	.8514	-.8907	.7808	-.7675					.8410	-.9012	.8308	-.9114	.8201	-.9220
3.3294	.9413	-.9737	.8873	-.8785					.9413	-.9737	.9413	-.9737	.9413	-.9737
4.4392	.9977	-1.0257	.9620	-.9553										
5.5490	1.0328	-1.0528	1.0110	-1.0110										
6.6588	1.0536	-1.0627	1.0451	-1.0468										
7.7686	1.0632	-1.0632	1.0594	-1.0634										
8.8784	1.0603	-1.0514	1.0610	-1.0630										
9.9882	1.0472	-1.0248	1.0496	-1.0427										
11.0980	1.0257	-.9802	1.0274	-.9951										
12.2078	.9962	-.9136	.9924	-.9182										
13.3176	.9573	-.8064	.9425	-.8079										
13.8725	.9342	-.7305	.		.9331	-.7316	.9313	-.7334						
14.4274	.9080	-.6421	.8820	-.6676	.9052	-.6450	.9005	-.6497						
14.9823	.8776	-.5471			.8723	-.5525	.8651	-.5597						
15.5372	.8421	-.4521	.8662	-.5089	.8330	-.4612	.8183	-.4693						
16.0921	.8013	-.3633			.7864	-.3782	.7624	-.4022						
16.6470	.7558	-.2841	.7138	-.3425	.7329	-.3070	.6947	-.3451						
17.2019	.7047	-.2157			.6714	-.2490	.6159	-.3045						
17.7568	.6441	-.1594	.6001	-.1903	.5975	-.2060	.5209	-.2826						
18.3117	.5722	-.1170			.5098	-.1793	.4080	-.2812						
18.8666	.4921	-.0894	.4559	-.0728	.4100	-.1716	.2746	-.3070						
19.4215	.3944	-.0792			.2879	-.1858	.1148	-.3589						
19.9764	.2903	-.0886	.2791	-.0416	.1554	-.2235	-.0659	-.4448						
20.5313	.1687	-.1210			-.0044	-.2941	-.2895	-.5792						
21.0862	.0386	-.1831	.0572	-.1282	-.1796	-.4014	-.5337	-.7555						
21.6411	-.1083	-.2797			-.3778	-.5491	-.8186	-.9899						
22.1960	-.2584	-.4251	-.2427	-.3665	-.5886	-.7553	-1.1291	-1.2536						

TABLE 6.3 UNTWISTED ORDINATES, OUTBOARD TARGET AIRFOILS ~ INCHES (1/6TH SCALE)

CASE	2		4		9-2		9-4		9-6		9-8		9-10	
η	z_U	z_L	z_U	z_L	z_U	z_L	z_U	z_L	z_U	z_L	z_U	z_L	z_U	z_L
0	0	0	0	0	▲	▲	▲	▲	-.2271	-.2271	-.4542	-.4542	-.6813	-.6813
.01536	.0573	-.0611							-.1671	-.2854	-.3916	-.5099	-.6157	-.7341
.0307	.0777	-.0843	.0633	-.0802					-.1437	-.3057	-.3651	-.5271	-.5866	-.7486
.0461	.0940	-.1007							-.1238	-.3185	-.3416	-.5364	-.5592	-.7539
.0614	.1076	-.1147							-.1067	-.3291	-.3211	-.5434	-.5354	-.7578
.0768	.1196	-.1271	.1003	-.1098					-.0918	-.3386	-.3033	-.5500	-.5147	-.7615
.1152	.1434	-.1525							-.0602	-.3561	-.2638	-.5597	-.4674	-.7633
.1919	.1755	-.1858							-.0112	-.3733	-.1995	-.5608	-.3869	-.7482
.3839	.2246	-.2405							.0719	-.3932	-.0809	-.5460	-.2337	-.6988
.7678	.2850	-.3073	.2681	-.2604					.1886	-.4037	.0921	-.5001	-.0043	-.5965
1.1516	.3260	-.3502							.2702	-.4060	.2145	-.4617	.1588	-.5175
1.5355	.3559	-.3817	.3477	-.3385					.3278	-.4098	.2997	-.4379	.2716	-.4660
2.3033	.3992	-.4227	.3962	-.3900					.3957	-.4263	.3922	-.4298	.3886	-.4333
3.0710	.4279	-.4476	.4306	-.4259										
3.8388	.4476	-.4619	.4525	-.4525										
4.6065	.4608	-.4682	.4681	-.4667										
5.3743	.4694	-.4694	.4714	-.4715										
6.1420	.4742	-.4659	.4685	-.4685										
6.9098	.4759	-.4574	.4593	-.4532										
7.6775	.4745	-.4435	.4440	-.4269										
8.4453	.4700	-.4204	.4224	-.3910										
9.2130	.4617	-.3826	.3945	-.3439	SAME AS CASE #2	SAME AS CASE #2	SAME AS CASE #2	SAME AS CASE #2	SAME AS CASE #2	SAME AS CASE #2	SAME AS CASE #2	SAME AS CASE #2	SAME AS CASE #2	SAME AS CASE #2
9.5969	.4557	-.3538			.4553	-.3544	.4540	-.3557						
9.9808	.4482	-.3154	.3619	-.2946	.4465	-.3171	.4431	-.3205						
10.3646	.4384	-.2666			.4532	-.2698	.4300	-.2749						
10.7485	.4259	-.2137	.3201	-.2419	.4204	-.2193	.4103	-.2294						
11.1324	.4104	-.1664			.4015	-.1754	.3846	-.1922						
11.5163	.3911	-.1282	.2743	-.1905	.3773	-.1420	.3510	-.1683						
11.9001	.3671	-.0995			.3472	-.1195	.3088	-.1578						
12.2840	.3355	-.0806	.2218	-.1409	.3079	-.1083	.2557	-.1605						
12.6679	.3005	-.0729			.2629	-.1106	.1922	-.1812						
13.0518	.2578	-.0739	.1561	-.0980	.2082	-.1235	.1142	-.2174						
13.4356	.1973	-.0866			.1328	-.1511	.0131	-.2709						
13.8195	.1408	-.1092	.0763	-.0885	.0610	-.1890	-.0941	-.3441						
14.2034	.0665	-.1368			-.0382	-.2415	-.2351	-.4384						
14.5873	-.0195	-.1812	-.0268	-.1365	-.1504	-.3121	-.3958	-.5572						
14.9711	-.1172	-.2421			-.2798	-.4048	-.5847	-.7097						
15.3550	-.2248	-.3415	-.2104	-.2800	-.4241	-.5408	-.7980	-.9147						

TABLE 6.4 SUMMARY OF TRANSONIC FLOW COMPUTATIONS

One-Iteration, Inviscid, Bauer Computation

M=0.80, α =0°

Case No.	C_L	C_D	C_M	Airfoil
1	0.9593	0.00534	-0.2286	TACT (Inboard)
2	0.9994	0.00501	-0.2385	TACT (Outboard)
3	0.9284	0.00421	-0.2220	CSC- (Inboard)
4	0.8478	0.00456	-0.1979	CSC- (Outboard)
9-1	1.4102	0.01441	-0.3243	TACT+TE#5 (Inboard)
9-2	1.3852	0.01456	-0.3231	TACT+TE#5 (Outboard)
9-3	1.9690	0.03860	-0.4438	TACT+TE#6 (Inboard)
9-4	2.0006	0.04908	-0.4636	TACT+TE#6 (Outboard)
9-5	0.9495	0.00281	-0.2319	TACT, δ_{LE}=5° (Inboard)
9-7	0.9379	0.00218	-0.2353	TACT, δ_{LE}=10° (Inboard)
9-9	0.9275	0.00297	-0.2384	TACT, δ_{LE}=15° (Inboard)
9-6	0.9853	0.00043	-0.2435	TACT, δ_{LE}=5° (Outboard)
9-8	0.9673	0.00085	-0.2490	TACT, δ_{LE}=10° (Outboard)
9-10	0.9498	0.00018	-0.2527	TACT, δ_{LE}=15° (Outboard)

Airfoils from Reference 10

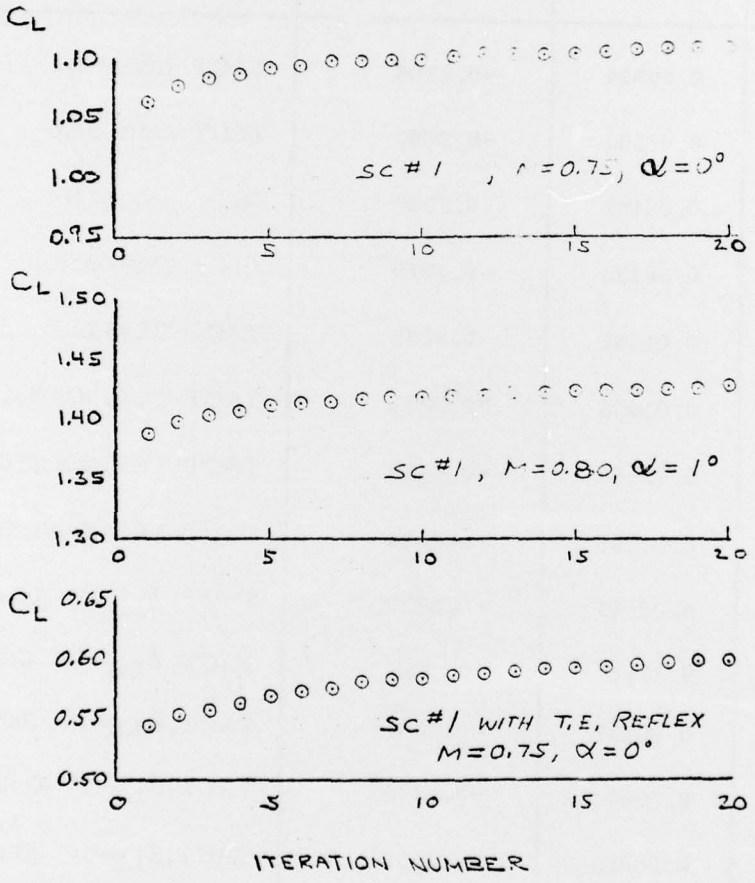

Figure 6.1 Variation of Lift Coefficient with Iteration Number for Bauer Computer Program, Inviscid Analysis

Symbol	Case	Airfoil	C_L	C_M	C_D	α_{0L}
	I	TACT, W_{52}, 0.348b/2	0.9593	-0.2286	0.00534	-5.044°
	II	CSC, 9.58%	0.9284	-0.222	0.00421	-4.878°

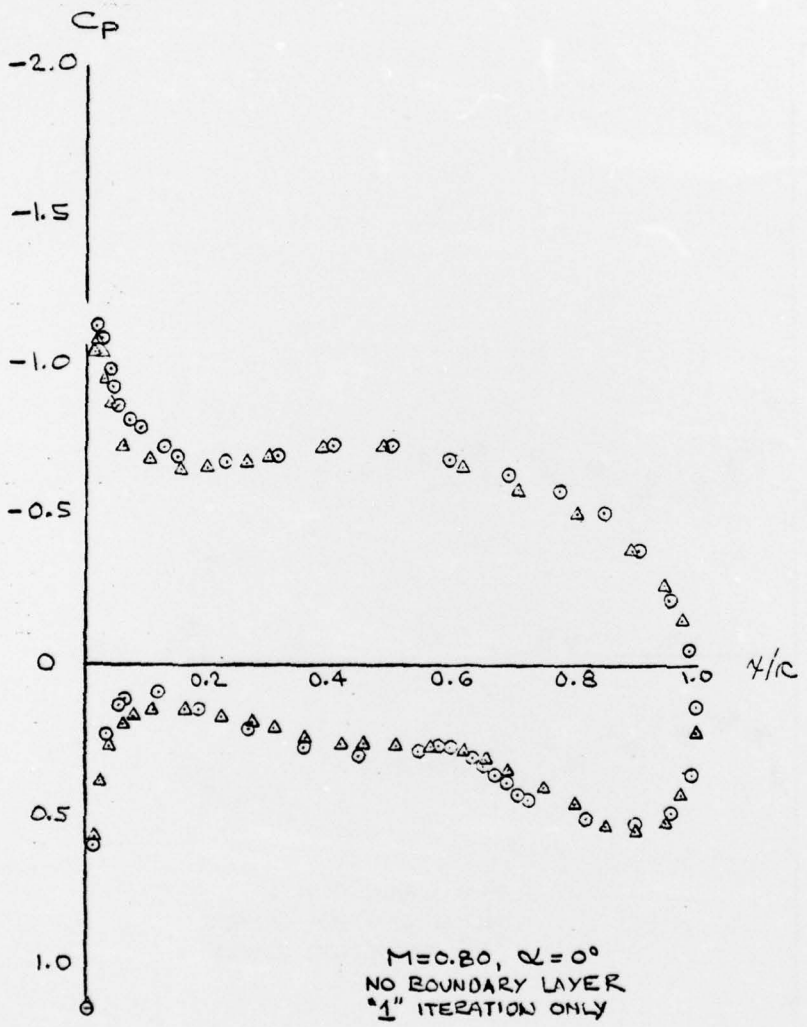

Figure 6.2 Comparison of TACT and CSC Airfoil Characteristics from Bauer Version of Jameson Program, Inboard Station

Symbol	Case	Airfoil	C_L	C_M	C_D	α_{0L}
⊙	II	TACT, W_{52}, 0.913 b/2	0.999	-.2385	.0050	-5.380
⧈	4	CSC, 6.12%	0.8478	-.1979	.0046	-4.54

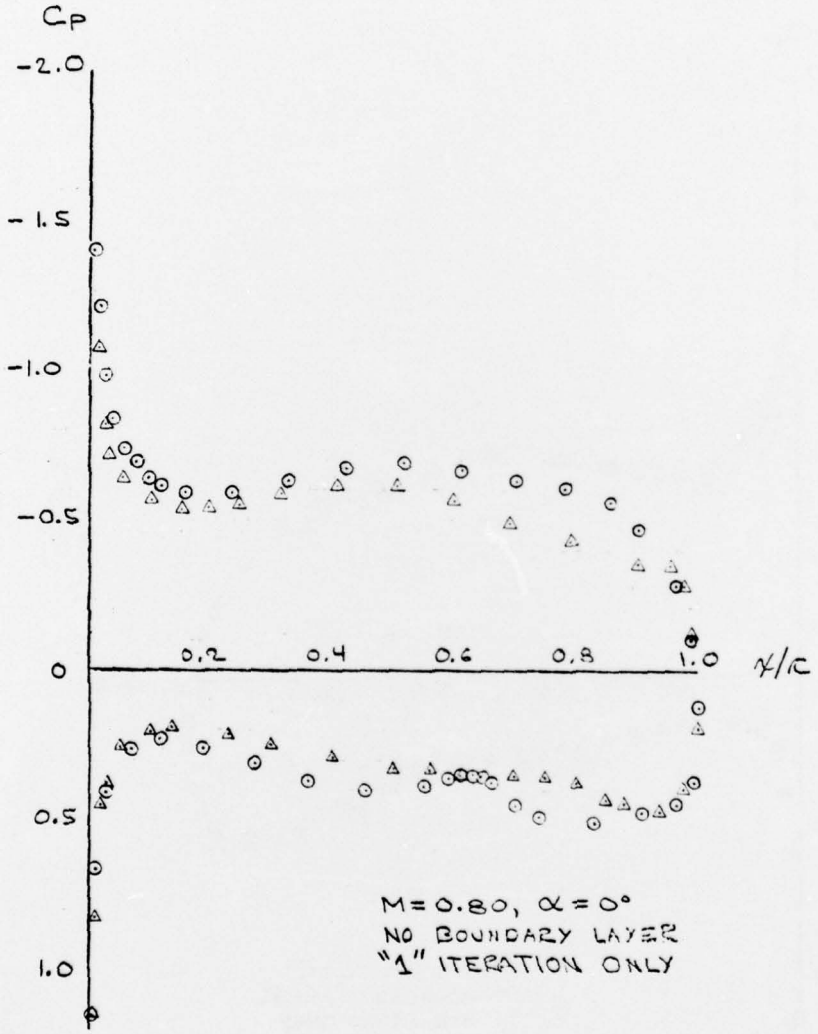

Figure 6.3 Comparison of TACT and CSC Airfoil Characteristics from Bauer Version of Jameson Program, Outboard Station

7.0 CONCLUSIONS AND RECOMMENDATIONS

The present interim technical report has dealt with progress made under Phase I of the Self Optimizing Flexible Technology Wing wind tunnel program. The Phase I investigation, which included preliminary and detailed design of a 1/6'th scale semi-span model; loads, stress and flutter analyses; fabrication of a kinematic model, the computer programming of an optimization program; simulation studies; and various aerodynamic analyses has been completed. The Phase II program, which deals with model fabrication and testing at AEDC, is now well underway, and plans call for testing in mid summer of 1977. Specific conclusions and recommendations with regard to the Phase I investigation are listed below.

(i) Detailed design of the wind tunnel model has been completed and fabrication is currently underway. The model was designed with the planform, thickness distribution and twist distribution of the TACT I wing and includes 12 independent hydraulic actuation systems, three flexible skin panels with sliding joints and a split spar. The articulation is sufficiently general to encompass proposed AFTI-111 wing contours, as well as transonic wings with more general camber and thickness variations, and provides for conformal spanwise as well as chordwise changes in wing shape. The design permits increasing the number of independent actuators to 20 and inserting small chord extensions between the spars, with only minor rework, to even further increase the generality of the model.

(ii) All design objectives appear to have been met, except that problems are anticipated in achieving differential twist variations along the span (primarily along the leading edge, but also possibly along the trailing edge), and the articulation may be severely limited for the inboard trailing actuators when the wing is swept at 58°. In addition, the trailing edge thickness was compromised at 1% chord (instead of the 0.75% chord desired), and fasteners were allowed to protrude above the skin, because of problems in designing the sliding trailing edge joints

(iii) The stress analysis of the split spar design showed an adequate minimum safety factor SF=5.7, based on ultimate, for the primary wing structure at the nominal test dynamic pressure q=500 lbs/ft^2. Safety factors have also been shown to be marginally adequate for the various lever arms and brackets comprising the actuators (lowest SF=3.9, based on ultimate). On the other hand, it has proven difficult to estimate the maximum stress levels in the flexible skin panels. It is therefore recommended that up to 50 strain gages be implanted on the skins during the pretest calibrations and the maximum skin deflection limits be established.

(iv) The wing flutter analysis has predicted positive aerodynamic damping at transonic test conditions for $q \leq 1250$ lbs/ft^2. Thus, no flutter problems are anticipated for the actual dynamic pressure levels($q \sim 500$ lbs/ft^2). However, because of the unusual wing design, and because of the many simplifying approximations in the flutter analysis, it is recommended that static deflection checks be made during the pretest calibrations (to verify the stiffness assumptions), and that aerodynamic damping runs at gradually increasing q levels be made at the beginning the the test.

(v) Preliminary estimates of panel flutter have shown the upper rear skin panel to be somewhat marginal. It is therefore recommended that two strain gages be premanently implanted on this panel, and that the corresponding RMS strain reading be monitored during the test for any indication of panel flutter.

(vi) A wind tunnel scale kinematic model with 10 actuators has been fabricated and was used to verify the function of the leading and trailing edge actuators and the form of the wing shapes produced. Conclusions reached through operation of the kinematic model were that reasonably good transonic (and possible low speed) airfoil sections could be produced with the present design, and that the anticipated level of articulation should be obtainable, except that wrinkling of

the leading edge skin was observed when differential deflection of the leading edge actuators was attempted. In addition, the push rod (for changing leading edge radius) was found to be too flexible, and was also observed to unport from the skin when the leading edge was deflected downward. The design of the push rod has been modified and the calibration procedure has been altered to accommodate the above difficulties. However, problems are still anticipated for leading edge differential twist.

The kinematic model may also be used for estimating actuator force (and hydraulic pressure) requirements and for predicting areas of skin stress concentration and skin stress levels, both unloaded and loaded. However, funding and scheduling considerations prevented these applications from being carried out. It is recommended that future SOFT Wing programs take fuller advantage of the analytical tools which the kinematic model offers.

(vii) The 2D optimization program has been completely rewritten for the SOFT Wing test. The new optimization program allows up to 20 independent variables (actuators, angle of attack, tail incidence) to be involved in the optimization, and permits the merit function being optimized to be selected from among 18 different aerodynamic and geometric functions being measured. The remaining 17 functions may then be selected as equality or inequality constraints. The program features a simple means of freezing (locking out) various independent variables, in order to represent wings with reduced articulation and includes a provision for tabular limits on pitching moment when optimizing with a fixed tail. The program may be controlled interactively from a remote video or teletype terminal.

The optimization program has been demonstrated on a DEC 10 computer, and delivery to AEDC/ARO has been carried out.

(viii) A series of test simulation and check out runs were made on the DEC 10 by linking the optimization program to a Pseudo-Aerodynamic Module for computing aerodynamic coefficients. The majority of the simulations dealt with maximizing C_L or minimizing C_D, subject to equality constraints on C_D or C_L, respectively, and on C_M, and to inequality constraints on $C_{P_{TE_1}}$, $C_{P_{TE_2}}$ and on differential actuator deflection. These simulations, which were made with all twelve actuators active and also with variable tail incidence angle, demonstrated reasonable convergence of the optimization procedure, even with standard testing errors, provided that the various control parameters could be fine tuned during interactive control.

(ix) Convergence was not demonstrated for similar optimization problems with testing errors, when the tail was held fixed and the equality constraint on C_M was replaced by tabular inequality constraints to limit C_M between values for which adequate trail trim control was available.

(x) It is recommended that the simulations be completed for the problems with a fixed tail and with tabular limits on C_M. In addition, it is strongly recommended that no optimization problems of any kind be attempted in the wind tunnel, until adequate simulation and fine tuning of the optimization parameters has been achieved including effects of testing errors This is required to insure that valuable wind tunnel occupancy time will not be squandered on procedures which could be carried out at very low cost on the DEC 10.

(xi) The "fast" Bauer computer program should be converted for running on the DEC 10 and used to evaluate the accuracy of the one-iteration inviscid approximation made in the aerodynamic analyses.

8.0 REFERENCES

1. "A Self Optimizing Flexible Technology Wing Program, Semispan Wind Tunnel Test of a Generalized Variable Geometry Wing Panel, Phase I Model Design and Aerodynamic Analyses, Technical," General Dynamics Convair Division Proposal GDC CM 75-2410, 14 November 1975.

2. "Minutes and Presentations - SOFT Wing Prefabrication, Planning and Coordination Meeting, Held at WPAFB, Ohio, 14 October 1976," General Dynamics Convair Division Aerodynamics Memo AM-76-CRAD-16, 15 October 1976.

3. "Minutes - SOFT Wing Pretest and Computer Programming Conference," General Dynamics Convair Division Aerodynamics Memo AM-76-CRAD-22, 20 December 1976.

4. Levinsky, E.S.; McClain, A. A., and Schappelle, R. H., "Pretest Report, Wind Tunnel Test of a Self-Optimizing Flexible Technology (SOFT) Wing 1/6'th Scale Semispan Model in AEDC Tunnel 16T," General Dynamics Convair Report GDC TR-77-CRAD-01 (P), December 1976.

5. Brady, A. E., "Stress Analysis of 1/6'th Scale F-111 SOFT Wing Model Tested in AEDC 16T Tunnel, General Dynamics Convair Aero-Test Report 4048, 3 December 1976.

6. Rodriguez, M. B., and Peters, D. W.; "Theoretical Subsonic Flutter Analysis Results of the Self Optimizing Flexible Technology (SOFT) 1/6'th Scale Wind Tunnel Model Wing," General Dynamics Convair Aerodynamics Memo AM-76-CRAD-17, 12 October 1976.

7. McClain, A. A., "1/6'th Scale SOFT Wing Semispan Model - AEDC 16T," General Dynamics Convair Wind Tunnel Drawings WT-76-1111-01 through WT-76-1111-08, 1976.

8. Status Report No. 7, Mission Adaptive Wing, Aerodynamic Design and Analysis, Project 1431, General Dynamics Fort Worth Division Report, 17 November 1976.

9. Levinsky, E. S., and Schappelle, R. H.; "Airfoil Optimization Utilizing A remotely Controlled Flexible Model, Phase I. Low Speed Wind Tunnel Test," General Dynamics Convair Report CASD-NSC-74-007, 31 August 1974.

10. Levinsky, E. S., Schappelle, R. H., and Pountney, S.: "Airfoil Optimization through the Adaptive Control of Camber and Thickness, Phase II. Transonic Wind Tunnel Test and Program Summary," General Dynamics Convair Report CASD-NSC-75-004, 30 September 1975.

11. Levinsky, E. S., Schappelle, R. H., and Pountney, S.: "Transonic Testing of a Self Optimizing Flexible Airfoil," Proceedings of the AIAA 9th Aerodynamic Testing Conference, June 7-9, 1976.

12. "Introduction to the PWT DEC System 10 Real Time Data System," ARO, Inc. PWT, AEDC, Tennessee.

13. Palko, R L., "A Computer -Controlled Closed-Loop Vehicle Trim System Developed in the PWT at AEDC, "Proceedings of the AIAA 9th Aerodynamic Testing Conference, June 7-9, 1976.

14. Yoshihara, H., Benepe, D. B., and Whiooden, P.D., "Transonic Performance of Jet Flaps on an Advanced Fighter Configuration," Air Force Flight Dynamic Laboratory Technical Report AFFDL-TR-73-97, September 1973.

15. Lemley, C. E., "Design Criteria for the Prediction and Prevention of Panel Flutter, Vol. I: Criteria Presentation," Air Force Flight Dynamic Laboratory Report AFFDL-TR-67-140, August 1968.

16. "Evaluation of Kinematic Model," General Dynamics Convair Division Aerodynamics Memo AM-76-CRAD-19, 6 October 1976.

17. Hicks R. M., Murman, E.M. and Vanderplaats, G. N.: "An Assessment of Airfoil Design by Numerical Optimization," NASA TM X-3092, July 1974.

18. Hicks, R. M. and Murman, E. M.: "Application of Numerical Optimization to the Design of Low-Speed Airfoils," NASA TM X-3213, March 1975.

19. Hicks, R. M., Vanderplaats, G. N., Murman, E. M., and King, R. R.: "Airfoil Section Drag Reduction at Transonic Speeds by Numerical Optimization," S.A.E. Report 760477, April 1976.

20. "Inclusion of a Trim Correction to the Tail-Fixed Optimization Computer Program," General Dynamics Convair Aerodynamics Memo AM-CRAD-76-15, 15 September 1976.

21. "Monthly Progress Letter No. 3., SOFT Wing Program," General Dynamics Convair Aero Memo AM-76-CRAD-10, 30 July 1976.

22. "Monthly Progress Letter No. 5., SOFT Wing Program," General Dynamics Convair Aero Memo AM-76-CRAD-14, 5 October 1976.

23. Jameson, A., "Transonic Flow Calculations for Airfoils and Bodies of Revolution," Grumman Report 390-71-1, 1971.

24. Bauer, F., et al., "A Theory of Supercritical Wing Sections with Computer Programs and Examples," in Lecture Notes in Economics and Mathematical Systems, 66, Springer-Verlag, 1972.

DISTRIBUTION LIST

Chief of Naval Research
Department of the Navy
Arlington, VA 22217
ATTN: Vehicles and Propulsion Program, Code 211 — 5

Chief of Naval Development
Department of the Navy
Washington, DC 20360
ATTN: NAVMAT 0331 — 1

Naval Air Systems Command
Department of the Navy
Washington, DC 20361
ATTN: NAVAIR 320D — 1
NAVAIR 5301 — 1
NAVAIR 53013 — 1

David Taylor Naval Ship Research & Development Center
Aviation and Surface Effects Department
Bethesda, MD 20034
ATTN: Code 16 — 1
Code 522.3 — 1

Naval Research Laboratory
Washington, DC 20375
ATTN: Technical Information Office, Code 2627 — 1
Library, Code 2629 — 1

Superintendent
U. S. Naval Academy
Annapolis, MD 21402 — 1

Superintendent
U. S. Naval Postgraduate School
Monterey, CA 93940 — 1

U. S. Naval Air Development Center
Warminster, PA 18974
ATTN: Aeromechanics Department — 1
Code 3015 — 1

Commandant of the Marine Corps
Washington, DC 26320
ATTN: Dr. A. L. Slafkosky
Scientific Advisor
(Code RD-1) — 1

Defense Documentation Center
Cameron Station, Bldg. 5
Alexandria, VA 22314 — 12

Contract Administrator
Southeastern Area
2110 G. Street, N.W.
Washington, DC 20037 — 1

Office of Naval Research Resident Representative
Room 582 Federal Building
300 East 8th Street
Austin, TX 78701 — 1

Department of the Army
DCS for Research Development and Acquisition
Washington, DC 20310
ATTN: DAMA-WSA (Mr. R. L. Ballard) — 1

U. S. Army Material Command
5001 Eisenhower Avenue
Alexandria, VA 22333
ATTN: AMCRD-F — 1

Director, Headquarters
U. S. Army Air Mobility R&D Lab.
Ames Research Center
Moffett Field, CA 94035 — 1

Director, Ames Directorate
U. S. Army Air Mobility R&D Lab.
Ames Research Center
Moffett Field, CA 94035 — 1

Director, Langley Directorate
U. S. Army Air Mobility R&D Lab.
Langley Research Center
Hampton, VA 23665 — 1

Director, Eustis Directorate
U. S. Army Air Mobility R&D Lab.
Fort Eustis, VA 23564 1

U. S. Air Force Flight Dynamics Laboratory
Wright-Patterson AFB, OH 45433
ATTN: Mr. R. DeCamp (FXS) 1

Air Force Office of Scientific Research
Bldg. 410
Bolling AFB, DC 20332
ATTN: Aerospace Sciences (NA) 1

Arnold Engineering Development Center
Arnold Air Force Station
Tennessee 37389
ATTN: MAJ B. Harwood (DYR) 1
Mr. R. Palko (PWT) 1

National Aeronautics and Space Administration
600 Independence Avenue, SW
Washington, DC 20546
ATTN: Code RAA 1
Code RAV 1

National Aeronautics and Space Administration
Ames Research Center
Moffett Field, CA 94035
ATTN: Large-Scale Aerodynamics Branch 1

National Aeronautics and Space Administration
Langley Research Center
Hampton, VA 23665
Subsonic, Transonic Aerodynamic Division
ATTN: James F. Campbell 1

Commander, Air Force Plant Representative Office
Lockheed-Georgia Company
Lockheed-Georgia Company
Marietta, GA 30060 1

Office of Naval Research
Department of the Navy
Arlington, VA 22217
ATTN: Mr. M. Cooper, Code 430B 1

Office of Naval Research Branch Office
495 Summer Street
Boston, MA 02210
ATTN: Dr. A. D. Wood 1

ONR Branch Office Chicago
536 South Clark Street
Chicago, IL 60605
ATTN: Mr. M. A. Chaszeyka 1

Lockheed Missiles & Space Co., Inc.
Huntsville Research & Engineering Ctr.
P. O. Box 1103
Huntsville, AL 35807
ATTN: Mr. A. Zalay 1

Lockheed-Georgia Company
Department 72-74, Zone 503
Marietta, GA 30063
ATTN: Mr. Charles Dixon 1